Copyright Warning & Restrictions

The copyright law of the United States (Title 17, United States Code) governs the making of photocopies or other reproductions of copyrighted material.

Under certain conditions specified in the law, libraries and archives are authorized to furnish a photocopy or other reproduction. One of these specified conditions is that the photocopy or reproduction is not to be "used for any purpose other than private study, scholarship, or research." If a, user makes a request for, or later uses, a photocopy or reproduction for purposes in excess of "fair use" that user may be liable for copyright infringement,

This institution reserves the right to refuse to accept a copying order if, in its judgment, fulfillment of the order would involve violation of copyright law.

Please Note: The author retains the copyright while the New Jersey Institute of Technology reserves the right to distribute this thesis or dissertation

Printing note: If you do not wish to print this page, then select "Pages from: first page # to: last page #" on the print dialog screen

ABSTRACT

A FULL WAVE METHOD FOR ROUGH SURFACE SCATTERING USING FICTITIOUS CURRENT DISTRIBUTIONS

by
Anthony A. Triolo

Rough surface scattering is a current topic of interest in many diverse fields. But, despite its importance, the two most widely used solution methods, the Kirchhoff and first order perturbation methods, are valid only for a restricted range of surface types. There is a large range of surface statistics for which neither of these theories is valid. There are purely numerical solutions to the problem, i.e., the integral equation technique and FDTD method, but these methods require a prohibitively large amount of computer time and storage space for use in practical applications. A full wave method has been introduced by E. Bahar which agrees with the Kirchhoff method in its range of validity, but does not bridge the gap between the later two standard theories and does not provide understanding of the physical processes involved in rough surface scattering. Consequently, it has been a center of controversy since modifications made to improve the method seem arbitrary and are without mathematical or physical justification.

The method presented here is a new full wave method which uses equivalent currents to provide insight into the physical scattering processes. This full wave method analytically reduces to the two standard theories in their respective regions of validity and bridges the gap between the two, which was shown by comparison to the integral equation method. The results presented here are for statistically rough surfaces with Gaussian distributed heights and slopes. A Monte Carlo procedure is used to generate the radar cross section data for this new full wave method.

A FULL WAVE METHOD FOR ROUGH SURFACE SCATTERING USING FICTITIOUS CURRENT DISTRIBUTIONS

by
Anthony A. Triolo

A Dissertation
Submitted to the Faculty of
New Jersey Institute of Technology
in Partial Fulfillment of the Requirements for the Degree of
Doctor of Philosophy

Department of Electrical and Computer Engineering

May 1996

APPROVAL PAGE

A FULL WAVE METHOD FOR ROUGH SURFACE SCATTERING USING FICTITIOUS CURRENT DISTRIBUTIONS

Anthony A. Triolo

Gerald M. Whitman, Ph.D., Dissertation Advisor — Date
Director, Center for Microwave and Lightwave Engineering, NJIT

Felix K. Schwering, Ph.D., Committee Member — Date
Cheif Scientist, U.S. Army CECOM

Gregory A. Kriegsmann. Ph.D., Committee Member — Date
Chairman, Department of Applied Mathematics, NJIT

Edip Niver, Ph.D., Committee Member — Date
Associate Professor, Electrical and Computer Engineering, NJIT

Haim Grebel, Ph.D., Committee Member — Date
Associate Professor, Electrical and Computer Engineering, NJIT

BIOGRAPHICAL SKETCH

Author: Anthony A. Triolo

Degree: Doctor of Philosophy

Date: May 1996

Undergraduate and Graduate Education:

- Attended Graduate School
  Massachussetts Institute of Technology, Cambridge, MA, 1992
- Bachelor of Science in Electrical Engineering (*suma cum laude*, valedictorian)
  New Jersey Institute of Technology, Newark, NJ, 1992

Publications:

G.M. Whitman, F. Schwering, A.A. Triolo, and N.Y. Cho, "A Transport Theory of Pulse Propagation in a Strongly Forward Scattering Random Medium," *IEEE Trans. Antennas Propag.*, Vol. 44, No. 1, January 1996, p. 118-128.

F. Schwering, G. Whitman, A. Triolo, and W-Y. Chen, "The Dielectric Wedge Antenna Fed by a Slab Waveguide Using Local Mode Theory and Equivalent Current Distributions: TE Case," Submitted for publication in *IEEE Trans. Antennas Propag.*, 1996.

G.M. Whitman, A. Triolo, and N. Cho, "Transport Theory of Pulse Propagation in Vegetation Using the PN Method: Validation Study," *U.S. Army Research Office*, Contract No. DAAL03-86-D-0001, June 30, 1992, 34 pages.

F. Schwering, G. Whitman, A. Triolo, and W-Y. Chen, "The Dielectric Wedge Antenna Fed by a Slab Waveguide Using Local Mode Theory and Equivalent Current Distributions: TE Case," *International IEEE AP-S Symposium and URSI Meeting*, Newport Beach, CA, June 19-23, 1995.

F. Schwering, G.M. Whitman, A. Triolo, and N. Cho, "Millimeter-Wave Pulse Propagation in Vegetation," *International IEEE AP-S Symposium and URSI Radio Science Meeting*, Ann Arbor, MI, June 28-July 2, 1993.

To my ever patient wife, Maria

ACKNOWLEDGEMENT

I extend my sincerest gratitute to Dr. Gerald Whitman who, by guidance and example, has taught me an immeasurable amount about science and life. This work would not have been possible if not for Dr. Felix Schwering, whose generosity of ideas and time were greatly appreciated. I would also like to thank my family, especially my parents, for their continuing support, encouragement, and love; without them, I would not be where I am today. A debt of gratitude is owed to Dr. Eric I. Thorsos for the Integral Equation data he provided.

They say love can conquer all. Well, Maria has shown me that this statement is truer than I had ever imagined. When I thought I could not go on, she gave me the courage and strength to continue. She has contributed to this thesis in more ways than she knows, and for that and many other things, I thank her.

TABLE OF CONTENTS

LIST OF FIGURES

CHAPTER 1

INTRODUCTION

Rough surface scattering has been the subject of scientific investigation in many diverse research areas for many decades. This is because all real surfaces are rough, and it is important to determine exactly how and to what extent wave propagation is affected by surface roughness. For example, in line-of-sight communication and cellular communication in particular, the electromagnetic field at the receiver consists of a directly received wave and a wave scattered by the earth's surface. For a smooth earth, the scattered wave can be accurately predicted. However, along the path between the transmitter and receiver a rough surface of dimensions comparable to a wavelength is often encountered. An accurate theory of scattering by rough surfaces could be used to predict and compensate for the scattered field to avoid signal fading. If the communication path is above the sea surface, the surface will be rough and time varying, causing the type of fading to change with the character of the water waves.

Another use for rough surface scattering is that of predicting "sea clutter" in radar return. This "sea clutter" is caused by rapidly fluctuating reflections from facets of the surface of the sea and can seriously affect target recognition above a water surface, sometimes totally obscuring the target. A theory that is accurate over a wide range of frequencies and statistical surface parameters is used to formulate effective measures for reducing interference in radar return from the sea. In the area of medical imaging, rough interfaces between tissues and organs affect propagation and scattering characteristics of a wave. To get an accurate image of internal organs, a theory of scattering from rough interfaces must be used to properly analyze the scattering data. In antenna design, the roughness of the reflector in reflector antennas can lead to performance degradation. Compensating for this effect can result in

improved efficiency and hence lower power requirements for reflector antennas. In radar astronomy, the characteristics of reflected radar pulses from planetary surfaces is used to deduce the roughness of the surface. In acoustics, rough surface scattering is used in many ways, some of which include sonar detection, ultrasonic non-destructive testing, and sound engineering for room acoustics. Rough surface scattering is also very important for remote sensing of the environment. For example, to determine the depth and extent of an oil deposit, the theory of layered media with random interfaces can be employed to analyze radar or sonar return data. Also, the thickness of an oil slick on the ocean surface can be determined precisely using satellite data and an accurate theory of rough surface scattering.

Despite all the applications and interest in rough surface scattering, the two methods most widely used are of restricted applicability. These two methods are the small-perturbation method, which is valid for small heights and slopes, and the physical optics (Kirchhoff) method, which is valid for high frequency, large radii of curvature, and small slope. The so called "full-wave" methods have received much attention as of late due to the efforts of E. Bahar. Full wave methods are those methods where the fields are taken to satisfy Maxwell's equations and the exact boundary conditions by expanding the fields in terms of a basis that includes all wave constituents. The full wave method of E. Bahar [1] uses a local basis function expansion to convert Maxwell's equations into the generalized telegraphist's equations. He then solves this system of coupled integro-differential equations using the method of successive approximations, taking the surface slope as a small parameter. This method is not easily explained in terms of physical scattering processes, has no means of providing an internal check of accuracy, and provides no mathematically justifiable procedure for extension to the full three dimensional case. It has also been the center of controversy since it was introduced [2]. Recently, R.E. Collin [3] furnished a mathematical explanation of the Bahar's method, but did

not provide a way to extend the method to include higher order scattering terms. Without such terms, Bahar's method does not include a mechanism to asses its accuracy. To the contrary, the full wave method presented here provides physical insight into the rough surface scattering processes, and does provide a quantitative measure of its accuracy. The new theory is shown to reduce to the first order perturbation and physical optics (Kirchhoff) approximations in their respective regions of validity. It has also been numerically applied to surfaces with Gaussian height and slope variation for which it is shown to be more accurate than the first order perturbation, Kirchhoff, and Bahar's full wave methods in regions where none of these methods are considered valid.

In Chapter 2, the new full-wave method is formulated in general and used to treat the specific cases of TE and TM polarization in Sections 2.1 and 2.2, respectively. The method consists of initially postulating the total field above the rough surface, called the primary or zero-order field approximation. The primary field is chosen to satisfy the boundary conditions, but does not satisfy Maxwell's source-free equations. To be a field solution, the primary field is forced to satisfy Maxwell's equations with fictitious volume current sources. These zero-order fictitious volume current sources compensate for the difference, or error, between the true total field and the primary field, i.e., the initial approximate solution. Since the fictitious volume current sources are not physically present in the original problem, they must be eliminated. This is accomplished by introducing fictitious first-order sheet current densities to fill the region above the rough surface, which is occupied by the zero-order fictitious volume current sources. The sheet current densities cancel the fictitious volume current sources. These sheet current densities excite first-order fields which consist of a superposition of modal fields that do not satisfy the source free Maxwell's equations. They are forced to satisfy Maxwell's equations with first-order fictitious volume current sources. These volume current sources must be small in order for the

first-order field to be a good approximation to the true solution. The formulation will be performed explicitly for the first-order approximation and the general term of the series solution will be presented as a multidimensional integral representation. A procedure for finding a quantitative measure of the accuracy of this method using current densities induced in the conducting surface is presented in Chapter 3.

Comparison to other standard methods, such as the Kirchhoff method, first-order perturbation method, and Bahar's full wave method are made in Chapters 4 and 5. The comparisons are made for field expressions using a deterministic surface profile in Chapter 4. These expressions are derived in Appendices B, C and D. Statistical analysis is then performed on all these field expressions in Chapter 5, using results obtained in Appendix A, and the resulting expressions are qualitatively compared. The statistical expressions (formal averages) for these fields due to a rough surface with Gaussian height and slope profile are evaluated and compared in Chapter 6 by plotting the new method versus the other methods. Data for plots of the new method were produced using Monte Carlo method. All methods are compared, as done in the literature, to a numerical evaluation of an integral equation using the Monte Carlo method. It is shown through these comparisons that the full wave method presented here produces results that agree with the integral equation results extremely well and much more closely than results form any of the previously mentioned methods for all parameter ranges.

CHAPTER 2

FORMULATION

The two-dimensional geometry under consideration is that of an infinite perfect conductor with a rough surface segment of length $2L$ embedded in air, as shown in Figure 2.1. The rough surface in the region $-L \leq z \leq L$, $-\infty < y < \infty$, is

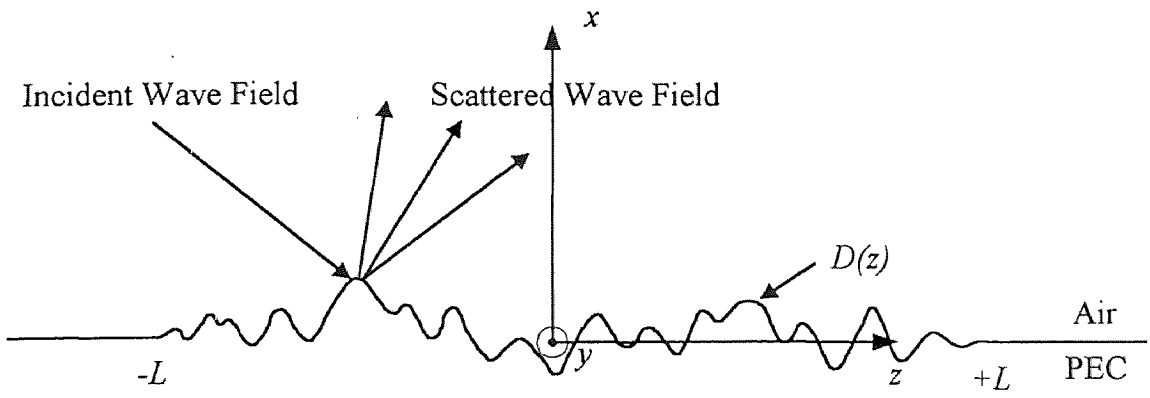

Figure 2.1 The physical geometry under consideration.

taken to be an arbitrary deterministic surface $x = D(z)$ with $D(\pm L) = D'(\pm L) = 0$ throughout the general formulation[1]. A plane wave is assumed incident upon the surface. The total field above the perfect conductor must satisfy the time-harmonic source-free Maxwell's equations with time dependence $e^{j\omega t}$ assumed and suppressed:

$$\nabla \times \mathbf{E} = -j\omega\mu_0\mathbf{H} \tag{2.1a}$$

$$\nabla \times \mathbf{H} = j\omega\epsilon_0\mathbf{E} \tag{2.1b}$$

$$\nabla \cdot \mathbf{E} = 0 \tag{2.1c}$$

$$\nabla \cdot \mathbf{H} = 0. \tag{2.1d}$$

[1]After the total field expression is obtained, statistical analysis is performed in Chapter 5.

The total wave field also satisfies the boundary conditions that the electric field tangential to the surface is zero and that the magnetic field normal to the surface is zero, i.e.,

$$\widehat{n} \times \mathbf{E}\big|_{x=D(z)} = 0 \tag{2.2a}$$

$$\widehat{n} \cdot \mathbf{H}\big|_{x=D(z)} = 0. \tag{2.2b}$$

It is a direct consequence of Maxwell's equations that if one of the two boundary conditions in (2.2a,b) is satisfied then the other is automatically satisfied.

An initial postulate for the total field solution above the metal surface, called the primary field or the zero-order field, is chosen to include an incident plane wave plus a plane wave that is reflected from a flat perfectly conducting surface of infinite extent adjusted to the local elevation. The primary field is chosen to satisfy the boundary conditions (2.2a,b) but does not satisfy the source-free Maxwell's equations. However, the field is chosen to satisfy Maxwell's equations with fictitious electric and magnetic current densities $\mathbf{J}$ and $\mathbf{M}$, respectively, given by

$$\nabla \times \mathbf{E} = -j\omega\mu_0\mathbf{H} - \mathbf{M} \tag{2.3a}$$

$$\nabla \times \mathbf{H} = j\omega\epsilon_0\mathbf{E} + \mathbf{J} \tag{2.3b}$$

$$\nabla \cdot \mathbf{E} = 0 \tag{2.3c}$$

$$\nabla \cdot \mathbf{H} = 0. \tag{2.3d}$$

The fictitious primary volume current densities are imagined to be present in the geometry to support the primary field. Since these current distributions do not physically exist, they must be eliminated by postulating the presence of other current distributions of equal magnitude but 180° out of phase with the primary volume current densities. This is accomplished by introducing sheets of current in planes $z = z_1$, $-L \leq z_1 \leq L$ which extend to $\pm$ infinity in the y direction and from $D(z)$ to ∞ in the x direction. The superposition of these first-order current sheets are used

to cancel the primary volume current densities in the region where they are assumed to exist, namely at points (x, z), for $x \in [D(z), \infty)$[2] and $z \in [-L, L]$.

The first-order sheet currents that are introduced at $z = z_1$ radiate a wave constituent which travels to the right when $z > z_1$ and a wave constituent that travels to the left when $z < z_1$. A superposition of such wave constituents, called the first-order field, is a correction to the primary field and is composed of orthogonal modes, each with spatial wavenumber u_1 in the x direction and β_1 in the z direction, see Figure 2.2. The wavenumber u_1 takes on values between 0 and ∞; u_1 and β_1 are related by $\beta_1^2 = k_0^2 - u_1^2$; and $k_0 = \omega\sqrt{\epsilon_0\mu_0}$ is the free-space wavenumber. Each mode of the first-order field must satisfy the source-free Maxwell's equations

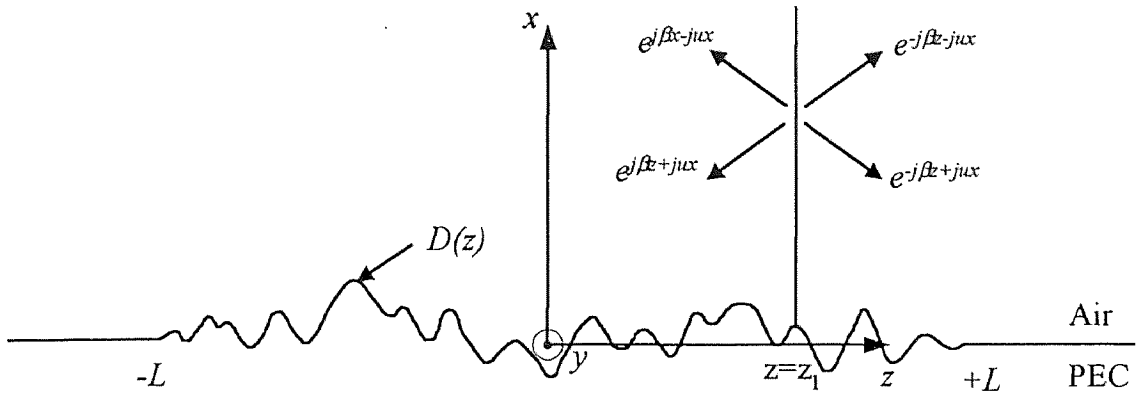

Figure 2.2 Field radiated by sheet current.

plus boundary conditions to be a solution to the problem. However, Maxwell's equations can only be satisfied by a mode if fictitious current densities are introduced again; these are designated first-order volume current densities. If the first-order volume current densities are "small", the total field will be approximately equal to the primary plus first-order fields.

The procedure above can easily be generalized to include higher order field contributions which may improve the accuracy of the solution. For each mode corre-

[2]This notation means $D(z) \leq x < \infty$.

sponding to a particular value of u_1, there will be a fictitious first-order volume current density remaining in the region where the primary volume current densities had existed. This first-order volume current density can be cancelled by introducing second-order sheet currents in the plane $z = z_2$, $|z_2| \leq L$, $D(z) \leq x < \infty$, of equal magnitude but 180° out of phase with the first-order volume current density. These second-order sheet currents cancel the first-order volume current densities corresponding to u_1 and require another set of modes with x directed wavenumbers u_2. This implies that the resulting field will be a triple superposition. In other words, there will be a superposition of modes summing over u_2 for each u_1. There will also be a superposition of modes summing over u_1 for each position $z = z_2$. All of the previous terms are then superimposed for all z_2, $|z_2| \leq L$. It should be kept in mind that z_1, z_2, u_1 and u_2 are continuous variables, and the summations actually represent integrations. The field radiated by the second-order sheet currents require additional fictitious volume current densities (denoted as being second-order) in order to satisfy Maxwell's equations. The entire process can be repeated to obtain higher order terms in the scattered field. The procedure is applied to the specific cases of TE and TM wave scattering from a rough surface in the following two sections.

2.1 The TE Case

In TE case the only non-zero components of the electric and magnetic fields are E_y, H_x and H_z, as shown in Figure 2.3. Maxwell's equations with sources reduce to

$$\frac{\partial E_y}{\partial z} = jk_0\eta_0 H_x + M_x \tag{2.4a}$$

$$\frac{\partial E_y}{\partial x} = -jk_0\eta_0 H_z - M_z \tag{2.4b}$$

$$\eta_0\left[\frac{\partial H_x}{\partial z} - \frac{\partial H_z}{\partial x}\right] = jk_0 E_y + \eta_0 J_y, \tag{2.4c}$$

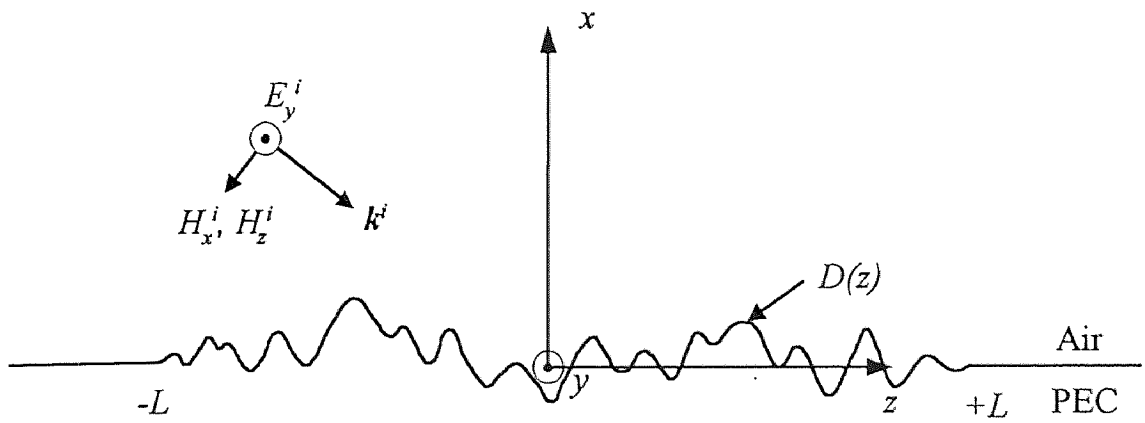

Figure 2.3 Geometry for TE case.

where $\eta_0 = \sqrt{\mu_0/\epsilon_0}$ and $k_0 = \omega\sqrt{\mu_0\epsilon_0}$. The boundary conditions become

$$E_y|_{x=D(z)} = 0, \tag{2.5a}$$

$$[H_x - D'(z)H_z]_{x=D(z)} = 0, \tag{2.5b}$$

where the prime denotes differentiation with respect to z. The total electric field is written as the sum of incident and scattered fields:

$$E_y^t = E_y^i + E_y^s. \tag{2.6}$$

The total field must satisfy Maxwell's source-free equations and boundary conditions to be the solution to the scattering problem.

The total electric field is initially assumed to have the form

$$\begin{aligned} E_y^p &= E_0^i e^{-j(\beta_0 z - u_0 D)} \sin u_0 (x - D) \\ &= \frac{E_0^i}{2j}\left[e^{-j(\beta_0 z - u_0 x)} - e^{-j(\beta_0 z + u_0 x - 2u_0 D)}\right], \end{aligned} \tag{2.7}$$

which will be referred to as the primary or zero-order solution. Substituting (2.7) into (2.4a,b) with $M_x = M_z = 0$ give the magnetic field components as

$$\eta_0 H_z^p = j\frac{u_0}{k_0} E_0^i e^{-j(\beta_0 z - u_0 D)} \cos u_0 (x - D) \tag{2.8}$$

$$\eta_0 H_x^p = -\frac{\beta_0}{k_0} E_0^i e^{-j(\beta_0 z - u_0 D)} \sin u_0 (x - D) + j\frac{u_0}{k_0} D' e^{-j(\beta_0 z + u_0 x - 2u_0 D)}, \tag{2.9}$$

where $D = D(z)$ and $\beta_0 = \sqrt{k_0^2 - u_0^2}$. The primary field, satisfies the boundary conditions (2.5a) and (2.5b) and is composed of an incident plane wave and a modified reflected plane wave. The modified reflected plane wave is equivalent to an incident plane wave reflected from a flat, perfectly conducting surface adjusted to the local elevation D. The remaining source-free Maxwell equation (i.e., (2.4c) with $J_y = 0$) is not satisfied by the primary field (2.7)–(2.9). The primary field does however satisfy Maxwell's equations (2.4a,b,c) with a single source term, namely, a fictitious electric current density J_y^p called the primary volume current density; it is found by substituting (2.7)–(2.9) into (2.4c) to be

$$J_y^p(x, z; u_0) = \frac{u_0}{\eta_0 k_0} E_0^i \left[2\beta_0 D' - 2u_0 D'^2 + jD''\right] e^{-j\beta_0 z + j2u_0 D - ju_0 x}. \tag{2.10}$$

Note that J_y^p is zero in the region $|z| > L$. Since this primary volume current density is not physically present in the original scattering problem, it may be cancelled in a plane $z = z_1$, $-\infty < y < \infty$ and $D(z_1) < x < \infty$ by introducing a superposition of first-order sheet current densities of equal magnitude and 180° phase difference. By allowing z_1 to vary over the region occupied by J_y^p, namely $|z_1| \leq L$, $D(z_1) < x < \infty$ the volume current density is removed. However, the sheet current densities produce an infinite superposition of orthogonal modes with x-directed wavenumbers u_1 ranging from 0 to ∞. Each mode, with a particular wavenumber u_1 and unknown amplitude factor, satisfies the boundary conditions (2.5a,b) and Maxwell's equations with $\mathbf{M} = 0$ and $\mathbf{J} = \hat{\mathbf{y}} J_y^{(1)}$, and is expressed in the same way as the primary field. Hence, a mode propagating to the right in the region $z > z_1$ is postulated to be given

by

$$E_{y>}^{(1)} = A^{(1)+}e^{-j\beta_1(z-z_1)-ju_1D}\sin u_1\,(x-D) \tag{2.11a}$$

$$\eta_0 H_{z>}^{(1)} = -\frac{u_1}{jk_0}A^{(1)+}e^{-j\beta_1(z-z_1)-ju_1D}\cos u_1\,(x-D) \tag{2.11b}$$

$$\eta_0 H_{x>}^{(1)} = -\frac{\beta_1}{k_0}A^{(1)+}e^{-j\beta_1(z-z_1)-ju_1D}\sin u_1\,(x-D) + j\frac{u_1}{k_0}D'A^{(1)+}e^{-j\beta_1(z-z_1)+ju_1x-j2u_1D}, \tag{2.11c}$$

and propagating to the left in the region $z < z_1$ is assumed to be given by

$$E_{y<}^{(1)} = A^{(1)-}e^{j\beta_1(z-z_1)-ju_1D}\sin u_1\,(x-D) \tag{2.12a}$$

$$\eta_0 H_{z<}^{(1)} = -\frac{u_1}{jk_0}A^{(1)-}e^{j\beta_1(z-z_1)-ju_1D}\cos u_1\,(x-D) \tag{2.12b}$$

$$\eta_0 H_{x<}^{(1)} = \frac{\beta_1}{k_0}A^{(1)-}e^{j\beta_1(z-z_1)-ju_1D}\sin u_1\,(x-D) + j\frac{u_1}{k_0}D'A^{(1)-}e^{j\beta_1(z-z_1)+ju_1x-j2u_1D}. \tag{2.12c}$$

By introducing the above modes, it is implicitly being assumed that the final representation of the scattered field will be an infinite superposition of modes over these wavenumbers u_1. Continuity of $E_y^{(1)}$ across $z = z_1$ implies $A^{(1)+} = A^{(1)-} = A^{(1)}(z_1, u_1; u_0)$. H_z is continuous across $z = z_1$. The discontinuity in H_x is used to determine the first-order sheet current density $J_{sy}^{(1)}$ *via*

$$\mathbf{J}_s = \widehat{\mathbf{z}} \times [\mathbf{H}_> - \mathbf{H}_<]_{z=z_1}\,, \tag{2.13}$$

which results in

$$J_{sy}^{(1)} = -\frac{2\beta_1}{k_0\eta_0}A^{(1)}(z_1, u_1; u_0)\sin u_1(x-D_1)e^{-ju_1D_1}, \tag{2.14}$$

where $D_1 = D(z_1)$ and $A^{(1)}(z_1, u_1; u_0)$ is the modal amplitude for each u_1. To cancel the primary volume current at a specific point (x, z_1), a superposition of all the sheet currents at this point is used

$$J_y^p(x, z_1; u_0) + \int_0^\infty J_{sy}^{(1)}(x, z_1, u'; u_0)\,du' = 0, \quad x \neq D_1, \quad -L \leq z_1 \leq L. \tag{2.15}$$

Recall that an infinite number of sheet currents superimposed over u_1 is required in order to obtain a modal representation of the scattered field. Substituting (2.10) and (2.14) into (2.15), multiplying by $(2/\pi)\sin u_1(x - D_1)$, integrating with respect to x from D_1 to ∞ and using orthogonality (see Appendix E) yields

$$A^{(1)}(z_1, u_1; u_0) = -jE_0^i \frac{u_0\left[2\beta_0 D_1' - 2u_0 D_1'^2 + jD_1''\right]}{2\beta_1} \times e^{j(u_1+u_0)D_1 - j\beta_0 z_1}\zeta(u_1; u_0), \quad (2.16)$$

where

$$\zeta(u_1) \equiv \zeta(u_1; u_0) = \delta(u_1 - u_0) + j\frac{2}{\pi}\mathcal{P}\left\{\frac{u_1}{u_1^2 - u_0^2}\right\}. \quad (2.17)$$

The first-order field is obtained by superimposing the modes given in (2.11a,b,c) and/or (2.12a,b,c) with modal amplitude $A^{(1)}$ specified in (2.16). The superposition is a double integral which extends first over all wavenumbers $u_1 \in [0, \infty)$ and then over the physical space $z_1 \in [-L, L]$. The field expression depends on the location of the observation point relative to the spatial location of the sheet currents. Thus, for $z > L$ (region 1)

$$E_{y1}^{(1)}(x, z) = \int_{z_1=-L}^{L}\int_{u_1=0}^{\infty} A^{(1)}(z_1, u_1)e^{-j\beta_1(z-z_1)}\sin u_1 x du_1 dz_1, \quad (2.18)$$

for $-L \le z_1 \le L$ (region 2)

$$E_{y2}^{(1)}(x, z) = \int_{z_1=-L}^{z}\int_{u_1=0}^{\infty} A^{(1)}(z_1, u_1)e^{-j\beta_1(z-z_1)-ju_1 D}\sin u_1(x - D)du_1 dz_1 + \int_{z_1=z}^{L}\int_{u_1=0}^{\infty} A^{(1)}(z_1, u_1)e^{j\beta_1(z-z_1)-ju_1 D}\sin u_1(x - D)du_1 dz_1, \quad (2.19)$$

and for $z < -L$ (region 3)

$$E_{y3}^{(1)}(x, z) = \int_{z_1=-L}^{L}\int_{u_1=0}^{\infty} A^{(1)}(z_1, u_1)e^{j\beta_1(z-z_1)}\sin u_1 x du_1 dz_1, \quad (2.20)$$

where, as before, $D = D(z)$. The parameter u_0 is suppressed in the above expression, and is suppressed from this point forward.

To show that the field depends only on the surface height D and the square of the surface slope D'^2 it is necessary to obtain a convergent integral representation for the field. This is accomplished by using the path deformation in Figure 2.4 and Cauchy's theorem. It can be shown that

$$\int_0^\infty f(u_1)\zeta(u_1)du_1 = \int_\Omega f(u_1)\mathcal{P}\left\{\frac{2ju_1}{\pi\left(u_1^2 - u_0^2\right)}\right\}du_1, \tag{2.21}$$

where $\zeta(u_1)$ is given in (2.17) and the original integration over the real u_1-axis, which is the same as integrating over the path segments Γ_1 and Γ_2 with only the principal part of $\zeta(u_1)$ in the integrand, is now equivalent to the integral of the principal part of $\zeta(u_1)$ over the deformed path Ω. Equation (2.18), for example, is now written

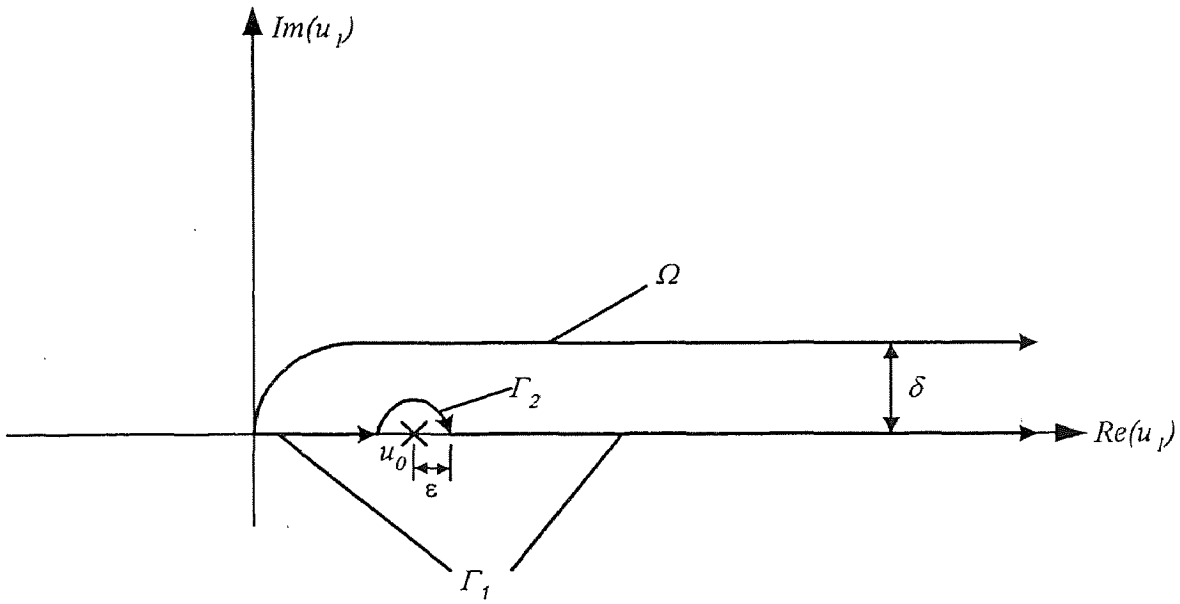

Figure 2.4 The integration path in the complex u_1 plane.

as

$$E_{y1}^{(1)}(x,z) = \frac{E_0^i u_0}{\pi} e^{-j\beta_0 z} \int_{z_1=-L}^{L} \int_{\Omega} \left[2\beta_0 D_1' - 2u_0 D_1'^2 + jD_1''\right] e^{j(u_1+u_0)D_1 - j(\beta_1-\beta_0)(z-z_1)} \times \frac{u_1}{u_1^2 - u_0^2} \sin u_1 x \frac{du_1}{\beta_1} dz_1. \quad (2.22)$$

There is a branch point at $u_1 = k_0$ (not shown in Figure 2.4) and the Riemann sheet on which the path lies is chosen such that $\mathrm{Im}\,(\beta_1) < 0$ when $u_1 > k_0$, which ensures that the above integrand decays for large u_1, i.e., the integral is convergent. The raised path avoids the singularity at $u_1 = u_0$, ensures that it is permissible to interchange the order of integration and leads to the following integration by parts of the integral over z_1:

$$\int_{-L}^{L} \left[2\beta_0 D_1' - 2u_0 D_1'^2 + jD_1''\right] e^{j2u_0 D_1 + j(\beta_1-\beta_0)z_1 + j(u_1-u_0)D_1} dz_1 = (u_0 - u_1) \int_{-L}^{L} \left\{1 - \left[1 + D_1'^2\right] e^{j(u_1+u_0)D_1}\right\} e^{j(\beta_1-\beta_0)z_1} dz_1, \quad (2.23)$$

where it has been assumed that $D(\pm L) = D'(\pm L) = 0$. Using this identity produces an expression for the first-order field in terms of only D and D'^2

$$E_{y1}^{(1)}(x,z) = -\frac{E_0^i u_0}{\pi} \int_{u_1=0}^{\infty} \int_{z_1=-L}^{L} \left\{1 - \left[1 + D_1'^2\right] e^{j(u_1+u_0)D_1}\right\} \frac{u_1}{u_1+u_0} \times e^{j(\beta_1-\beta_0)z_1} e^{-j\beta_1 z} \sin u_1 x dz_1 \frac{du_1}{\beta_1}. \quad (2.24)$$

The far field is obtained by using the stationary phase approximation [4]. For the scattering geometry shown in Figure 2.5, the following change of variables is introduced

$$\begin{aligned} u_0 &= k_0 \cos\phi_0 \quad , \quad \beta_0 = k_0 \sin\phi_0 \\ u_1 &= k_0 \cos w \quad , \quad \beta_1 = k_0 \sin w \\ x &= \rho \cos\phi \quad , \quad z = \rho \sin\phi \end{aligned} \quad (2.25)$$

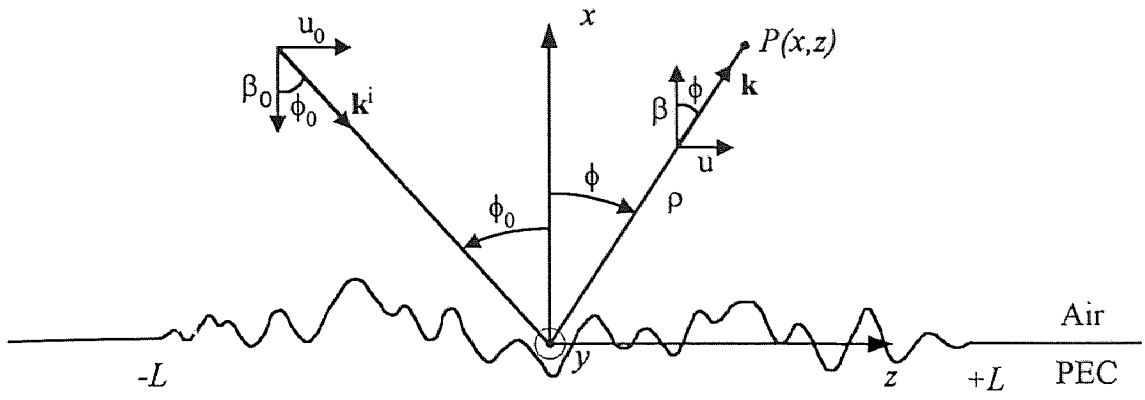

Figure 2.5 Scattering geometry for far field evaluation.

which produces the expression

$$E_{y1}^{(1)}(x,z) = \int_{w=0}^{\frac{\pi}{2}} \left[\int_{z_1=-L}^{L} K(w,z_1)dz_1 \right] e^{-jk_0\rho \sin w \sin\phi} \times \left[e^{jk_0\rho\cos w\cos\phi} - e^{-jk_0\rho\cos w\cos\phi} \right] dw \quad (2.26)$$

where

$$K(w,z_1) = j\frac{E_0^i k_0}{2\pi}\frac{\cos\phi_0\cos w}{\cos w+\cos\phi_0}\left\{1-\left[1+D_1'^2\right]e^{jk_0D_1(\cos w+\cos\phi_0)}\right\}e^{jk_0z_1(\sin w-\sin\phi_0)}. \quad (2.27)$$

The u_1 integration is terminated at k_0 to include only propagating modes. The w integration is evaluated using the stationary phase approximation (see Appendix E). If the u_1 integration is not terminated at k_0 then the w integration is evaluated along a path in the complex plane and the integration can be performed using the method of steepest descent [4]. The result is the same in either case, and is as follows (only the second term in the square bracket in (2.26) contributes to the integral):

$$E_{y1}^{(1)ff}(x,z) = \frac{k_0}{\sqrt{2\pi}}G_0A_0^iR^{TE}(\phi,\phi_0), \quad 0\le\phi<\pi/2, \quad (2.28)$$

where G_0 is the $2-D$ asymptotic Green's function

$$G_0 = \frac{e^{-j[k_0\rho-\pi/4]}}{\sqrt{k_0\rho}}, \quad (2.29)$$

the constant A_0^i is the amplitude of the incident field (see (2.7))

$$A_0^i = \frac{E_0^i}{2j}, \tag{2.30}$$

and the radar cross section can be obtained by taking the magnitude squared of the scatter pattern, which is

$$R^{TE}(\phi,\phi_0) = \frac{2\cos\phi\cos\phi_0}{\cos\phi+\cos\phi_0}\int_{-L}^{L}\left\{1-\left[1+D_1'^2\right]e^{jk_0D_1(\cos\phi+\cos\phi_0)}\right\}e^{jk_0z_1(\sin\phi-\sin\phi_0)}dz_1,$$

$$0\le\phi\le\pi/2. \tag{2.31}$$

The same procedure is performed for the case $z \le -L$ ($-\pi/2 \le \phi \le 0$) which yields the same expression. Since the rough surface is of finite extent, the scattering pattern expression in (2.31) remains valid for $-\pi/2 \le \phi \le \pi/2$.

Although the first-order field satisfies the boundary conditions (2.5a,b), it does not satisfy Maxwell's source-free equations; hence, it is forced to satisfy Maxwell's equations with a fictitious electric current density $J_y^{(1)}$ which is:

$$J_y^{(1)}(x,z_1,z,u_1) = \frac{u_1}{k_0\eta_0}\left[\mathrm{sgn}(z-z_1)2\beta_1D' + 2u_1D'^2 + jD''\right]A^{(1)}(z_1,u_1)$$

$$\times\, e^{-j|z-z_1|\beta_1+ju_1x-j2u_1D}, \tag{2.32}$$

where $\mathrm{sgn}(z-z_1) = \pm 1$ for $z \gtrless z_1$. Since the first-order fictitious volume current density is not physically present in the original scattering problem, it can be cancelled by introducing a superposition of second-order fictitious sheet current densities. This can mathematically be stated by the following relation

$$J_y^{(1)}(x,z_1,z_2,u_1) + \int_0^{\infty} J_{sy}^{(2)}(x,z_1,z_2,u_1,u_2)\,du_2 = 0,$$

$$x \ne D_2, \quad |z_2| \le L \tag{2.33}$$

(refer to (2.15) for a similar condition which was imposed to eliminate the primary volume current density $J_y^p(x,z_1;u_0)$). Note that in (2.33) u_0 is suppressed. In (2.33),

$J_y^{(1)}$ is obtained from (2.32) in the plane $z = z_2$. To eliminate the volume current density lying in this plane requires postulating a superposition of second-order sheet current densities $J_{sy}^{(2)}$, $0 \leq u_2 < \infty$. In order to find an expression for the sheet current densities $J_{sy}^{(2)}$, the mode structure is chosen to be identical to the mode structure introduced in (2.11a,b,c) and (2.12a,b,c) but with u_1 replaced by u_2 and z_1 replaced by z_2; the dependence on x, z_1, and u_1 in $J_{sy}^{(2)}$ comes from $J_y^{(1)}$ using (2.32) in (2.33). Recall that an infinite superposition of sheet current densities at $z = z_2$ is needed to generate the modal representation for the scattered field and hence is used to eliminate the volume current distribution at $z = z_2$. The modal representation for the second-order scattered field is obtained following the same procedure as was done before to get the first-order scattered field. For $z > L$ (region 1), the second-order scattered field is found to be

$$E_{y1}^{(2)}(x,z) = \int_{z_1=-L}^{L} \int_{z_2=-L}^{L} \int_{u_1=0}^{\infty} \int_{u_2=0}^{\infty} A^{(2)}(z_1,z_2,u_1,u_2) e^{-j\beta_2(z-z_2)} \sin u_2 x \, du_2 du_1 dz_2 dz_1, \tag{2.34}$$

for $-L \leq z \leq L$ (region 2),

$$\begin{aligned} E_{y2}^{(2)}(x,z) = &\int_{z_1=-L}^{L} \int_{z_2=-L}^{z} \int_{u_1=0}^{\infty} \int_{u_2=0}^{\infty} A^{(2)}(z_1,z_2,u_1,u_2) e^{-j\beta_2(z-z_2)-ju_2 D} \\ &\times \sin u_2(x-D) \, du_2 du_1 dz_2 dz_1 \\ &+ \int_{z_1=-L}^{L} \int_{z_2=z}^{L} \int_{u_1=0}^{\infty} \int_{u_2=0}^{\infty} A^{(2)}(z_1,z_2,u_1,u_2) e^{j\beta_2(z-z_2)-ju_2 D} \\ &\times \sin u_2(x-D) \, du_2 du_1 dz_2 dz_1, \end{aligned} \tag{2.35}$$

and for $z < -L$ (region 3),

$$E_{y3}^{(2)}(x,z) = \int_{z_1=-L}^{L} \int_{z_2=-L}^{L} \int_{u_1=0}^{\infty} \int_{u_2=0}^{\infty} A^{(2)}(z_1,z_2,u_1,u_2) e^{j\beta_2(z-z_2)} \sin u_2 x \, du_2 du_1 dz_2 dz_1. \tag{2.36}$$

For the second-order modal fields to satisfy Maxwell's equations, a second-order volume current density is required. This can then be cancelled by a third order sheet current, and so on. The general expression for the condition that the "$n+1$" order sheet current densities cancel the "n" order volume current density at (x, z_{n+1}) is written as

$$J_y^{(n)}(x, z_1, \ldots, z_n, z_{n+1}, u_1, \ldots, u_n) + \int_0^\infty J_{sy}^{(n+1)}(x, z_1, \ldots, z_n, z_{n+1}, u_1, \ldots, u_n, u_{n+1}) du_{n+1} = 0, \quad x \neq D_{n+1}, \quad |z_{n+1}| \leq L \tag{2.37}$$

where

$$J_y^{(n)}(x, z_1, \ldots, z_n, z, u_1, \ldots, u_n) = \frac{u_n}{k_0 \eta_0} \left[\mathrm{sgn}(z - z_n) 2\beta_n D' + 2u_n D'^2 + jD'' \right] \times A^{(n)}(z_1, \ldots, z_n, u_1, \ldots, u_n) e^{-j|z-z_n|\beta_n + ju_n x - j2u_n D}, \tag{2.38}$$

and $J_{sy}^{(n+1)}$ is of the same form as $J_{sy}^{(1)}$, but with all "1" replaced by "$n+1$". The modal amplitude $A^{(n)}$ can be written either as a recurrence relation given by

$$A^{(n+1)}(z_1, \ldots, z_{n+1}, u_1, \ldots, u_{n+1}; u_0) = j \frac{u_n}{2\beta_{n+1}} \varepsilon(u_n, z_n, z_{n+1}) e^{-j\beta_n |z_{n+1} - z_n| - jD_{n+1}(u_n - u_{n+1})} \times \zeta^*(u_{n+1}; u_n) A^{(n)}(z_1, \ldots, z_n, u_1, \ldots, u_n; u_0) \tag{2.39}$$

where

$$\varepsilon(u_n, z_n, z_{n+1}) = \left[\mathrm{sgn}(z_{n+1} - z_n) 2\beta_n D'_{n+1} + 2u_n D'^2_{n+1} + jD''_{n+1} \right], \tag{2.40}$$

and $\zeta^*(u_{n+1};u_n)$ is the complex conjugate of (2.17), or in the explicit form expressed as

$$A^{(n+1)}(z_1,\ldots,z_{n+1},u_1,\ldots,u_{n+1};u_0) = j\prod_{i=1}^{n}\left[\frac{u_n}{2\beta_{i+1}}\varepsilon(u_i,z_i,z_{i+1})\,e^{-j\beta_i|z_{i+1}-z_i|-jD_{i+1}(u_i-u_{i+1})}\zeta^*(u_{i+1};u_i)\right] \times A^{(1)}(z_1,u_1;u_0). \quad (2.41)$$

The "n" order field radiated by the "n" order sheet current takes the form for $z > L$ (region 1)

$$E_{y1}^{(n)}(x,z) = \int_{z_1=-L}^{L}\cdots\int_{z_n=-L}^{L}\int_{u_1=0}^{\infty}\cdots\int_{u_n=0}^{\infty} A^{(n)}(z_1,\ldots,z_n,u_1,\ldots,u_n)e^{-j\beta_n(z-z_n)} \times \sin u_n x\,du_n\ldots du_1 dz_n\ldots dz_1, \quad (2.42)$$

for $-L \le z \le L$ (region 2)

$$E_{y2}^{(n)}(x,z) = \int_{z_1=-L}^{L}\cdots\int_{z_n=-L}^{z}\int_{u_1=0}^{\infty}\cdots\int_{u_n=0}^{\infty} A^{(n)}(z_1,\ldots,z_n,u_1,\ldots,u_n)e^{-j\beta_n(z-z_n)-ju_nD} \times \sin u_n(x-D)du_n\ldots du_1dz_n\ldots dz_1 + \int_{z_1=-L}^{L}\cdots\int_{z_n=z}^{L}\int_{u_1=0}^{\infty}\cdots\int_{u_n=0}^{\infty} A^{(n)}(z_1,\ldots,z_n,u_1,\ldots,u_n)e^{j\beta_n(z-z_n)-ju_nD} \times \sin u_n(x-D)du_n\ldots du_1dz_n\ldots dz_1, \quad (2.43)$$

and for $z < -L$ (region 3)

$$E_{y3}^{(n)}(x,z) = \int_{z_1=-L}^{L}\cdots\int_{z_n=-L}^{L}\int_{u_1=0}^{\infty}\cdots\int_{u_n=0}^{\infty} A^{(n)}(z_1,\ldots,z_n,u_1,\ldots,u_n)e^{j\beta_n(z-z_n)} \times \sin u_n x\,du_n\ldots du_1dz_n\ldots dz_1. \quad (2.44)$$

The N-order total field approximation is given by

$$E_{yi}(x,z) = \sum_{n=0}^{N} E_{yi}^{(n)}, \qquad E_{yi}^{(0)} = E_y^p \quad (2.45)$$

where $i = 1,2,3$.

2.2 The TM Case

For the TM case, the only non-zero components of the electric and magnetic fields are H_y, E_x, and E_z, as shown in Figure 2.6. Maxwell's time-harmonic equations

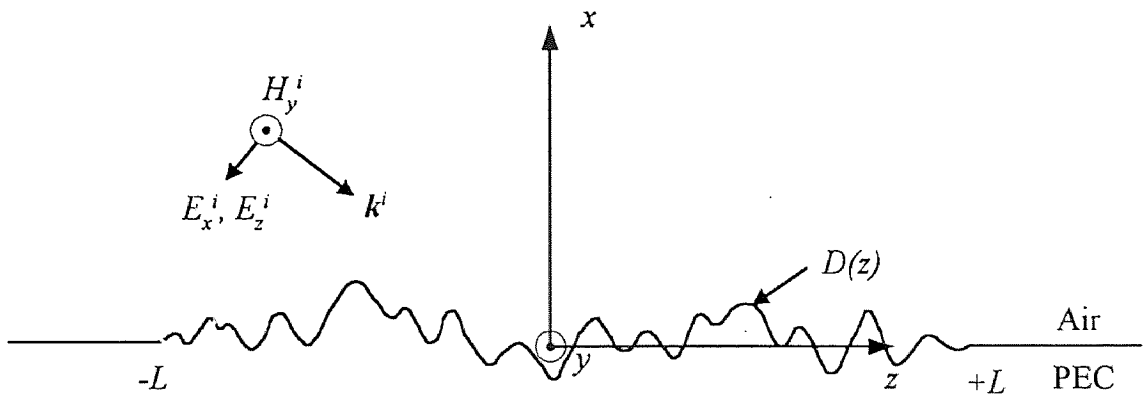

Figure 2.6 Geometry for TM case.

with source terms reduce to

$$\eta_0 \frac{\partial H_y}{\partial z} = -jk_0 E_x - J_x \tag{2.46a}$$

$$\eta_0 \frac{\partial H_y}{\partial x} = jk_0 E_z + J_z \tag{2.46b}$$

$$\frac{\partial E_x}{\partial z} - \frac{\partial E_z}{\partial x} = -jk_0\eta_0 H_y - M_y \tag{2.46c}$$

where, as before, $\eta_0 = \sqrt{\mu_0/\epsilon_0}$ and $k_0 = \omega\sqrt{\mu_0\epsilon_0}$. The boundary conditions become

$$H_x - D'(z)H_z|_{x=D(z)} = 0 \tag{2.47a}$$

$$E_z + D'(z)E_x|_{x=D(z)} = 0 \tag{2.47b}$$

where the prime denotes differentiation with respect to z. Since the magnetic field has no x or z component, the first boundary condition (2.47a) is trivially satisfied; therefore, the second (2.47b) must be used. The total magnetic field is written as the sum of an incident and scattered field, i.e.,

$$H_y^t = H_y^i + H_y^s. \tag{2.48}$$

The total field must satisfy Maxwell's source free equations, i.e., (2.46a,b,c) with $J_x = J_z = M_y = 0$, and the boundary condition (2.47b) to be the solution to the scattering problem. From this point forward, field quantities without superscripts will represent total fields.

Instead of writing the total field as an incident and scattered field as in (2.48), it is written as a primary field plus higher order field terms, where the primary field is the zero-order solution for the total field, i.e.,

$$H_y = H_y^p + H_y^{ho} \quad , \quad E_x = E_x^p + E_x^{ho} \quad , \quad E_z = E_z^p + E_z^{ho} \; . \tag{2.49}$$

The higher order components are expressed in terms of partial fields:

$$F^{ho} = \int_{z_1=-L}^{L} \int_{u_1=0}^{\infty} F^{(1)}(x,z,z_1,u_1)du_1dz_1 + \cdots + \int_{\overline{z}_n} \int_{\overline{u}_n} F^{(n)}(x,z,\overline{z}_n,\overline{u}_n)d\overline{u}_nd\overline{z}_n + \cdots \; , \tag{2.50}$$

where F represents any of the three field components H_y, E_x, E_z; $\overline{u}_n$ and $\overline{z}_n$ are vectors composed of the variables $u_1, \ldots, u_n$ and $z_1, \ldots, z_n$, respectively; the integrals over $\overline{u}_n$ and $\overline{z}_n$ are

$$\int_{\overline{z}_n} \int_{\overline{u}_n} (\cdot)\, d\overline{u}_nd\overline{z}_n \equiv \int_{z_1=-L}^{L} \cdots \int_{z_n=-L}^{L} \int_{u_1=0}^{\infty} \cdots \int_{u_n=0}^{\infty} (\cdot)\, du_1 \ldots du_ndz_1 \ldots dz_n. \tag{2.51}$$

A primary field is postulated, which satisfies the flat surface boundary condition, (2.47b) with $D' = 0$; thus,

$$H_y^p = \frac{E_0^i}{\eta_0} e^{-j\beta_0 z + ju_0 D} \cos u_0(x - D). \tag{2.52}$$

Taking $J_x = J_z = 0$ in Maxwell's equations (2.46a,b) gives the remaining field components

$$E_x^p = j\frac{E_0^i}{k_0} e^{-j\beta_0 z + ju_0 D} \left[u_0 D' \sin u_0(x - D) - j\left(\beta_0 - u_0 D'\right) \cos u_0(x - D)\right] \tag{2.53}$$

and

$$E_z^p = ju_0 \frac{E_0^i}{k_0} e^{-j\beta_0 z + ju_0 D} \sin u_0(x - D). \tag{2.54}$$

The forms for the higher order terms with $J_x^{(n)} = J_z^{(n)} = 0$ are assumed as follows for $z > z_1$,

$$H_{y>}^{(n)}(x, z, z_n, u_n; u_0) = A^{+(n)} e^{-j\beta_n(z-z_n) - ju_n D} \cos u_1(x - D) \tag{2.55a}$$

$$E_{x>}^{(n)}(x, z, z_n, u_n; u_0) = \frac{\eta_0}{k_0} A^{+(n)} e^{-j\beta_n(z-z_n) - ju_n D} \times \left[u_n D' e^{ju_n(x-D)} + \beta_n \cos u_n(x - D)\right] \tag{2.55b}$$

$$E_{z>}^{(n)}(x, z, z_n, u_n; u_0) = ju_n \frac{\eta_0}{k_0} A^{+(n)} e^{-j\beta_n(z-z_n) - ju_n D} \sin u_n(x - D) \tag{2.55c}$$

and for $z < z_1$

$$H_{y<}^{(n)}(x, z, z_n, u_n; u_0) = A^{-(n)} e^{j\beta_n(z-z_n) - ju_n D} \cos u_1(x - D) \tag{2.56a}$$

$$E_{x<}^{(n)}(x, z, z_n, u_n; u_0) = \frac{\eta_0}{k_0} A^{-(n)} e^{j\beta_n(z-z_n) - ju_n D} \times \left[u_n D' e^{ju_n(x-D)} - \beta_n \cos u_n(x - D)\right] \tag{2.56b}$$

$$E_{z<}^{(n)}(x, z, z_n, u_n; u_0) = ju_n \frac{\eta_0}{k_0} A^{-(n)} e^{j\beta_n(z-z_n) - ju_n D} \sin u_n(x - D) \tag{2.56c}$$

where the variables $[u_1, \ldots, u_n]$ and $[z_1, \ldots, z_n]$ are suppressed in the amplitude terms $A^{\pm(n)}$. These higher order terms also satisfy only the flat surface boundary condition and not the rough surface boundary condition. In the strict sense, these terms cannot be called modes since they do not satisfy the rough surface boundary conditions. It will be shown, however, that these terms can be forced to satisfy the boundary conditions and, hence, will be modes.

$H_y^{(n)}$ and $E_z^{(n)}$ are continuous across $z = z_n$, but $E_x^{(n)}$ is discontinuous due to the postulation of a fictitious sheet current density $M_{sy}^{(n)}$ at z_n. The boundary conditions

at $z = z_n$ are explicitly given by

$$J_{sx}^{(n)} = \left[H_{y>}^{(n)} - H_{y<}^{(n)}\right]_{z=z_n} = 0 \tag{2.57a}$$

$$M_{sy}^{(n)} = -\left[E_{x>}^{(n)} - E_{x<}^{(n)}\right]_{z=z_n} \neq 0 \tag{2.57b}$$

$$\rho_s^{(n)}/\epsilon_0 = \left[E_{z>}^{(n)} - E_{z<}^{(n)}\right]_{z=z_n} = 0 \tag{2.57c}$$

The boundary condition (2.57a) makes $A^{+(n)} = A^{-(n)} = A^{(n)}$, and the condition (2.57b) specifies the magnetic sheet current density as

$$M_{sy}^{(n)}(x, z_1, \ldots z_n, u_1, \ldots, u_n) = -\frac{2\beta_n \eta_0}{k_0} A^{(n)}(z_1, \ldots z_n, u_1, \ldots, u_n) e^{-ju_n D_n} \cos u_n (x - D_n) \tag{2.58}$$

where $D_n = D(z_n)$.

The condition for all the fictitious sheet current densities to cancel all the fictitious volume current densities is

$$M_y(x, z) + M(x, z) = 0 \tag{2.59}$$

where

$$M_y(x, z) = M_y^p(x, z; u_0) + \int_{z_1=-L}^{L} \int_{u_1=0}^{\infty} M_y^{(1)}(x, z, z_1, u_1; u_0) du_1 dz_1 + \cdots$$
$$+ \int_{\overline{z}_n} \int_{\overline{u}_n} M_y^{(n)}(x, z, z_1, \ldots, z_n, u_1, \ldots, u_n; u_0) d\overline{u}_n d\overline{z}_n + \cdots, \tag{2.60}$$

$$M_y^{(n)} = \frac{\partial E_z^{(n)}}{\partial x} - \frac{\partial E_x^{(n)}}{\partial z} - j\omega\mu_0 H_y^{(n)}, \tag{2.61}$$

and

$$M(x, z) = \int_{u=0}^{\infty} M_{sy}^{(1)}(x, z, u; u_0) du + \int_{z_1=-L}^{L} \int_{u_1=0}^{\infty} \int_{u=0}^{\infty} M_{sy}^{(2)}(x, z_1, z, u_1, u; u_0) du du_1 dz_1 + \cdots$$
$$+ \int_{\overline{z}_n} \int_{\overline{u}_n} \int_{u=0}^{\infty} M_{sy}^{(n+1)}(x, z_1, \ldots, z_n, z, u_1, \ldots, u_n, u; u_0) du d\overline{u}_n d\overline{z}_n + \cdots. \tag{2.62}$$

Substituting (2.60) and (2.62) into (2.59) results in the following integral equation for the order n

$$\int_{\overline{z}_n}\int_{\overline{u}_n}\left[M_y^{(n)}(x,z)+\int_{u=0}^{\infty}M_{sy}^{(n+1)}(x,z,u)du\right]d\overline{u}_n d\overline{z}_n = 0,$$
$$n = 0,1,2,\ldots \qquad (2.63)$$

where the variables $[z_1,\ldots,z_n,u_1,\ldots,u_n;u_0]$ have been suppressed, and $n=0$ refers to the primary field. Factoring out the integration over u in (2.62) and substituting into (2.59) gives

$$M_y(x,z)+\int_{u=0}^{\infty}K_M(x,z,u)du=0 \qquad (2.64)$$

where

$$K_M(x,z,u)=M_{sy}^{(1)}(x,z,u)+\int_{z_1=-L}^{L}\int_{u_1=0}^{\infty}M_{sy}^{(2)}(x,z_1,z,u_1,u)du_1dz_1+\cdots$$
$$+\int_{\overline{z}_n}\int_{\overline{u}_n}M_{sy}^{(n+1)}(x,z_1,\ldots,z_n,z,u_1,\ldots,u_n,u)d\overline{u}_n d\overline{z}_n+\cdots \qquad (2.65)$$

and u_0 has been suppressed. Since the modal sheet currents densities in (2.65) are all proportional to $\cos u(x-D)$, the integration over u in (2.64) can be removed using the orthogonality properties of the cosine function. Hence, multiplying (2.64) by $2/\pi\cos u'(x-D)$ and integrating with respect to x from D to ∞ gives

$$\frac{2}{\pi}\int_{D}^{\infty}M_y(x,z)\cos u'(x-D)dx=-\frac{2}{\pi}\int_{D}^{\infty}\int_{u=0}^{\infty}K_M(x,z,u)\cos u'(x-D)dudx. \qquad (2.66)$$

Referring to Maxwell's equation (2.46c), M_y is written as

$$M_y=\left(\frac{\partial E_z}{\partial x}-\frac{\partial E_x}{\partial z}\right)-j\omega\mu_0 H_y, \qquad (2.67)$$

and the left side of (2.66) now becomes

$$\frac{2}{\pi}\int_D^\infty M_y \cos u'(x-D)dx = \frac{2}{\pi}\int_D^\infty \frac{\partial E_z}{\partial x}\cos u'(x-D)dx$$
$$-\frac{2}{\pi}\int_D^\infty \frac{\partial E_x}{\partial z}\cos u'(x-D)dx - j\omega\mu_0\frac{2}{\pi}\int_D^\infty H_y \cos u'(x-D)dx. \quad (2.68)$$

Employing the relations

$$\frac{\partial E_x}{\partial z}\cos u'(x-D) = \frac{\partial}{\partial z}\left(E_x \cos u'(x-D)\right) - u'D'E_x \sin u'(x-D), \quad (2.69)$$

and

$$\frac{\partial}{\partial z}\int_{D(z)}^\infty E_x \cos u'(x-D)dx = \int_D^\infty \frac{\partial}{\partial z}\left(E_x \cos u'(x-D)\right)dx - E_x D' \cos u'(x-D)|_{x=D}\,, \quad (2.70)$$

and integration by parts, (2.68) becomes

$$\frac{2}{\pi}\int_D^\infty M_y \cos u'(x-D)dx = \frac{2}{\pi}u'\int_D^\infty [E_z + E_x D']\sin u'(x-D)dx - \frac{2}{\pi}\frac{\partial}{\partial z}\int_D^\infty E_x \cos u'(x-D)dx$$
$$-j\omega\mu_0\frac{2}{\pi}\int_D^\infty H_y \cos u'(x-D)dx - \frac{2}{\pi}\left[E_z + E_x D'\right]\cos u'(x-D)|_{x=D}\,. \quad (2.71)$$

The last term in (2.71) is recognized as the boundary condition for the tangential electric field (2.47b). The boundary term is not zero for the field as represented by (2.49) and (2.50); it is equal to the magnetic current induced on the metal surface. This induced magnetic surface current can be forced to be zero by adding a fictitious magnetic surface current 180° out of phase with the induced magnetic surface current. This fictitious magnetic surface current also needs to be cancelled by the sheet current density. The fictitious magnetic surface current density is absorbed into the volume current density in order to be cancelled by the sheet current densities. This is accomplished by representing the fictitious surface current density using the delta

function, i.e., (2.71) becomes

$$\frac{2}{\pi}\int_D^\infty M_y^{eff}\cos u'(x-D)dx = \frac{2}{\pi}u'\int_D^\infty [E_z + E_x D']\sin u'(x-D)dx$$
$$-\frac{2}{\pi}\frac{\partial}{\partial z}\int_D^\infty E_x\cos u'(x-D)dx - j\omega\mu_0\frac{2}{\pi}\int_D^\infty H_y\cos u'(x-D)dx, \quad (2.72)$$

where the effective fictitious current densities are

$$M_y^{eff} = M_y + [E_z + E_x D']\,\delta(x-D). \quad (2.73)$$

This procedure effectively forces the entire field in (2.49) and (2.50), and hence, each mode of the expansion to satisfy the boundary conditions. Effectively, this means that the field is expanded into the sum of primary field and higher order terms as in (2.49) and (2.50), such that each effective fictitious volume current density is canceled by the next higher order sheet current density. The primary volume current density is cancelled as follows

$$\frac{2}{\pi}u'\int_D^\infty [E_z^p + E_x^p D']\sin u'(x-D)dx - \frac{2}{\pi}\frac{\partial}{\partial z}\int_D^\infty E_x^p\cos u'(x-D)dx$$
$$-j\omega\mu_0\frac{2}{\pi}\int_D^\infty H_y^p\cos u'(x-D)dx = --\frac{2}{\pi}\int_D^\infty\int_0^\infty M_{sy}^{(1)}(x,z,u)\cos u'(x-D)dudx, \quad (2.74)$$

and since the fictitious surface current density is included in the volume current density, both are cancelled by the first-order sheet current density. After substituting the primary field expressions (2.52)–(2.54) into (2.74), this integral equation is solved by using the orthogonality properties of sines and cosines (E.6)–(E.8). If this is done, the modal amplitude becomes

$$A^{(1)}(z_1,u_1) = A_a^{(1)}(z_1,u_1) + A_b^{(1)}(z_1,u_1) \quad (2.75)$$

where

$$A_a^{(1)}(z_1,u_1) = \frac{E_0^i}{\pi\beta_1\eta_0}e^{-j\beta_0 z_1 + j(u_0+u_1)D_1}\left[\beta_0 - u_0 D_1'\right]D_1', \quad (2.76)$$

$$A_b^{(1)}(z_1,u_1) = -j\frac{E_0^i}{2\beta_1\eta_0}u_0 e^{-j\beta_0 z_1 + j(u_0+u_1)D_1}\left[2\beta_0 D_1' - 2u_0 D_1'^2 + jD_1''\right] \times \left\{\delta(u_1-u_0) - j\frac{2}{\pi}\frac{u_0\mathcal{P}}{u_0^2-u_1^2}\right\}, \quad (2.77)$$

and z and u have been replaced by z_1 and u_1, respectively. The next higher order modal amplitude is found by taking

$$\frac{2}{\pi}u'\int_D^\infty \left[E_z^{(1)} + E_x^{(1)}D'\right]\sin u'(x-D)dx - \frac{2}{\pi}\frac{\partial}{\partial z}\int_D^\infty E_x^{(1)}\cos u'(x-D)dx$$
$$- j\omega\mu_0\frac{2}{\pi}\int_D^\infty H_y^{(1)}\cos u'(x-D)dx = --\frac{2}{\pi}\int_D^\infty\int_0^\infty M_{sy}^{(2)}(x,z,u)\cos u'(x-D)dudx, \quad (2.78)$$

and solving for $A^{(2)}$ which is included in $M_{sy}^{(2)}$. The process can be generalized to order n.

The order "n" field is generated by superimposing the partial fields (2.55a,b,c) and/or (2.56a,b,c) over all $u_1,\ldots,u_n$ and all $z_1,\ldots,z_n$. The field must be divided into three regions as in the TE case. Hence, for $z > L$ (region 1)

$$H_{y1}^{(n)}(x,z) = \int_{z_1=-L}^{L}\cdots\int_{z_n=-L}^{L}\int_{u_1=0}^{\infty}\cdots\int_{u_n=0}^{\infty} A^{(n)}(z_1,\ldots,z_n,u_1,\ldots,u_n)e^{-j\beta_n(z-z_n)} \times \cos u_n x du_n\ldots du_1 dz_n\ldots dz_1, \quad (2.79)$$

for $-L \le z \le L$ (region 2)

$$H_{y2}^{(n)}(x,z) = \int_{z_1=-L}^{L}\cdots\int_{z_n=-L}^{z}\int_{u_1=0}^{\infty}\cdots\int_{u_n=0}^{\infty} A^{(n)}(z_1,\ldots,z_n,u_1,\ldots,u_n)e^{-j\beta_n(z-z_n)-ju_nD} \times \cos u_n(x-D)du_n\ldots du_1dz_n\ldots dz_1$$
$$+\int_{z_1=-L}^{L}\cdots\int_{z_n=z}^{L}\int_{u_1=0}^{\infty}\cdots\int_{u_n=0}^{\infty} A^{(n)}(z_1,\ldots,z_n,u_1,\ldots,u_n)e^{j\beta_n(z-z_n)-ju_nD} \times \cos u_n(x-D)du_n\ldots du_1dz_n\ldots dz_1, \quad (2.80)$$

and for $z \leq -L$ (region 3)

$$H_{y3}^{(n)}(x,z) = \int_{z_1=-L}^{L} \cdots \int_{z_n=-L}^{L} \int_{u_1=0}^{\infty} \cdots \int_{u_n=0}^{\infty} A^{(n)}(z_1,\ldots,z_n,u_1,\ldots,u_n) e^{j\beta_n(z-z_n)} \times \cos u_n x du_n \ldots du_1 dz_n \ldots dz_1. \quad (2.81)$$

The total field in each region is expressed in terms of its partial fields,

$$H_{yi}(x,z) = H_{yi}^{p}(x,z) + H_{yi}^{(1)}(x,z) + \cdots + H_{yi}^{(n)}(x,z) + \cdots . \quad (2.82)$$

where $i = 1, 2, 3$.

Consider only the first-order field in region 1 which is written as a sum of two pieces

$$H_{y1}^{(1)} = H_{y1}^{(1)a} + H_{y1}^{(1)b} \quad (2.83)$$

where,

$$H_{y1}^{(1)a} = \int_{-L}^{L} \int_{u_1=0}^{\infty} A_a^{(1)}(z_1,u_1) e^{-j\beta_1(z-z_1)} \cos u_1 x du_1 dz_1 \quad (2.84a)$$

$$= \frac{E_0^i}{\pi\eta_0} \int_{u_1=0}^{\infty} \int_{-L}^{L} \left[\beta_0 D_1' - u_0 D_1'^2\right] e^{j(\beta_1-\beta_0)z_1 + j(u_0+u_1)D_1} dz_1 \times e^{-j\beta_1 z} \cos u_1 x \frac{du_1}{\beta_1} \quad (2.84b)$$

and

$$H_{y1}^{(1)b} = \int_{-L}^{L} \int_{u_1=0}^{\infty} A_b^{(1)}(z_1,u_1) e^{-j\beta_1(z-z_1)} \cos u_1 x du_1 dz_1 \quad (2.85a)$$

$$= -j\frac{E_0^i}{2\eta_0} \int_{u_1=0}^{\infty} \int_{-L}^{L} u_0 \left[2\beta_0 D_1' - 2u_0 D_1'^2 + jD_1''\right] e^{j(\beta_1-\beta_0)z_1 + j(u_0+u_1)D_1} dz_1 \times e^{-j\beta_1 z} \cos u_1 x \left\{\delta(u_1-u_0) - j\frac{2}{\pi}\mathcal{P}\frac{u_0}{u_0^2-u_1^2}\right\} \frac{du_1}{\beta_1}. \quad (2.85b)$$

The integral over z_1 in $H_{y1}^{(1)a}$, which will be called I_a, is split into two pieces:

$$I_a = \int_{-L}^{L} \beta_0 D_1' e^{j(u_0+u_1)D_1} e^{-j(\beta_0-\beta_1)z_1} dz_1 - \int_{-L}^{L} u_0 D_1'^2 e^{j(u_0+u_1)D_1 - j(\beta_0-\beta_1)z_1} dz_1. \tag{2.86}$$

The first integral can be re-expressed by performing an integration by parts recognizing that

$$D_1' e^{j(u_0+u_1)D_1} = \frac{1}{j(u_0+u_1)} \frac{d}{dz_1} \left(e^{j(u_0+u_1)D_1} \right). \tag{2.87}$$

When the integration by parts is done, a term arises which is due to the endpoints of the integration region. This term can be rewritten as an integral in order to combine it with the other integrated terms by using the relation

$$e^{-j(\beta_0-\beta_1)L} - e^{j(\beta_0-\beta_1)L} = -j(\beta_0-\beta_1) \int_{-L}^{L} e^{-j(\beta_0-\beta_1)z_1} dz_1. \tag{2.88}$$

I_a is now rewritten as

$$I_a = \beta_0 \frac{(\beta_1-\beta_0)}{(u_1+u_0)} \int_{-L}^{L} \left\{ 1 - \left[1 + \frac{u_0(u_1+u_0)}{\beta_0(\beta_1-\beta_0)} D_1'^2 \right] e^{j(u_0+u_1)D_1} \right\} e^{-j(\beta_0-\beta_1)z_1} dz_1. \tag{2.89}$$

The integral over z_1 in $H_{y1}^{(1)b}$, which will be called I_b, has already been transformed by using integration by parts for the TE case in (2.23) and is rewritten here for convenience

$$\begin{aligned} I_b &= \int_{-L}^{L} \left[2\beta_0 D_1' - 2u_0 D_1'^2 + j D_1'' \right] e^{j(\beta_1-\beta_0)z_1 + j(u_0+u_1)D_1} dz_1 \\ &= (u_0-u_1) \int_{-L}^{L} \left\{ 1 - \left[1 + D_1'^2 \right] e^{j(u_0+u_1)D_1} \right\} e^{j(\beta_1-\beta_0)z_1} dz_1. \end{aligned} \tag{2.90}$$

Because the term $(u_0 - u_1)$ multiplies all of (2.85b), the delta function term can be dropped. Hence, the first-order field is expressed in terms of I_a and I_b:

$$H_{y1}^{(1)} = \frac{E_0^i}{\pi\eta_0} \int_{u_1=0}^{\infty} \left\{ I_a - \frac{u_0^2 \mathcal{P}}{u_0^2 - u_1^2} I_b \right\} e^{-j\beta_1 z} \cos u_1 x \frac{du_1}{\beta_1} \tag{2.91}$$

or

$$H_{y1}^{(1)} = \int_{u_1=0}^{\infty} K(u_1) e^{-j\beta_1 z} \cos u_1 x \frac{du_1}{\beta_1}, \tag{2.92}$$

where

$$K(u_1) = -\frac{E_0^i}{\pi\eta_0} \frac{k_0^2 - \beta_0\beta_1}{u_1 + u_0} \int_{-L}^{L} \left\{ 1 - \left[1 - \frac{u_0 u_1}{k_0^2 - \beta_0\beta_1} D_1'^2 \right] e^{j(u_0+u_1)D_1} \right\} e^{j(\beta_1-\beta_0)z_1} dz_1. \tag{2.93}$$

The integral in (2.92) is evaluated asymptotically to obtain the far field, as was done for the TE case, using the change of variables

$$\begin{aligned} u_0 &= k_0 \cos\phi_0 \quad , \quad \beta_0 = k_0 \sin\phi_0, \\ u_1 &= k_0 \cos w \quad , \quad \beta_1 = k_0 \sin w \\ x &= \rho\cos\phi \quad , \quad z = \rho \sin\phi, \end{aligned} \tag{2.94}$$

which refer to Figure 2.5, and (E.9)–(E.11) with I_e equal to zero, which produces:

$$H_{y1}^{(1)ff} \sim \frac{k_0}{\sqrt{2\pi}} G_0 B_0^i R^{TM}(\phi, \phi_0), \quad 0 \le \phi \le \pi/2, \tag{2.95}$$

where G_0 is the $2-D$ asymptotic Green's function defined in (2.29), the amplitude constant from the incident field part of (2.52) is

$$B_0^i = \frac{E_0^i}{2\eta_0}. \tag{2.96}$$

and the scatter pattern becomes

$$\begin{aligned} R^{TM}(\phi, \phi_0) = 2\frac{1 - \sin\phi \sin\phi_0}{\cos\phi + \cos\phi_0} \\ \times \int_{-L}^{L} \left\{ 1 - \left[1 - \frac{\cos\phi\cos\phi_0}{1 - \sin\phi\sin\phi_0} D_1'^2 \right] e^{jk_0 D_1(\cos\phi + \cos\phi_0)} \right\} \\ \times e^{-jk_o z_1(\sin\phi_0 - \sin\phi)} dz_1, \qquad 0 \le \phi \le \pi/2. \end{aligned} \tag{2.97}$$

Again, as in the TE case, the same procedure is performed for the case $z \le -L$ $(-\pi/2 \le \phi < 0)$ to obtain the same expression. The complete scattering pattern is now the same as (2.97) except it is valid over $-\pi/2 \le \phi \le \pi/2$.

CHAPTER 3

ACCURACY CHECK FOR THE FIRST ORDER FIELD

In the previous chapter, the first-order field was determined. This is an approximate solution which includes only two terms in the summation (2.45). All higher-order terms are small in the numerical comparisons made in Chapter 6 between the fictitious current first-order solution and the integral equation solution, which is considered to be a reference solution. This check on the accuracy of the solution is limited since it is a purely numerical check and is performed for a finite number of surface parameters. Calculation of higher order terms are prohibitively cumbersome, and to evaluate the overall accuracy would require evaluation of a number of additional higher order terms to ascertain that they are negligible. A simpler estimate of the validity of the first-order solution, however, can be obtained by finding the scattered fields radiated by the physical currents induced in the surface by the first-order approximation of the total solution.

In the first-order approximation, the total field above the rough surface is

$$\mathbf{E}^{tot} \simeq \mathbf{E}^{p} + \mathbf{E}^{(1)} = \mathbf{E}^{tot(1)}. \tag{3.1}$$

The current induced in the metal scatterer is given by

$$\mathbf{K}_{ind}^{tot(1)} = \hat{\mathbf{n}} \times \mathbf{H}^{tot(1)} \qquad on\ S_0, \tag{3.2}$$

where $\mathbf{H}^{tot(1)}$ is found from Maxwell's equation

$$\mathbf{H}^{tot(1)} = -\frac{1}{j\omega\mu_0} \nabla \times \mathbf{E}^{tot(1)} \tag{3.3}$$

and S_0 is the entire metal surface $x = D(z)$ over $-\infty < z < \infty$, with $D(z) = 0$ for $|z| > L$. The scattered field radiated by $\mathbf{K}_{ind}^{tot(1)}$ is found from [5]

$$\mathbf{E}_{ind}^{s} = -j\omega\mu_0 \int_{S_0} G_f^{2-D} \mathbf{K}_{ind}^{tot(1)} dS_0, \tag{3.4}$$

where G_f^{2-D} is the two-dimensional free-space Green's function

$$G_f^{2-D} = -\frac{j}{4} H_0^{(2)} \left(k_0 \left| \boldsymbol{\rho} - \boldsymbol{\rho}_0 \right| \right). \tag{3.5}$$

The total first order field is now expressed as

$$\mathbf{E}^{tot(1)} = \mathbf{E}^s_{ind} + \mathbf{E}_{vol} + \mathbf{E}^p, \tag{3.6}$$

which includes the field $\mathbf{E}_{vol}$ due to the first-order volume current density $\mathbf{J}^{(1)}$. Equating (3.1) and (3.6) gives

$$\mathbf{E}^{(1)} - \mathbf{E}^s_{ind} = \mathbf{E}_{vol}. \tag{3.7}$$

This shows that the field radiated by the volume current is a measure of the accuracy of the first-order solution. Note that if $\mathbf{E}^{(1)} = \mathbf{E}^s_{ind}$ then $\mathbf{E}_{vol}$ is zero, i.e., $\mathbf{J}^{(1)}$ is zero and $\mathbf{E}^{(1)}$ would be the exact scattered field.

It is now necessary to determine the fields radiated by the induced current densities in the metal and the field radiated by the volume current density. Returning to (3.2) for the TE case, it follows that

$$K_y^{tot} = - \left. \frac{[H_z^{tot} + D' H_x^{tot}]}{\sqrt{1 + D'^2}} \right|_{x=D}, \tag{3.8}$$

where $\widehat{\mathbf{n}}$ is given by

$$\widehat{\mathbf{n}} = \frac{[\widehat{\mathbf{x}} - D'\widehat{\mathbf{z}}]}{\sqrt{1 + D'^2}}. \tag{3.9}$$

Since the total field can be written as a sum of incident, reflected and scattered fields the total induced current density (over the entire surface for $z \in (-\infty, +\infty)$) can be expressed as the sum of incident, reflected and scattered current densities K_y^i, K_y^r and K_y^s. Recall that the incident and reflected fields are given in (2.7). For the region $|z| > L$, the reflected field reduces to the form of the field reflected from an infinite flat plate, namely,

$$E_y^r(x, z) = -\frac{E_0^i}{2j} e^{-j\beta_0 z - j u_0 x}, \quad |z| > L \tag{3.10}$$

whereas in the middle region, $|z| \leq L$, the reflected field is adjusted to the local elevation, i.e.,

$$E_y^R(x,z) = -\frac{E_0^i}{2j} e^{-j\beta_0 z - ju_0 x - j2u_0 D}, \quad |z| \leq L. \tag{3.11}$$

The induced surface current density is expressed in the different regions as

$$K_y^{tot} = \begin{cases} K_y^i + K_y^r + K_y^s, & |z| > L \\ K_y^i + K_y^R + K_y^s, & |z| \leq L \end{cases}, \tag{3.12}$$

with K_y^r due to E_y^r, and K_y^R due to E_y^R. In order to examine only the scattered field, the surface current density $K_y^i + K_y^R$ over a length $2L$ is added to and subtracted from the total surface current density (see Figure 3.1). The resultant current

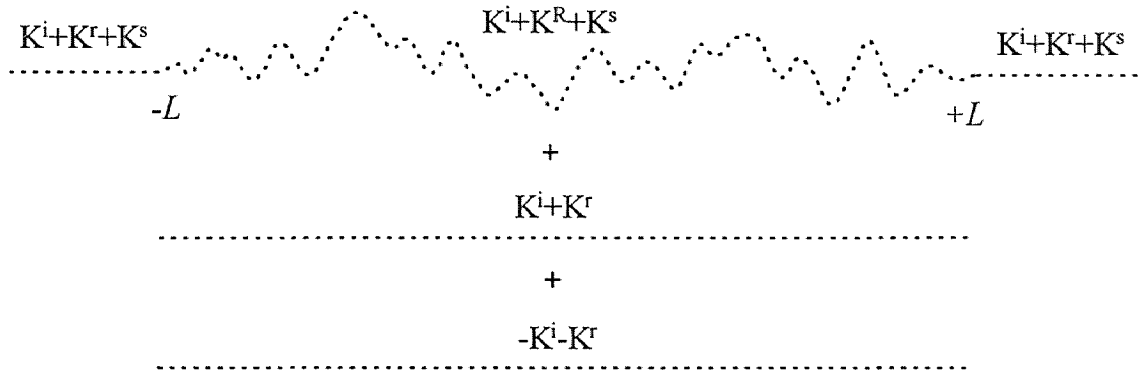

Figure 3.1 Induced surface current densities.

density is then split into five pieces as shown in Figure 3.2, each of which will now be examined independently. Part E of the total induced current density (see Figure 3.2) consists of the current density that is induced in an infinite flat metal surface irradiated by an incident plane wave. Since this current density gives no contribution to the scattered field, this field constituent is not included in the final result.

To find the contributions to the scattered field from the remaining current densities, it is convenient to find the magnetic vector potential $\mathbf{A}(\mathbf{r})$ from which the electric field is readily obtained. Since all current distributions flow in the y-direction,

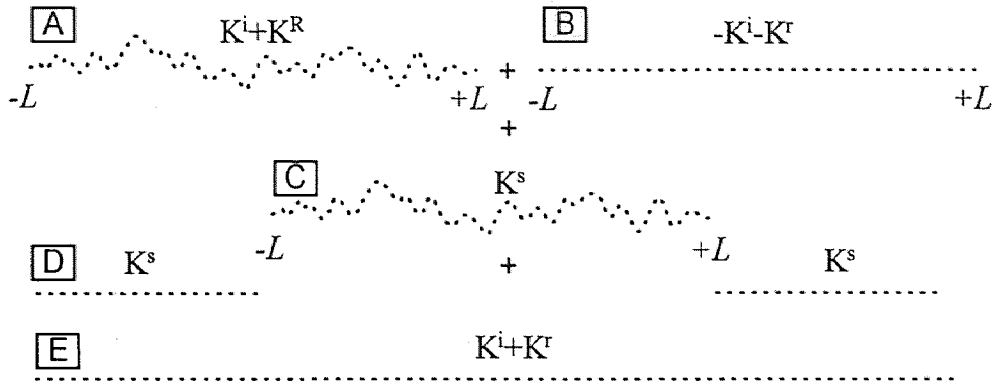

Figure 3.2 Partitioning the total surface current density into five pieces which are designated A: $K^i + K^R$ over the rough surface $|z| \leq L$; B: $-K^i - K^r$ over the smooth surface $|z| \leq L$; C: K^s over the rough surface $|z| \leq L$; D: K^s over the smooth surface $|z| > L$; and E: $K^i + K^r$ over the infinite smooth surface, $-\infty < z < \infty$.

only the y component of the magnetic vector potential exists; it takes the form [5]

$$A_y(x,z) = -j\frac{\mu}{4}\int_{-L}^{L} K_y(z_0) H_0^{(2)}\left(k_0\left|\boldsymbol{\rho}-\boldsymbol{\rho}_0\right|\right)\sqrt{1+D_0'^2}\,dz_0, \tag{3.13}$$

where

$$\left|\boldsymbol{\rho}-\boldsymbol{\rho}_0\right| = \sqrt{x^2-(z-z_0)^2}, \tag{3.14}$$

and $H_0^{(2)}$ is the zero-order Hankel function of the second kind. The associated electric field also has only a y component, it is given by

$$E_y(x,z) = -j\omega A_y. \tag{3.15}$$

Returning to the partitioned current densities in Figure 3.2, consider Part A which involves $K^i + K^R$ on the rough surface in $|z| \leq L$. The induced current density for Part A is found by using (2.8)–(2.9) and the corresponding portion of the total induced current density due to the incident and reflected fields. Hence,

$$K_y^A = \frac{\left[1+D_0'^2\right]}{\sqrt{1+D_0'^2}}\frac{E_0^i u_0}{jk_0\eta_0}e^{-j\beta_0 z_0 + ju_0 D_0}. \tag{3.16}$$

Using (3.13) and (3.15), the scattered field due to this current density is

$$E_y^A(x,z) = \frac{j}{4} E_0^i u_0 \int_{-L}^{L} \left[1 + D_0'^2\right] e^{-j\beta_0 z_0 + j u_0 D_0} H_0^{(2)}\left(k_0 \left|\rho - \rho_0\right|\right) dz_0. \tag{3.17}$$

The current density of Part B gives the field scattered by a finite flat metal strip of width $2L$. The induced current on this finite metal strip is $K_y^B = K_y^i - K_y^r$, which is explicitly given by

$$K_y^B = -\frac{E_0^i u_0}{j k_0 \eta_0} e^{-j\beta_0 z_0}. \tag{3.18}$$

The scattered field due to K_y^B is

$$E_y^B(x,z) = -j\frac{E_0^i u_0}{4} \int_{-L}^{L} e^{-j\beta_0 z_0} H_0^{(2)}\left(k_0 \left|\rho - \rho_0\right|\right) dz_0. \tag{3.19}$$

Assume that the scattered electric field is given by the first-order field approximation in (2.18)–(2.20). The induced current density that gives rise to this scattered field is obtained from the first-order magnetic field which is found by using (2.18)–(2.20) in the Maxwell equation similar to (3.3) and by substituting this magnetic field into (3.8). However, when the total scattered field is approximated by the first-order field, a first-order volume current density (2.32) is left over, as shown in Figure 3.3. This volume current density radiates a field which should be small compared to the total first-order field for the first-order field to be an accurate approximation to the total scattered field. The field due to this first-order volume current density is the remainder term in the series solution (2.45). Since the scattered field is approximated by the first-order field, the induced current density is $K_y^s = K_y^{(1)}$. Hence, the surface current density K_y^C,which is used for part C, is found by using (2.19) to be

$$K_y^C = K_y^s = -\frac{E_0^i u_0}{2k_0\eta_0} \frac{\left[1 + D_0'^2\right]}{\sqrt{1 + D_0'^2}} \int_{-L}^{L} \int_{0}^{\infty} \left[2\beta_0 D_1' - 2u_0 D_1'^2 + j D_1''\right]$$
$$\times e^{j[(u_1+u_0)D_1 - \beta_0 z_1 - \beta_1 |z_0 - z_1| - u_1 D_0]} \zeta(u_1) \frac{u_1}{\beta_1} du_1 dz_1, \tag{3.20}$$

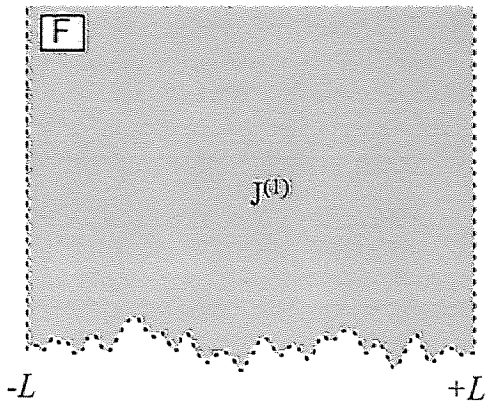

Figure 3.3 The remaining volume current density.

where

$$\zeta(u_1) = \delta(u_1 - u_0) + j\frac{2}{\pi}\mathcal{P}\left\{\frac{u_1}{(u_1^2 - u_0^2)}\right\}. \tag{3.21}$$

Hence, using (3.13) and (3.15), the radiated field for Part C becomes

$$E_y^C(x,z) = \frac{E_0^i u_0}{8}\int_{-L}^{L}\int_{-L}^{L}\int_{0}^{\infty}\left[2\beta_0 D_1' - 2u_0 D_1'^2 + jD_1''\right] \times e^{j[(u_1+u_0)D_1 - \beta_0 z_1 - \beta_1|z_0 - z_1| - u_1 D_0]}\zeta(u_1)\frac{u_1}{\beta_1}du_1 dz_1 \times \left[1 + D_0'^2\right] H_0^{(2)}(k_0|\boldsymbol{\rho} - \boldsymbol{\rho}_0|)\, dz_0. \tag{3.22}$$

To find the radiated field from Part D, K_y^s on the smooth surface $x = 0$ in $|z| > L$ is used. The field expressions (2.18) and (2.20) then give

$$E_y^D(x,z) = \frac{E_0^i u_0}{8}\int_{-L}^{L}\int_{0}^{\infty}\left[2\beta_0 D_1' - 2u_0 D_1'^2 + jD_1''\right] \times e^{j[(u_1+u_0)D_1 - \beta_0 z_1 - u_1 D_0]}\zeta(u_1)\frac{u_1}{\beta_1} \times \left(\int_{-\infty}^{-L} + \int_{L}^{\infty}\right) e^{-j\beta_1|z_0 - z_1|}H_0^{(2)}(k_0|\boldsymbol{\rho} - \boldsymbol{\rho}_0|)\, dz_0 du_1 dz_1. \tag{3.23}$$

The scattered field due to the volume current density is found using the radiation integral [5]:

$$E_y^F(x,z) = -\frac{\omega\mu_0}{4}\int_{-L}^{L}\int_{D_0}^{\infty} J_y^{(1)}(x_0,z_0)H_0^{(2)}\left(k_0\sqrt{(x-x_0)^2+(z-z_0)^2}\right)dx_0dz_0. \tag{3.24}$$

Using the volume current density (2.32) and making the change of variable $x_0 \rightarrow x_0 - D_0$, the scattered field becomes

$$\begin{aligned} E_y^F(x,z) = j\frac{u_0E_0^i}{8}\int_{x_0=0}^{\infty}\int_{z_1=-L}^{L}\int_{z_0=-L}^{L}\int_{u_1=0}^{\infty}&\left[\operatorname{sgn}(z_0-z_1)\,2\beta_1D_0' + 2u_1D_0'^2 + jD_0''\right] \\ &\times\left[2\beta_0D_1' + 2u_0D_1'^2 + jD_1''\right]\exp\left[(u_1+u_0)D_1 - \beta_0|z_0-z_1| - u_1D_0\right] \\ &\times\zeta(u_1)\frac{u_1}{\beta_1}du_1dz_1H_0^{(2)}\left(k_0\overline{R}_V\right)e^{ju_1x_0}dx_0dz_0, \end{aligned} \tag{3.25}$$

where

$$\overline{R}_V = \sqrt{(x-x_0-D_0)^2+(z-z_0)^2}. \tag{3.26}$$

In the far field, the Hankel functions in the above expressions are asymptotically expanded and the parallel ray approximation is used, as is done in Appendix C, to give the following relations

$$H_0^{(2)}\left(k_0\sqrt{x^2+(z-z_0)^2}\right) \sim \sqrt{\frac{2}{\pi}}\frac{e^{-j[k_0\rho-\pi/4]}}{\sqrt{k_0\rho}}e^{jk_0z_0\sin\phi}, \tag{3.27a}$$

$$H_0^{(2)}\left(k_0\sqrt{(x-a)^2+(z-z_0)^2}\right) \sim \sqrt{\frac{2}{\pi}}\frac{e^{-j[k_0\rho-\pi/4]}}{\sqrt{k_0\rho}}e^{jk_0[z_0\sin\phi+a\cos\phi]}, \tag{3.27b}$$

Substituting these relations into all the expressions for the scattered fields, Parts A–D and F, adding them and performing some very involved manipulations returns the expression for the first-order scattered field, whose scatter pattern is

$$R^{TE}(\phi,\phi_0) = \frac{2\cos\phi\cos\phi_0}{\cos\phi+\cos\phi_0}\int_{-L}^{L}\left\{1-\left[1+D_1'^2\right]e^{jk_0D_1(\cos\phi+\cos\phi_0)}\right\}e^{jk_0z_1(\sin\phi-\sin\phi_0)}dz_1. \tag{3.28}$$

Note that these evaluations show that (3.7) is satisfied and provides a check on the scatter pattern (2.31) for the first-order scattered field $E_y^{(1)}$.

In order to compare the magnitude of the field radiated by the volume current density E_y^F, to the total first-order field $E_y^{(1)}$, the scatter pattern for (3.25) is obtained in the form

$$R_V^{TE} = 2j\frac{u_0}{k_0}\int_{-L}^{L}\int_{\Omega}\left[2\beta_0 D_0' - 2u_0 D_0'^2 + jD_0''\right]\xi_1 \times\left\{\frac{1-e^{-j(u_1-k_0\cos\phi)D_0}}{u_1^2-k_0^2\cos^2\phi}+\frac{j}{2\beta}\int_{-L}^{L}\left[1-\left(1+D_1'^2\right)e^{-j(u_1-k_0\cos\phi)D_1}\right]\xi_2 dz_1\right\} \times\frac{u_1^2}{u_1^2-u_0^2}du_1 dz_0, \quad (3.29)$$

where

$$\xi_1 = \exp\left[-j\beta_0 z_0 + j\left(u_1+u_0\right)D_0 + jk_0 z_0\sin\phi\right], \quad (3.30a)$$

$$\xi_2 = \exp\left[-j\beta_1\left|z_1-z_0\right| + jk_0\left(z_1-z_0\right)\sin\phi\right] \quad (3.30b)$$

and the integration path Ω is defined in Figure 2.4. Many attempts were made to estimate the relative magnitude of R_V^{TE} in comparison to R^{TE}. One way is to perform a numerical integration using the Monte Carlo procedure. Having this capability will permit the determination of the surface parameters for which the fictitious current full wave method will give accurate results. Since the numerical results for the fictitious current full wave method agree very well with the integral equation reference solution (see Chapter 6), the evaluation mentioned above was deemed unnecessary at this point, but will be performed in future works.

CHAPTER 4

ANALYTIC COMPARISON TO OTHER METHODS

Even though rough surface scattering theories are usually used to predict scattering from random surface profiles, it is instructive to first examine the scattered field expressions found using various surface scattering theories with an arbitrary deterministic surface profile. The standard methods for computing the field scattered by rough surfaces are the Kirchhoff method, the first order perturbation method and Bahar's Full Wave method. The Kirchhoff theory is valid for high frequencies (radii of curvature large with respect to wavelength) and small slopes [6]. The Perturbation theory is valid for surfaces with small heights and slopes [7]. Bahar's original full wave method is valid for small slopes. Thorsos and Winebrenner [8] have shown that Bahar's Modified Full Wave theory (see Appendix B) does not reduce to the Perturbation result in the limit of small heights and small slopes and is approximately equivalent to the Kirchhoff theory for all parameters that they examined; Bahar's Modified Full Wave theory is not included in this discussion. The expressions for the scattered field of all four methods have been derived in the appendices; the first three mentioned above are rewritten here for convenience.

Bahar's original full wave method for the TE case (see Appendix B) gives a scatter pattern

$$R_B^{TE}(\phi,\phi_0) = \frac{2\cos\phi\cos\phi_0}{\cos\phi+\cos\phi_0}\int_{-L}^{L}\left\{1-e^{jk_0D_0(\cos\phi+\cos\phi_0)}\right\}e^{jk_0z_0(\sin\phi-\sin\phi_0)}dz_0 \tag{4.31}$$

and for the TM case

$$R_B^{TM} = \frac{2\left(1-\sin\phi\sin\phi_0\right)}{\cos\phi+\cos\phi_0}\int_{-L}^{L}\left\{1-e^{jk_0D_0(\cos\phi+\cos\phi_0)}\right\}e^{jk_0z_0(\sin\phi-\sin\phi_0)}dz_0. \tag{4.32}$$

The Kirchhoff method (see Appendix C) gives a scatter pattern

$$R_K^{TE} = -R_K^{TM} = \frac{1+\cos(\phi+\phi_0)}{\cos\phi+\cos\phi_0}\int_{-L}^{L}\left\{1-e^{jk_0D_0(\cos\phi+\cos\phi_0)}\right\}e^{jk_0z_0(\sin\phi-\sin\phi_0)}dz_0. \tag{4.33}$$

The TE scatter pattern for the first-order Perturbation theory (see Appendix D) is:

$$R_P^{TE} = -2jk_0\cos\phi\cos\phi_0\int_{-L}^{L}D_0e^{jk_0z_0(\sin\phi-\sin\phi_0)}dz_0, \tag{4.34}$$

and for the TM case is:

$$R_P^{TM} = 2jk_0(1-\sin\phi\sin\phi_0)\int_{-L}^{L}D_0e^{jk_0z_0(\sin\phi-\sin\phi_0)}dz_0. \tag{4.35}$$

The full wave theory developed in this dissertation, referred to as the new method, gives a scatter pattern for the TE case of the form:

$$R^{TE}(\phi,\phi_0) = \frac{2\cos\phi\cos\phi_0}{\cos\phi+\cos\phi_0}\int_{-L}^{L}\left\{1-\left[1+D_0'^2\right]e^{jk_0D_0(\cos\phi+\cos\phi_0)}\right\}e^{jk_0z_0(\sin\phi-\sin\phi_0)}dz_0 \tag{4.36}$$

and for the TM case the form:

$$R^{TM} = \frac{2(1-\sin\phi\sin\phi_0)}{\cos\phi+\cos\phi_0}\int_{-L}^{L}\left\{1-\left[1-\frac{\cos\phi\cos\phi_0}{1-\sin\phi\sin\phi_0}D_0'^2\right]e^{jk_0D_0(\cos\phi+\cos\phi_0)}\right\} \times e^{jk_0z_0(\sin\phi-\sin\phi_0)}dz_0. \tag{4.37}$$

It should be noted that for small slopes, i.e., $D_0' \ll 1$, the new full wave method reduces exactly to Bahar's original full wave method.

It is easily seen that all methods are polarization dependent except the Kirchhoff method. This is a shortcoming of the Kirchhoff method, since it is widely known that electromagnetic waves depolarize when scattered by a rough surface [9]. Also, the Kirchhoff solution for the TE case does not satisfy the boundary conditions, i.e., $R_K^{TE} \neq 0$ for $\phi = \pm\pi/2$. It should be noted that when the TE

and TM cases for the new full wave method are added together, they produce the Kirchhoff approximation, as does Bahar's method:

$$R_K^{TE} = \frac{R^{TE} + R^{TM}}{2} = \frac{R_B^{TE} + R_B^{TM}}{2}. \tag{4.38}$$

The assumptions for the perturbation theory to be valid are

$$k_0 D_0 \ll 1 \quad ; \quad D_0' \ll 1. \tag{4.39}$$

If these assumptions are taken then the exponential involving D_0 in the new full wave solution (4.36) and (4.37) can be expanded in a Taylor series about $D_0 = 0$ as follows

$$e^{jk_0 D_0(\cos\phi + \cos\phi_0)} = 1 + jk_0 D_0 (\cos\phi + \cos\phi_0) + \cdots . \tag{4.40}$$

If only the first two terms in (4.40) are retained and the term $D_0'^2$ in either (4.36) or (4.37) is ignored, since it is very small compared to unity, then the new full wave method reduces to the perturbation result in its region of validity. The same procedure can be performed on Bahar's original solution with the same result.

Since the new full wave method and Bahar's original full wave method both reduce to the Kirchhoff and first order perturbation solutions in their limited regions of validity, these two full wave solutions will be compared over broader parameter ranges. This will be accomplished by comparing the two full wave theories to the "exact" integral equation method[1] of Eric I. Thorsos in Chapter 6.

[1]The solutions are exact in the sense that no approximations are made in the scattering physics, i.e., shadowing and multiple scattering effects are taken into account.

CHAPTER 5

STATISTICAL ANALYSIS

Rough surface scattering theories are useful for predicting the scattered field from many different types of surfaces, such as periodic, arbitrarily specified deterministic, or random surfaces. The most numerous types being random surfaces since any scattering application involving natural surfaces requires a statistical description of the surface. These naturally occurring rough surfaces are described using the theory of stationary random processes (see Appendix A). The most commonly used statistical description for these surfaces is the one where each point on the surface is taken to be a random variable which has a Gaussian probability density function and all points on the surface are related by a Gaussian correlation function. Therefore, this chapter, will discuss the average diffuse radar cross section (RCS) for surfaces with Gaussian distributed heights and slopes and with Gaussian correlation function (see [10] p. 221 for a discussion of the use of non-Gaussian distributions in rough surface scattering).

The average diffuse radar cross section is defined [10] as

$$\widetilde{\varrho}_d = \langle RR^* \rangle - \langle R \rangle \langle R \rangle^* \tag{5.1}$$

where the brackets $\langle \quad \rangle$ denote the ensemble average and R is the scatter pattern discussed in Chapter 2. Bahar's original full wave method (with the integrated term present as discussed in Appendix B) and the Kirchhoff theory have the same form for the scatter pattern given by

$$R = S(\phi, \phi_0) \int_{-L}^{L} \left\{ 1 - e^{j\overline{v}_x D_0} \right\} e^{-j\overline{v}_z z_0} dz_0, \tag{5.2}$$

where $\overline{v}_x = k_0 (\cos\phi + \cos\phi_0)$ and $\overline{v}_z = k_0 (\sin\phi_0 - \sin\phi)$; the only difference between the two is the function $S(\phi, \phi_0)$.

To simplify the analysis, R is split into two pieces, one containing the random variable (RV) D_0 and one without the RV, i.e.,

$$R = R_a + R_b, \tag{5.3}$$

where

$$R_a = -S(\phi, \phi_0) \int_{-L}^{L} e^{j\overline{v}_x D_0} e^{-j\overline{v}_z z_0} dz_0 \tag{5.4}$$

and

$$R_b = S(\phi, \phi_0) \int_{-L}^{L} e^{-j\overline{v}_z z_0} dz_0. \tag{5.5}$$

The diffuse RCS now becomes

$$\widetilde{\varrho}_d = \langle (R_a + R_b)(R_a^* + R_b^*) \rangle - \langle R_a + R_b \rangle \langle R_a + R_b \rangle^*. \tag{5.6}$$

The first term is expanded as follows

$$\langle (R_a + R_b)(R_a^* + R_b^*) \rangle = \langle R_a R_a^* \rangle + R_b \langle R_a^* \rangle + R_b^* \langle R_a \rangle + |R_b|^2, \tag{5.7}$$

and the second term as

$$\langle R_a + R_b \rangle \langle R_a + R_b \rangle^* = \langle R_a \rangle \langle R_a \rangle^* + R_b \langle R_a \rangle^* + R_b^* \langle R_a \rangle + |R_b|^2. \tag{5.8}$$

Subtracting the two gives

$$\widetilde{\varrho}_d = \langle R_a R_a^* \rangle - \langle R_a \rangle \langle R_a \rangle^* + R_b \left[\langle R_a^* \rangle - \langle R_a \rangle^* \right]. \tag{5.9}$$

Averaging R_a over the ensemble of realizations of D_0 results in

$$\langle R_a \rangle = -S(\phi, \phi_0) \int_{-L}^{L} \left\langle e^{j\overline{v}_x D_0} \right\rangle e^{-j\overline{v}_z z_0} dz_0 \tag{5.10}$$

using (A.51), which is

$$\chi(\overline{v}_x) \equiv \left\langle e^{j\overline{v}_x D_0} \right\rangle = e^{-\sigma^2 \overline{v}_x^2 / 2}. \tag{5.11}$$

where σ is the RMS height of the surface. Evaluation of (5.10) gives

$$\langle R_a \rangle = -2LS(\phi, \phi_0) e^{-\sigma^2 \overline{v}_x^2/2} \operatorname{sinc}(\overline{v}_z L), \tag{5.12}$$

the sinc function is defined as

$$\operatorname{sinc} x = \frac{\sin x}{x}. \tag{5.13}$$

The ensemble average of R_a^* is evaluated to give the same result as above, which when substituted into (5.9) results in

$$\widetilde{\varrho}_d = \langle R_a R_a^* \rangle - \langle R_a \rangle \langle R_a \rangle^*. \tag{5.14}$$

This expression is independent of the term R_b which does not contain an RV. A closed form expression for this average can be found by following the procedure outlined in [9] as follows. Referring to (A.52) gives the relation

$$\chi_2(\overline{v}_x, -\overline{v}_x) \equiv \left\langle e^{j\overline{v}_x(D_0 - D_1)} \right\rangle = e^{-\overline{v}_x^2 \sigma^2 (1 - r(\tau))}, \tag{5.15}$$

with $r(\tau)$, the correlation coefficient, taken as

$$r(\tau) = e^{-\tau^2/l^2}, \tag{5.16}$$

with correlation length l, $\tau = z_0 - z_1$ and $D_1 = D(z_1)$. The first term in the RCS (5.14) can now be rewritten as

$$\langle R_a R_a^* \rangle = |S(\phi, \phi_0)|^2 \int_{-L}^{L} \int_{-L}^{L} \left\langle e^{j\overline{v}_x(D_0 - D_1)} \right\rangle e^{-j\overline{v}_z(z_0 - z_1)} dz_0 dz_1 \tag{5.17}$$

$$= |S(\phi, \phi_0)|^2 \int_{-L}^{L} \int_{-L}^{L} \chi_2(\overline{v}_x, -\overline{v}_x) e^{-j\overline{v}_z \tau} dz_0 dz_1. \tag{5.18}$$

The diffuse RCS now becomes

$$\widetilde{\varrho}_d = |S(\phi, \phi_0)|^2 \int_{-L}^{L} \int_{-L}^{L} \left[\chi_2(\overline{v}_x, -\overline{v}_x) - \chi(\overline{v}_x) \chi(\overline{v}_x)^* \right] e^{-j\overline{v}_z \tau} dz_0 dz_1. \tag{5.19}$$

The correlation coefficient $r(\tau)$ measures how two points on a surface are correlated when they are separated by a distance τ. For $\tau = 0$, the two points are coincident and the correlation coefficient has its maximum value of unity (fully correlated). As the distance between the two points becomes very great, $\tau \rightarrow \infty$, the correlation coefficient reaches its minimum of zero, i.e., the two points are not correlated at all (independent). Between the two extremes of $\tau = 0$ and $\tau \rightarrow \infty$, the correlation coefficient decreases monotonically and reduces to a value of e^{-1} at one correlation length, $\tau = l$. In order for the surface to be truly rough, the correlation length l must be much smaller than the surface length $2L$, otherwise the rough surface would just have one or two irregularities. Thus, it is assumed

$$l \ll L. \tag{5.20}$$

This implies that the correlation coefficient is non-zero only in a small region about $\tau = 0$. If D_0 and D_1 are independent (which is true for $\tau = 0$), the second characteristic function becomes (see Appendix A)

$$\chi_2\left(\overline{v}_x, -\overline{v}_x\right) = \chi(\overline{v}_x)\chi(\overline{v}_x)^*, \tag{5.21}$$

and the integrand in (5.19) is non-zero only in the small region around $\tau = 0$.

The average diffuse RCS (5.19) is now simplified by transforming to a sum and difference coordinate system, $z_0 + z_1$ and $z_0 - z_1$. Since the integrand is only a function of the difference coordinate, the integration over the sum coordinate yields the surface length $2L$. To simplify the integration over the difference coordinate, it must be remembered that the integrand in (5.19) is non-zero only for a small region around $\tau = 0$ and hence the term of the form

$$\int_{-2L}^{2L} \left[\chi_2\left(\overline{v}_x, -\overline{v}_x\right) - \chi(\overline{v}_x)\chi(\overline{v}_x)^*\right] e^{-j\overline{v}_z\tau}\tau d\tau, \tag{5.22}$$

which arises from the transformation can be neglected. Therefore, the diffuse RCS is approximately given by

$$\widetilde{\varrho}_d = 2L\left|S(\phi,\phi_0)\right|^2 \int_{-2L}^{2L} \left[\chi_2\left(\overline{v}_x,-\overline{v}_x\right)-\chi(\overline{v}_x)\chi(\overline{v}_x)^*\right] e^{-j\overline{v}_z\tau}d\tau. \tag{5.23}$$

The average diffuse RCS is now normalized for surface length $2L$ and free space wavenumber k_0, i.e., $\varrho_d = k_0\widetilde{\varrho}_d/2L$, and the limits of integration are taken to infinity since the major contribution comes only from the neighborhood of $\tau = 0$, i.e.,

$$\varrho_d = k_0\left|S(\phi,\phi_0)\right|^2 \int_{-\infty}^{\infty} \left[\chi_2\left(\overline{v}_x,-\overline{v}_x\right)-\chi(\overline{v}_x)\chi(\overline{v}_x)^*\right] e^{-j\overline{v}_z\tau}d\tau. \tag{5.24}$$

This represents the radar cross section per surface length. In order to evaluate (5.24), $\chi_2\left(v_x,-v_x\right)$ is expanded in a Taylor series, which gives

$$\chi_2\left(\overline{v}_x,-\overline{v}_x\right)-\chi(\overline{v}_x)\chi(\overline{v}_x)^* = e^{-\sigma^2\overline{v}_x^2}\sum_{n=1}^{\infty}\frac{\sigma^{2n}\overline{v}_x^{2n}}{n!}e^{-n\tau^2/l^2}. \tag{5.25}$$

Using the integral [11]

$$\int_{-\infty}^{\infty} e^{-n\tau^2/l^2}\cos\overline{v}_z\tau d\tau = l\sqrt{\frac{\pi}{n}}e^{-\overline{v}_z^2l^2/4n}, \tag{5.26}$$

the average diffuse RCS for both the Kirchhoff and Bahar's original full wave method, assuming $l \ll L$, becomes

$$\varrho_d = (k_0l)\sqrt{\pi}\left|S(\phi,\phi_0)\right|^2 e^{-(k_0\sigma)^2v_x^2}\sum_{n=1}^{\infty}\frac{(k_0\sigma)^{2n}v_x^{2n}}{n!\sqrt{n}}e^{-v_z^2(k_0l)^2/4n}, \tag{5.27}$$

where $v_x = \overline{v}_x/k_0 = \cos\phi+\cos\phi_0$ and $v_z = \overline{v}_z/k_0 = \sin\phi_0-\sin\phi$. If the diffuse radar cross section for the Kirchhoff method is desired, the coefficient $S(\phi,\phi_0)$ becomes (see Appendix C)

$$S(\phi,\phi_0) = S_K(\phi,\phi_0) = \frac{1+\cos\left(\phi+\phi_0\right)}{\cos\phi+\cos\phi_0}. \tag{5.28}$$

If the diffuse RCS for Bahar's full wave method is desired, $S(\phi, \phi_0)$ is (see Appendix B)

$$S(\phi, \phi_0) = S_B^{TE}(\phi, \phi_0) = \frac{2\cos\phi\cos\phi_0}{\cos\phi + \cos\phi_0} \tag{5.29}$$

for the TE case, and

$$S(\phi, \phi_0) = S_B^{TM}(\phi, \phi_0) = \frac{2\left(1 - \sin\phi\sin\phi_0\right)}{\cos\phi + \cos\phi_0} \tag{5.30}$$

for the TM case.

For comparison to the other statistical results, the statistical analysis for the fictitious current full wave case will be included, even though Monte Carlo results are used for the numerical comparisons. The scatter pattern for the fictitious current full wave method is

$$R_F = R_{Fa} + R_{Fb}, \tag{5.31}$$

where

$$R_{Fa} = S(\phi, \phi_0) \int_{-L}^{L} \left[1 + S_N(\phi, \phi_0) D_0'^2\right] e^{j\overline{v}_x D_0} e^{-j\overline{v}_z z_0} dz_0 \tag{5.32}$$

and

$$R_{Fb} = S(\phi, \phi_0) \int_{-L}^{L} e^{-j\overline{v}_z z_0} dz_0, \tag{5.33}$$

where S and S_N are arbitrary functions of ϕ and ϕ_0. The diffuse RCS for the new full wave method is defined as

$$\widetilde{\varrho}_d^F = \langle R_F R_F^* \rangle - \langle R_F \rangle \langle R_F \rangle^* . \tag{5.34}$$

Since the term R_{Fb} does not contain a random variable, the same argument used to obtain (5.14) is used to give

$$\widetilde{\varrho}_d^F = \langle R_{Fa} R_{Fa}^* \rangle - \langle R_{Fa} \rangle \langle R_{Fa} \rangle^* . \tag{5.35}$$

Dropping the ϕ and ϕ_0 dependence, the average of R_{Fa} is

$$\langle R_{Fa}\rangle = S\int_{-L}^{L}\left\langle\left[1+S_N D_0'^2\right]e^{j\overline{v}_x D_0}\right\rangle e^{-j\overline{v}_z z_0}dz_0. \tag{5.36}$$

Since for a stationary RP the heights and slopes at a given point are uncorrelated, the average can be simplified to

$$\langle R_{Fa}\rangle = S\left[1+S_N\alpha^2\right]\chi(\overline{v}_x)\int_{-L}^{L}e^{-j\overline{v}_z z_0}dz_0, \tag{5.37}$$

where α^2 is the variance of the random variable D' (surface slope), which from (A.57) is

$$\alpha^2 \equiv \left\langle D'^2\right\rangle = \frac{2\sigma^2}{l^2}. \tag{5.38}$$

The characteristic function $\chi(\overline{v}_x)$ is the same as defined in (5.11). The term $\langle R_{Fa}\rangle\langle R_{Fa}\rangle^*$ is now given by

$$\langle R_{Fa}\rangle\langle R_{Fa}\rangle^* = |S|^2\left[1+S_N\alpha^2\right]^2\chi(\overline{v}_x)\chi(\overline{v}_x)^*\int_{-L}^{L}\int_{-L}^{L}e^{-j\overline{v}_z\tau}dz_0dz_1, \tag{5.39}$$

where it is assumed that S_N is real. Using (5.32) the term $\langle R_{Fa}R_{Fa}^*\rangle$ becomes

$$\langle R_{Fa}R_{Fa}^*\rangle = |S|^2\int_{-L}^{L}\int_{-L}^{L}\left\langle\left[1+S_N D_0'^2\right]\left[1+S_N D_1'^2\right]e^{j\overline{v}_x(D_0-D_1)}\right\rangle e^{-j\overline{v}_z\tau}dz_0dz_1. \tag{5.40}$$

In general, heights and slopes at different points are correlated and the average inside the integral must be performed using the four dimensional probability density function as in [8]. For short correlation lengths, the heights can be considered uncorrelated to the slopes and the average $\langle R_{Fa}R_{Fa}^*\rangle$ can be written as

$$\langle R_{Fa}R_{Fa}^*\rangle = |S|^2\int_{-L}^{L}\int_{-L}^{L}\left\langle\left[1+S_N D_0'^2\right]\left[1+S_N D_1'^2\right]\right\rangle\left\langle e^{j\overline{v}_x(D_0-D_1)}\right\rangle e^{-j\overline{v}_z\tau}dz_0dz_1. \tag{5.41}$$

Note, however, that a height (slope) at one point is correlated to a height (slope)at a second point. Recalling the definitions of the autocorrelation of D'^2 in (A.59) and the characteristic function $\chi_2(\overline{v}_x, -\overline{v}_x)$ in (5.15), $\langle R_{Fa} R^*_{Fa} \rangle$ becomes

$$\langle R_{Fa} R^*_{Fa} \rangle = |S|^2 \left[1 + 2S_N\alpha^2\right] \int_{-L}^{L}\int_{-L}^{L} \chi_2(\overline{v}_x, -\overline{v}_x) e^{-j\overline{v}_z\tau} dz_0 dz_1 + |SS_N|^2 \int_{-L}^{L}\int_{-L}^{L} R_{D'^2}(\tau)\chi_2(\overline{v}_x, -\overline{v}_x) e^{-j\overline{v}_z\tau} dz_0 dz_1. \quad (5.42)$$

Combining (5.42) with (5.39) and using (A.60) and (5.23) gives

$$\widetilde{\varrho}^F_d = \left[1 + S_N\alpha^2\right]^2 \widetilde{\varrho}_d + |SS_N|^2 \int_{-L}^{L}\int_{-L}^{L} 2R^2_{D'}(\tau)\chi_2(\overline{v}_x, -\overline{v}_x) e^{-j\overline{v}_z\tau} dz_0 dz_1. \quad (5.43)$$

The autocorrelation of D' is given in (A.57) and is rewritten here for convenience:

$$R_{D'^2}(\tau) = \frac{4\sigma^4}{l^4} e^{-2\tau^2/l^2} \left[1 - \frac{2\tau^2}{l^2}\right]^2. \quad (5.44)$$

For short correlation lengths, the function $R_{D'^2}(\tau)\chi_2(\overline{v}_x, -\overline{v}_x)$ strongly peaks about $\tau = 0$ and the double integral in the second term of (5.43) reduces to

$$K = 2L \int_{-2L}^{2L} 2R^2_{D'}(\tau)\chi_2(\overline{v}_x, -\overline{v}_x) e^{-j\overline{v}_z\tau} d\tau. \quad (5.45)$$

If the limits of integration are removed to infinity as before and the expansion of the characteristic function given in (5.25) is used in (5.45), K is expressed in terms of an infinite series, i.e.,

$$K = 2Le^{-(\sigma\overline{v}_x)^2} \sum_{n=0}^{\infty} \frac{(\sigma\overline{v}_x)^{2n}}{n!} \int_{-\infty}^{\infty} 2R^2_{D'}(\tau) e^{-n\tau^2/l^2} e^{-j\overline{v}_z\tau} d\tau. \quad (5.46)$$

Using the relations [11]

$$\int_{-\infty}^{\infty} e^{-(2+n)\tau^2} \tau^2 \cos\overline{v}_z\tau d\tau = \frac{l^3}{4}\sqrt{\frac{\pi}{(2+n)^5}} \left[2(2+n) - (l\overline{v}_z)^2\right] e^{-(l\overline{v}_z)^2/4(2+n)}, \quad (5.47)$$

$$\int_{-\infty}^{\infty} e^{-(2+n)\tau^2}\tau^4\cos\overline{v}_z\tau d\tau =$$

$$\frac{l^5}{16}\sqrt{\frac{\pi}{(2+n)^9}}\left[12\left(2+n\right)^2+12\left(2+n\right)\left(l\overline{v}_z\right)^2+\left(l\overline{v}_z\right)^4\right]e^{-(l\overline{v}_z)^2/4(2+n)}, \quad (5.48)$$

and (5.26), K becomes

$$K = 8Ll\sqrt{\pi}\frac{\sigma^4}{l^4}e^{-(k_0\sigma v_x)^2}\sum_{n=0}^{\infty}a_n\frac{\left(k_0\sigma v_x\right)^{2n}}{n!}, \quad (5.49)$$

where

$$a_n = \frac{e^{-(k_0lv_z)^2/4(2+n)}}{\sqrt{2+n}}\left\{2-2\frac{\left[2\left(2+n\right)-\left(k_0lv_z\right)^2\right]}{\left(2+n\right)^2}\right\}$$
$$+\frac{e^{-(k_0lv_z)^2/4(2+n)}}{\sqrt{2+n}}\left\{\frac{1}{2}\frac{\left[12\left(2+n\right)^2+12\left(2+n\right)\left(k_0lv_z\right)^2+\left(k_0lv_z\right)^4\right]}{\left(2+n\right)^4}\right\}, \quad (5.50)$$

$v_x = \overline{v}_x/k_0 = \cos\phi + \cos\phi_0$, and $v_z = \overline{v}_z/k_0 = \sin\phi_0 - \sin\phi$. Therefore, the normalized average diffuse radar cross section $\left(\varrho_d^F = k_0\widetilde{\varrho}_d^F/2L\right)$for the new full wave method is for short correlation lengths

$$\varrho_d^F = \left[1+S_N\alpha^2\right]^2\varrho_d + \left|SS_N\right|^2\left(k_0l\right)\alpha^4\sqrt{\pi}e^{-(k_0\sigma)^2v_x^2}\sum_{n=0}^{\infty}a_n\frac{\left(k_0\sigma\right)^{2n}v_x^{2n}}{n!}, \quad (5.51)$$

where ϱ_d is defined in (5.27). The coefficients S and S_N for the TE case are

$$S(\phi,\phi_0) = S^{TE}(\phi,\phi_0) = \frac{2\cos\phi\cos\phi_0}{\cos\phi+\cos\phi_0}, \quad (5.52)$$

and

$$S_N(\phi,\phi_0) = S_N^{TE}(\phi,\phi_0) = 1, \quad (5.53)$$

and for the TM case are

$$S(\phi,\phi_0) = S^{TM}(\phi,\phi_0) = \frac{2\left(1-\sin\phi\sin\phi_0\right)}{\cos\phi+\cos\phi_0}, \quad (5.54)$$

and

$$S_N(\phi,\phi_0) = S_N^{TM}(\phi,\phi_0) = \frac{\cos\phi\cos\phi_0}{1-\sin\phi\sin\phi_0}. \quad (5.55)$$

It should be noted that the difference between the new full wave method and Bahar's full wave method are all terms of order α^2 and α^4, where α^2 is the mean squared value of the slope (variance). For surfaces with small slopes, i.e., $\alpha^2 \ll 1$, the new full wave method reduces to Bahar's full wave method.

In order to perform the formal average correctly for surfaces with long correlation lengths, the correlation between heights and slopes must be taken into account. The average in (5.40) must be performed by using the four dimensional probability density function. After transforming (5.40) to sum and difference coordinates it is written as

$$\langle R_{Fa} R_{Fa}^{*} \rangle = 2L\,|S|^2 \int_{-2L}^{2L} \left\langle \left[1 + S_N D_0'^2\right] \left[1 + S_N D_1'^2\right] e^{j\overline{v}_x (D_0 - D_1)} \right\rangle e^{-j\overline{v}_z \tau} dz_0 dz_1. \tag{5.56}$$

The averaged term in the integrand is expressed as

$$A(\tau) = \left\langle \left[1 + S_N D_0'^2\right] \left[1 + S_N D_1'^2\right] e^{j\overline{v}_x (D_0 - D_1)} \right\rangle. \tag{5.57}$$

By using the four dimensional Gaussian PDF $P_4\left(D_0, D_1, D_0', D_1', \tau\right)$ (5.57) is written as

$$A(\tau) = \int_{-\infty}^{\infty} \int_{-\infty}^{\infty} \int_{-\infty}^{\infty} \int_{-\infty}^{\infty} F\left(D_0'\right) F\left(D_1'\right) e^{j\overline{v}_x (D_0 - D_1)} P_4\left(\overline{w}, \tau\right) d\overline{w} \tag{5.58}$$

with

$$F\left(D_n'\right) = \left[1 + S_N D_n'^2\right], \qquad n = 0, 1 \tag{5.59}$$

and $\overline{w}$ is a vector with components $\overline{w} = [D_0, D_1, D_0', D_1'] = [w_1, w_2, w_3, w_4]$. The four dimensional Gaussian PDF for one height and one slope taken at z_0 and another height and one slope taken at $z_1 = z_0 - \tau$ [12] is

$$P_4\left(\overline{w}, \tau\right) = \frac{1}{(2\pi)^2 \sqrt{|\overline{K}|}} \exp\left[-\frac{1}{2} \overline{w}^T \overline{K}^{-1} \overline{w}\right] \tag{5.60}$$

where $\overline{K}$ is the symmetric 4×4 covariance matrix and $\left|\overline{K}\right|$ is the determinant of this matrix. The elements of $\overline{K}$ are given by (see Appendix A)

$$K_{11} = K_{22} = \left\langle D_1^2 \right\rangle = \sigma^2 \tag{5.61a}$$

$$K_{12} = \langle D_1 D_2 \rangle = R_D(\tau) = \sigma^2 e^{-\tau^2/l^2} \tag{5.61b}$$

$$K_{13} = K_{24} = \langle D_1 D_1' \rangle = 0 \tag{5.61c}$$

$$K_{14} = -K_{23} = \langle D_1 D_2' \rangle = R_{DD'}(\tau) = \frac{2\sigma^2 \tau}{l^2} e^{-\tau^2/l^2} \tag{5.61d}$$

$$K_{33} = K_{44} = \left\langle D_1'^2 \right\rangle = \alpha^2 = \frac{2\sigma^2}{l^2} \tag{5.61e}$$

$$K_{34} = \langle D_1' D_2' \rangle = R_{D'}(\tau) = \alpha^2 \left(1 - \frac{2\tau^2}{l^2}\right) e^{-\tau^2/l^2} \tag{5.61f}$$

The determinant of $\overline{K}$ is found to be

$$\left|\overline{K}\right| = \left[\sigma^4 - R_D^2\right]\left[\alpha^4 - R_{D'}^2\right] - 2\left[\sigma^2\alpha^2 - R_D R_{D'}\right] + R_{DD'}^4. \tag{5.62}$$

The inverse of $\overline{K}$, which is also symmetric, has matrix elements $K_{nm}^{-1} = p_{nm}/\left|\overline{K}\right|$, where

$$p_{11} = p_{22} = \sigma^2\left[\alpha^4 - R_{D'}^2\right] - \alpha^2 R_{DD'}^2 \tag{5.63a}$$

$$p_{12} = -R_D\left[\alpha^4 - R_{D'}^2\right] + R_{DD'} R_D \tag{5.63b}$$

$$p_{13} = -p_{24} = R_{DD'}\left[\alpha^2 R_D - \sigma^2 R_{D'}\right] \tag{5.63c}$$

$$p_{14} = -p_{23} = R_{DD'}\left[\alpha^2\sigma^2 - R_D R_{D'} - R_{DD'}^2\right] \tag{5.63d}$$

$$p_{33} = p_{44} = \alpha^2\left[\sigma^4 - R_D^2\right] - \sigma^2 R_{DD'}^2 \tag{5.63e}$$

$$p_{34} = R_D R_{DD'}^2 - R_{D'}\left[\sigma^4 - R_D^2\right] \tag{5.63f}$$

After substituting (5.60) into (5.58), the double integration over D_0 and D_1 can be performed analytically (using a relation similar to (A.5)) to yield the closed form expression

$$\int_{-\infty}^{\infty}\int_{-\infty}^{\infty} e^{j\overline{v}_x(D_0 - D_1)} P_4\left(\overline{w}, \tau\right) dD_0 dD_1 = G\left(D_0', D_1', \tau\right) P_2\left(D_0', D_1', \tau\right) \tag{5.64}$$

where

$$G\left(D_0', D_1', \tau\right) = e^{-\overline{v}_x \sigma^2 [1 - r(\tau)]} \exp\left\{\frac{\overline{v}_x^2 R_{DD'}}{\left[\alpha^2 + R_{D'}\right]}\right\} \exp\left\{\frac{j\overline{v}_x R_{DD'}\left(D_0' + D_1'\right)}{\left[\alpha^2 + R_{D'}\right]}\right\} \tag{5.65}$$

and $P_2\left(D_0', D_1', \tau\right)$ is the joint PDF for the slope, which is

$$P_2\left(D_0', D_1', \tau\right) = \frac{1}{2\pi\sqrt{\alpha^4 - R_{D'}^2}} \exp\left\{\frac{-\left[\alpha^2 D_0'^2 - 2R_{D'} D_0' D_1' + \alpha^2 D_1'\right]}{2\left[\alpha^4 - R_{D'}^2\right]}\right\}. \tag{5.66}$$

The function $A(\tau)$ is now expressed as a two-dimensional integral, which makes (5.56) a three-fold integration that can be evaluated numerically. Is should be noted that the PDF $P_2\left(D_0', D_1', \tau\right)$ is singular at $\tau = 0$ and must be handled carefully in the same manner as was done in [8]. Once this three-fold integration is performed, the result can be combined with (5.39) and substituted into (5.35) to obtain the average diffuse RCS for the Fictitious Current Full Wave method for large correlation lengths. This integration was performed for a few cases and was found to require more computational time than the Monte Carlo method. Therefore, the Monte Carlo method was used to produce the data in Chapter 6.

The analysis for the first-order perturbation method is particularly simple. The scattering pattern for the perturbation method is

$$R_P = k_0 S_P(\phi, \phi_0) \int_{-L}^{L} D_0 e^{jk_0 v_z z_0} dz_0. \tag{5.67}$$

Its average is zero since the average height, $\langle D_0 \rangle$, is zero. Therefore, the diffuse RCS becomes

$$\widetilde{\varrho}_d^P = \langle R_P R_P^* \rangle = k_0^2 \left|S_P(\phi, \phi_0)\right|^2 \int_{-L}^{L} \int_{-L}^{L} \langle D_0 D_1 \rangle \, e^{jk_0 v_z \tau} dz_0 dz_1. \tag{5.68}$$

The definition of the autocorrelation of D from (A.50) is

$$\langle D_0 D_1 \rangle = R_D(\tau) = \sigma^2 e^{-\tau^2/l^2}. \tag{5.69}$$

The transformation to sum and difference coordinates is now performed on (5.68) which results in

$$\widetilde{\varrho}_d^P = k_0^2\sigma^2 \left|S_P(\phi,\phi_0)\right|^2 \left\{ 2L \int_{-2L}^{2L} e^{-\tau^2/l^2} e^{jk_0 v_z \tau} d\tau - 2 \int_{-2L}^{2L} \tau e^{-\tau^2/l^2} \cos\left(k_0 v_z \tau\right) d\tau \right\}. \tag{5.70}$$

If the surface is assumed to be very large, the first term in the brackets is much larger than the second and the average diffuse RCS becomes approximately

$$\widetilde{\varrho}_d^P = k_0^2\sigma^2 \left|S_P(\phi,\phi_0)\right|^2 2L \int_{-2L}^{2L} e^{-\tau^2/l^2} e^{jk_0 v_z \tau} d\tau. \tag{5.71}$$

Using relation (5.26) and the same normalization as used previously, i.e., $\varrho_d^P = k_0\widetilde{\varrho}_d^P/2L$, the average diffuse RCS is evaluated to be

$$\varrho_d^P = (k_0\sigma)^2 (k_0 l) \sqrt{\pi} \left|S_P(\phi,\phi_0)\right|^2 e^{-(k_0 l)^2 v_z^2/4}. \tag{5.72}$$

For the TE case, the coefficient S_P is

$$S_P^{TE}(\phi,\phi_0) = -2j \cos\phi \cos\phi_0, \tag{5.73}$$

and for the TM case it is

$$S_P^{TM}(\phi,\phi_0) = 2j \left(1 - \sin\phi \sin\phi_0\right). \tag{5.74}$$

CHAPTER 6

NUMERICAL RESULTS

For the fictitious current full wave method, the evaluation of the average diffuse radar cross section per unit length can be performed in one of two ways. The first is to evaluate the formal average given in Chapter 5 using numerical integration. The second, called the Monte Carlo method, is to evaluate repeatedly the simpler integrals for the TE and TM scatter patterns, as given in (4.36) and (4.37), respectively, using many different realizations of the surface to calculate a collection of radar cross sections. This collection of radar cross sections is then averaged over the ensemble of realizations. In order to perform the Monte Carlo method, a procedure for generating random surfaces with the appropriate statistics must be developed.

6.1 Random Surface Generation

To calculate the average RCS, a random surface profile must be generated with the appropriate statistics, i.e., a surface profile with Gaussian correlated heights and slopes. This is accomplished using either the moving average, autoregressive, or spectral method of random number generation. A discussion of the moving average and autoregressive methods is found in [10]. For the present work, the spectral method [6] is used because it numerically more efficient than the others.

The pth realization of the rough surface D_n, called D_n^p, is represented as a summation of Fourier components as long as the surface roughness is of finite extent and is considered one period of length $2L$ of an infinite periodic surface, i.e.,

$$D_n^p = \frac{1}{2L} \sum_{i=-N/2}^{(N/2)-1} F^p\left(K_i\right) e^{jk_i z_n}, \tag{6.1}$$

where $z_n = n\Delta z$ and $D_n^p = D^p(z_n)$ and the surface extends over $-L \leq z_n \leq L$. The spatial wavenumber K_i is given by $K_i = \pi i/L$, with $2L = N\Delta z$. The coefficients

$F^p(K_i)$ are random and uncorrelated when D_n is random, and are expressed as

$$F^p(K_i) = \sum_{i=-N/2}^{(N/2)-1} D_n^p e^{-jk_i z_n}. \tag{6.2}$$

The power spectrum of the discrete random process D_n^p is [13]

$$P(K_i) = \frac{1}{2\pi} \lim_{2L\to\infty} \left\{ \frac{1}{2L} \left\langle |F^p(K_i)|^2 \right\rangle \right\}, \tag{6.3}$$

where the brackets $\langle \quad \rangle$ represent averaging over all the realizations. If the coefficients $F^p(K_i)$ are chosen using the relation

$$F^p(K_i) = \begin{cases} [4\pi L P(K_i)]^{1/2} X_p, & i \geq 0 \\ F^{p*}(K_i), & i < 0 \end{cases} \tag{6.4}$$

where * denotes complex conjugation and X_p is an uncorrelated random process. The new process D_n^p has the power spectrum $P(K_i)$. The choice of $F^{p*}(K_i)$ for $i < 0$ makes the resultant process D_n^p real. For the case under consideration, i.e., a surface with Gaussian heights and slopes, the coefficients $F^p(K_i)$ become [6]

$$F^p(K_i) = [4\pi L P(K_i)]^{1/2} \begin{cases} [G(0,1) + jG(0,1)]/\sqrt{2}, & i \neq 0, N/2 \\ G(0,1), & i = 0, N/2 \end{cases}, \tag{6.5}$$

for $i = 0, \ldots, N/2$ and $F^p(K_i) = F^{p*}(K_i)$ for $i < 0$. Each $G(0,1)$ represents an independent sample of a Gaussian (Normally) distributed random variable with zero mean and unit variance. The power spectrum is Gaussian and is taken as

$$P(K_i) = \left(\frac{l\sigma^2}{2\sqrt{\pi}} \right) e^{-K_i^2 l^2/4} \tag{6.6}$$

where σ is the RMS height and l is the correlation length of the surface.

The evaluation of (6.1) is performed efficiently using an inverse fast Fourier transform (IFFT). In order to implement this IFFT using a standard package, the index i in (6.1) is shifted so that it extends over the interval $[1, N]$. A new index is

introduced such that $m = j + (N/2) + 1$; this yields an alternative expression for the pth realization of the surface height:

$$D_n^p = e^{-j(n-1)\pi} \frac{1}{N\Delta z} \sum_{m=1}^{N} Q_m e^{j\frac{2\pi}{N}(m-1)(n-1)}, \tag{6.7}$$

where

$$Q_m = F^p\left(\overline{K}_{m-N/2-1}\right) e^{j\frac{2\pi}{N}\left[m-\frac{N}{2}-1\right]}, \tag{6.8}$$

$$F^p\left(\overline{K}_{m-N/2-1}\right) = \left[4\pi LP\left(\overline{K}_{m-N/2-1}\right)\right]^{1/2} \begin{cases} \left[G(0,1) + jG(0,1)\right]/\sqrt{2}, & m \neq \frac{N}{2}+1, N+1 \\ G(0,1), & m = \frac{N}{2}+1, N+1 \end{cases}, \tag{6.9}$$

for $m = N/2+1, \ldots, N+1$ and $\overline{K}_{m-N/2-1} = 2\pi\left[m - N/2 - 1\right]/(N\Delta z)$. Also, only the coefficients for $m < N/2+1$ need to be calculated from (6.9), since the remaining terms are found using $F^p\left(\overline{K}_{m-N/2-1}\right) = F^{p*}\left(\overline{K}_{-m+N/2-1}\right)$ for $m < N/2+1$. The surface height profile is now written as

$$D_n^p = \frac{e^{-j(n-1)\pi}}{\Delta z} IFFT\left[Q_m\right], \tag{6.10}$$

and, by taking the first derivative, the surface slope profile becomes

$$D_n'^p = \frac{e^{-j(n-1)\pi}}{\Delta z} IFFT\left[jK_{m-N/2-1}Q_m\right]. \tag{6.11}$$

6.2 Numerical Comparisons

Since the formal average method is numerically very cumbersome for the Fictitious Current Full Wave method, the Monte Carlo method is used, which is performed as follows. Once the discrete surface profile D_n^p is generated, it is substituted into the expression for the scattering pattern (2.31), which is

$$R^{TE}(\phi,\phi_0) = \frac{2\cos\phi\cos\phi_0}{\cos\phi+\cos\phi_0} \int_{-L}^{L} \left\{1 - \left[1 + D_0'^2\right] e^{jk_0 D_0(\cos\phi+\cos\phi_0)}\right\} e^{jk_0 z_0(\sin\phi-\sin\phi_0)} dz_0 \tag{6.12}$$

for the TE case. Since the surface height and slope profiles are discrete variables, the integrand is only known at the specific points $z_n = n\Delta z$, where $\Delta z = 2L/N$. A simple, but effective, method to evaluate the integral in (6.12) is to use the extended trapezoidal rule [14]:

$$R^{TE}(\phi,\phi_0) = \frac{2\cos\phi\cos\phi_0}{\cos\phi+\cos\phi_0}\left\{\sum_{n=1}^{N} f_n(\phi) + \frac{1}{2}f_0(\phi) + \frac{1}{2}f_N(\phi)\right\}\Delta z, \tag{6.13}$$

where

$$f_n(\phi) = \left\{1 - \left[1+D_n'^2\right]e^{jk_0D_n(\cos\phi+\cos\phi_0)}\right\}e^{jk_0z_n(\sin\phi-\sin\phi_0)}, \tag{6.14}$$

with $D_n \equiv D_n^p$, since only one realization is being considered. The function f_n is a function of ϕ, which means the summation is performed for each value of ϕ. In the numerical results presented, ϕ is taken at 180 discrete values ranging form -90^o to $+90^o$ in 1^o increments. All the Monte Carlo data generated for the fictitious current full wave method use $N = 1024$ with $2L = 80\lambda_0$ and $x = 0.078\lambda_0$. In order to verify that the results are not contaminated by edge effect scattering, surfaces with lengths $2L = 160\lambda_0$ and $2L = 320\lambda_0$ were used in the simulation which produced no change in the results. Spatial resolution in the simulation was also increased to $N = 2048$ and $N = 4096$ for $2L = 80\lambda_0$, which also yielded no change in the results. Fifty surface realizations are used in the Fictitious Current Full Wave method Monte Carlo plots, and accuracy was checked by increasing this number to 100 with, again, no change in the results.

The methods that are used in the comparisons are all formally averaged (see Chapter 5), except for the integral equation method and fictitious current full wave method. The integral equation method is normally used for comparison in the literature and is considered very accurate. Data presented for the integral equation method was supplied for use in the plots by Eric I. Thorsos, much of which

was previously published [8],[6],[7]. Details of the method are found in [6], but is summarized here.

To find the field scattered by a 1-D surface for the TE, case the Helmholtz integral (see Appendix C) is used. For the TE case, the tangential electric field is zero on the perfectly conducting boundary and the unknown total field above the surface is written as

$$E_y(\mathbf{r}) = E_y^i(\mathbf{r}) + \frac{1}{4j}\int_S H_0^{(2)}(k_0|\mathbf{r}-\mathbf{r}'|)\frac{\partial E_y(\mathbf{r}')}{\partial n'}dS', \tag{6.15}$$

where $H_0^{(2)}$ is the zero-order Hankel function of the second kind and $\partial E_y(\mathbf{r}')/\partial n'$ is the normal derivative of the total field on the surface, which is also unknown. An integral equation for the unknown term $\partial E_y(\mathbf{r}')/\partial n'$ is formulated by letting $\mathbf{r}$ approach the surface and using the boundary condition that $E_y(\mathbf{r}) = 0$ on the surface, i.e.,

$$E_y^i(\mathbf{r}) = -\frac{1}{4j}\int_S H_0^{(2)}(k_0|\mathbf{r}-\mathbf{r}'|)\frac{\partial E_y(\mathbf{r}')}{\partial n'}dS', \tag{6.16}$$

with $\mathbf{r}$ and $\mathbf{r}'$ both on the surface. This integral equation is a linear integral equation of the first kind for $\partial E_y(\mathbf{r}')/\partial n'$. An alternative formulation can be obtained by applying the operator $\partial/\partial n = \hat{\mathbf{n}}\cdot\nabla$ to (6.15), where $\hat{\mathbf{n}}$ is the surface normal, and taking $\mathbf{r}$ to approach the surface, i.e.,

$$\frac{\partial E_y(\mathbf{r})}{\partial n} = 2\frac{\partial E_y^i(\mathbf{r})}{\partial n} + \frac{1}{2j}\int_S \frac{\partial}{\partial n}H_0^{(2)}(k_0|\mathbf{r}-\mathbf{r}'|)\frac{\partial E_y(\mathbf{r}')}{\partial n'}dS'. \tag{6.17}$$

This is a linear integral equation of the second kind for $\partial E_y(\mathbf{r}')/\partial n'$. Once $\partial E_y(\mathbf{r}')/\partial n'$ is found, the total field can be calculated by placing the result in (6.15).

Both integral equations are solved by using a quadrature method to convert the integral into a summation and, hence, the integral equation into a matrix equation which is solved by standard methods. The generation of the matrices and the

solutions of the matrix equations require considerable computer resources and were performed on a CRAY supercomputer for the large matrices required to give sufficiently accurate results. Many checks were performed to ensure the accuracy of the solution (see [6],[7],[8]). Note, to reduce "edge" effect scattering by the edges of the rough surface, the incident field was taken to be a tapered Gaussian beam instead of a plane wave.

The first set of eight plots are for the TE case. The parameters $k_0\sigma$, $k_0 l$ and γ are the normalized RMS height, normalized correlation length and RMS slope angle, respectively, where k_0 is the free-space wavenumber. The RMS slope angle is found from the RMS height and correlation length using the relation $\tan\gamma = \sqrt{2}\sigma/l$. The formally averaged results appear as smooth lines in the plots. The Monte Carlo data is jagged compared to the formal averages because the results using the Monte Carlo methods are only averaged over a finite number of surface realizations. The formal averages are analytically averaged for an infinite number of surface realizations. All curves, except the integral equation curve represent the diffuse scattering strength, which is the diffuse RCS divided by 2π. The integral equation curve is a plot of the total scattering strength, which is equal to the diffuse scattering strength plus a coherent component that contributes around the specular direction $\phi_0 = 45^o$ which is seen as a large peak in the plots, and slightly near grazing $\phi_0 = \pm 90^o$. The integral equation data for Figures 6.1 and 6.2 was originally published in [7], for Figures 6.3 and 6.4 in [8], and for Figures 6.5 and 6.6 in [15]. The integral equation data for Figures 6.7–6.10 is previously unpublished.

Figure 6.1 demonstrates the agreement between the Fictitious Current (F.C.) Full Wave results and the "exact" integral equation results in a region where neither the Kirchhoff or first order perturbation results are valid. Bahar's results fall below the integral equation result for $-90^o \leq \phi < -30^o$, and is approximately 3dB below it at -70°. Figure 6.2 shows the results from all the methods under consideration

for an increased RMS slope angle. The disagreement between Bahar's result and the integral equation result is even more pronounced than in the previous plot. This should be expected since Bahar's method is only valid for small RMS slopes. Disagreement between Bahar's result and the integral equation result now starts to occur for $\phi < 0°$ and reaches a maximum disagreement of 5dB around $\phi = -70°$. Figures 6.3 and 6.4 present two cases where the first order perturbation result is valid. It is seen that the F.C. Full Wave, Bahar's Full Wave and the integral equation results all overlap with the perturbation result. Results in Figure 6.5 are plotted for the region where the Kirchhoff result is valid. The F.C. Full Wave, integral equation and Kirchhoff results all overlap for this case. Bahar's Full Wave result disagrees with the aforementioned results for $\phi < 0°$; specifically, at $\phi = -60°$ Bahar's result is about 10dB below the three results mentioned above. For this case, the first order perturbation result is not accurate, except for $\phi > 70°$. Figures 6.6–6.8 present cases where the Kirchhoff, first order perturbation and Bahar's results are not valid, but the F.C. Full Wave method agrees very well with the "exact" integral equation results. Figures 6.9 and 6.10 present results for TM polarization. It can be seen that the Kirchhoff, F.C. Full Wave and Bahar's Full Wave results all agree for these parameters, but the integral equation results do not agree with these others around grazing angles $\phi = \pm 90°$. This may be explained because of the difference in the formulation between the integral equation method and the other methods examined. All the other methods under consideration are formulated for infinite surfaces illuminated by a plane wave. The integral equation method is formulated for a finite surface illuminated by a tapered Gaussian beam. Although the integral equation solution is considered an "exact" solution, it is an exact solution to a problem that is slightly different than the one considered in the other methods. The discrepancy appears most distinctly in the TM case, since the scattered field is non-zero on the surface ($\phi = \pm 90°$). The integral equation result is smaller than

the others for $\phi = \pm 90^o$ since the beam does not illuminate the surface far from the origin. The scattered field that reaches the observation point on the surface at $\phi = \pm 90^o$ is a wave that has propagated along the surface but has lost some energy to multiple scattering effects in the surface troughs.

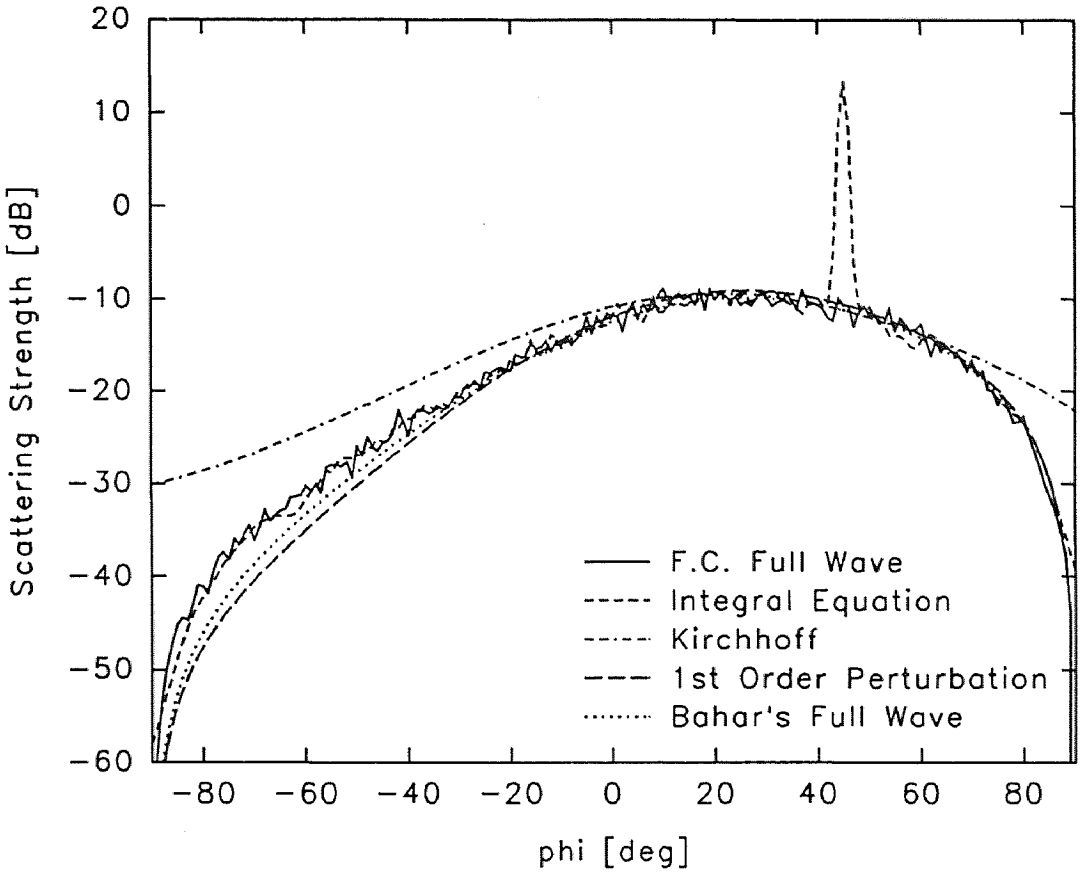

Figure 6.1 Comparison of rough surface scattering methods for $k_0\sigma = 0.333$, $k_0 l = 2.83$, $\gamma = 9.48^o$, $\phi_0 = 45^o$, TE polarization, where σ is the RMS surface height, l is the surface correlation length, γ is the RMS surface slope angle and ϕ_0 is the angle of incidence. The large peak in the specular direction for the integral equation method is due to the coherent field and is subtracted from all the other results.

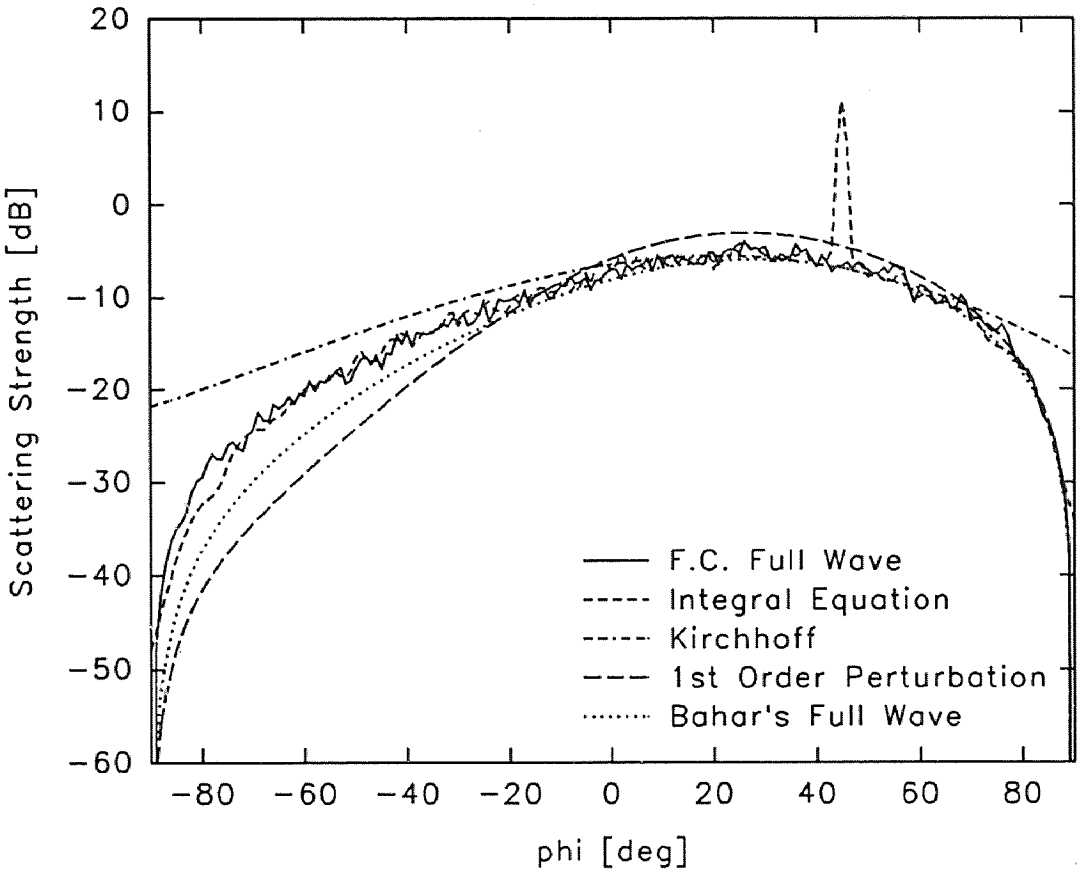

Figure 6.2 Comparison of rough surface scattering methods for $k_0\sigma = 0.666$, $k_0 l = 2.83$, $\gamma = 18.4^o$, $\phi_0 = 45^o$, TE polarization.

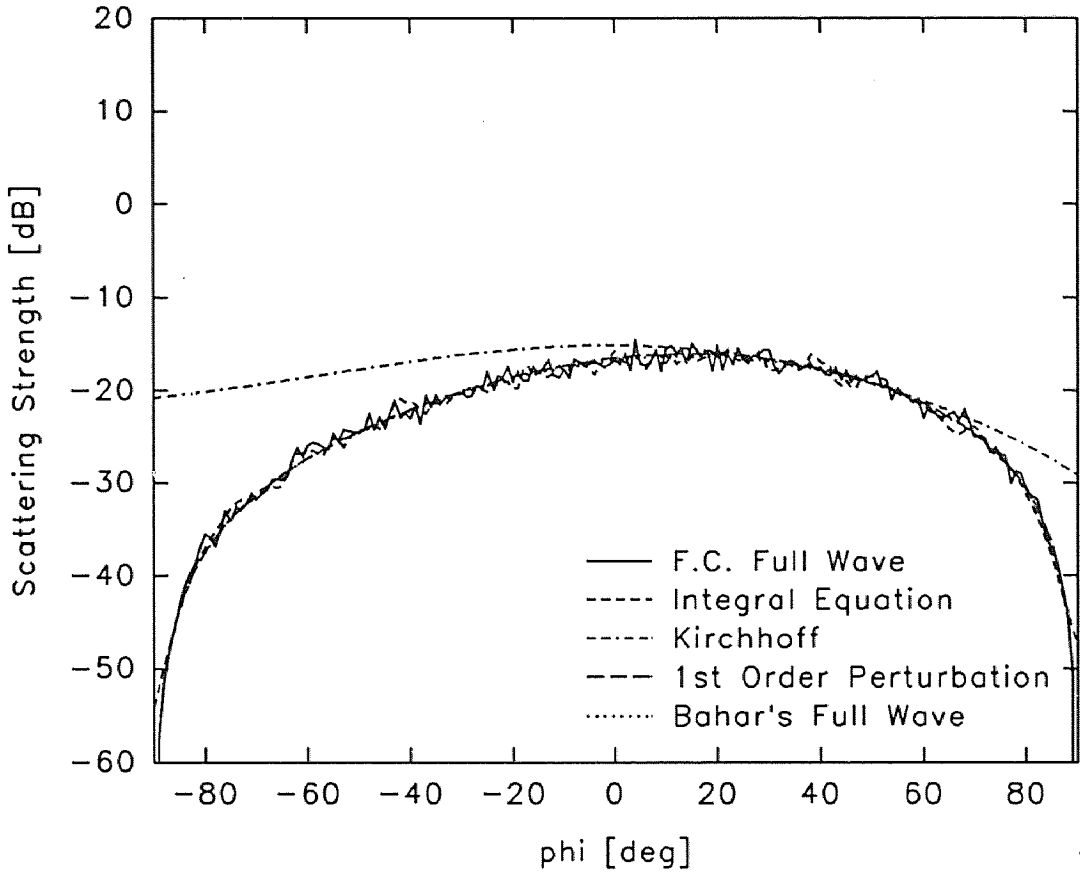

Figure 6.3 Comparison of rough surface scattering methods for $k_0\sigma = 0.187$, $k_0 l = 1.5$, $\gamma = 10°$, $\phi_0 = 45°$, TE polarization.

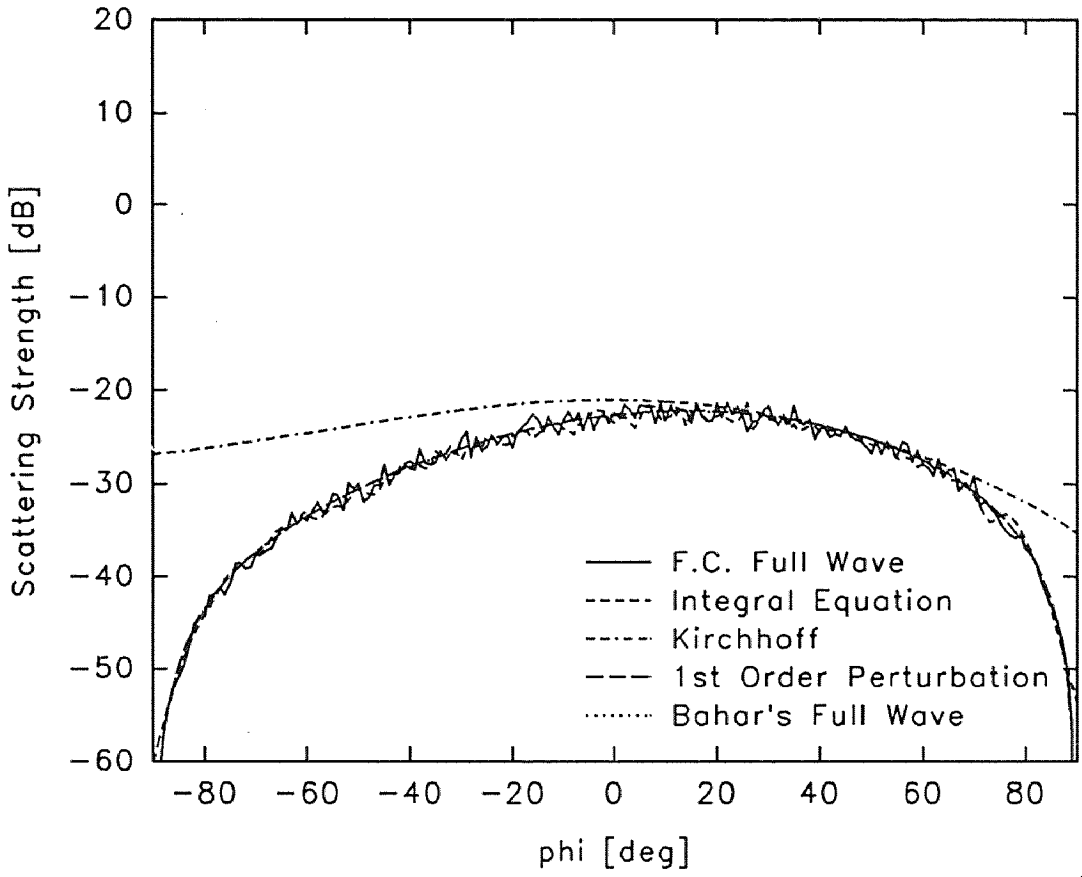

Figure 6.4 Comparison of rough surface scattering methods for $k_0\sigma = 0.0928$, $k_0 l = 1.5$, $\gamma = 5^o$, $\phi_0 = 45^o$, TE polarization.

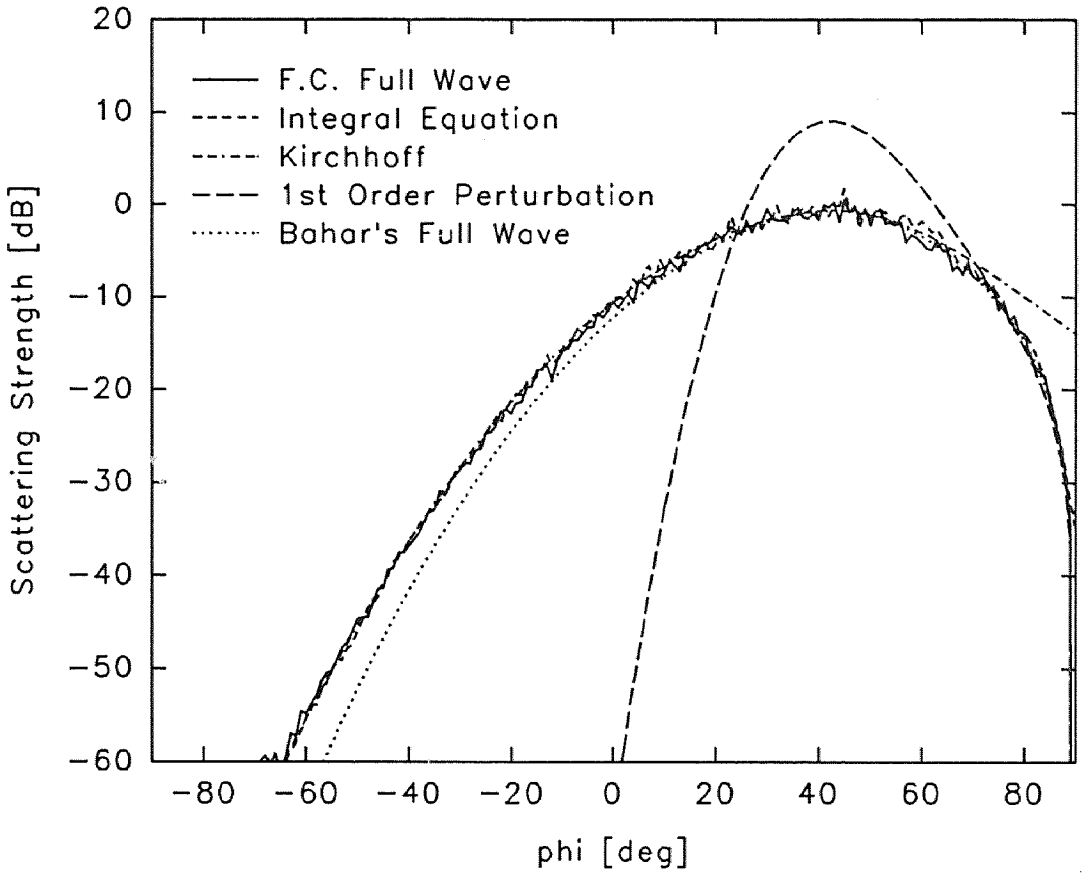

Figure 6.5 Comparison of rough surface scattering methods for $k_0\sigma = 1.5$, $k_0 l = 12.0$, $\gamma = 10.02^o$, $\phi_0 = 45^o$, TE polarization.

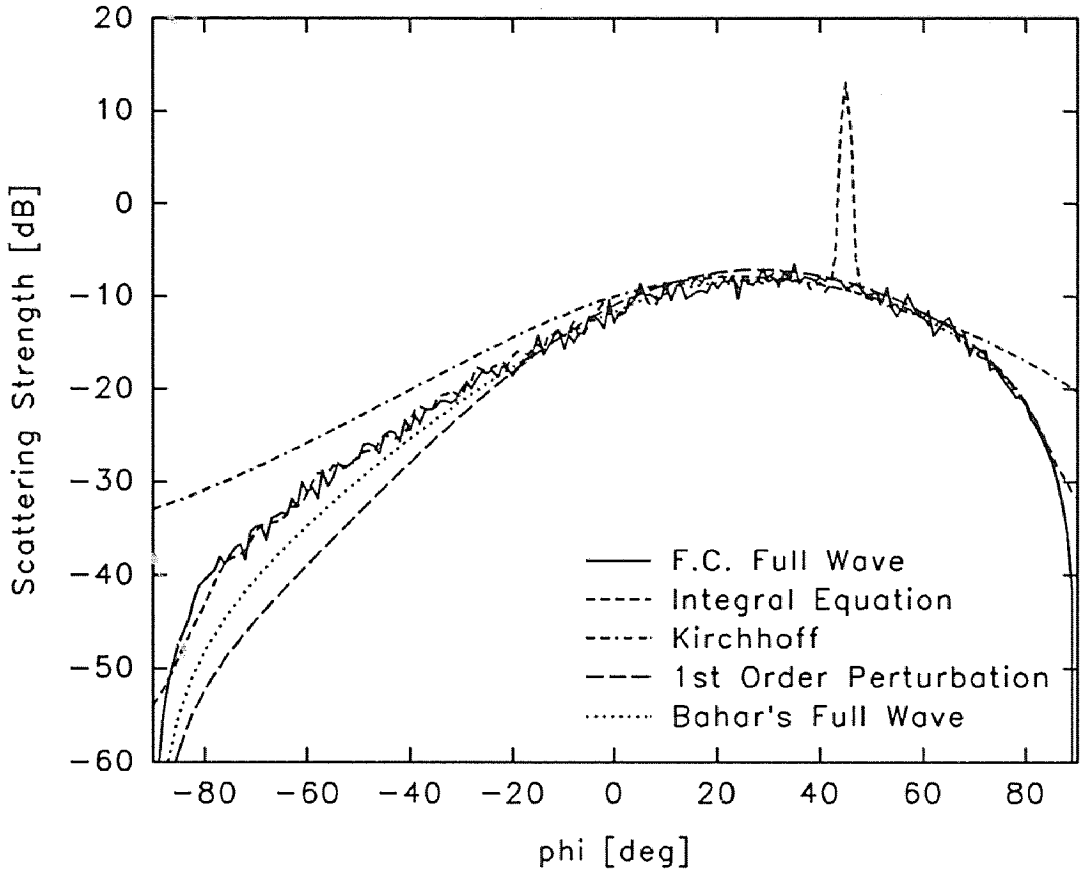

Figure 6.6 Comparison of rough surface scattering methods for $k_0\sigma = 0.399$, $k_0 l = 3.2$, $\gamma = 10°$, $\phi_0 = 45°$, TE polarization.

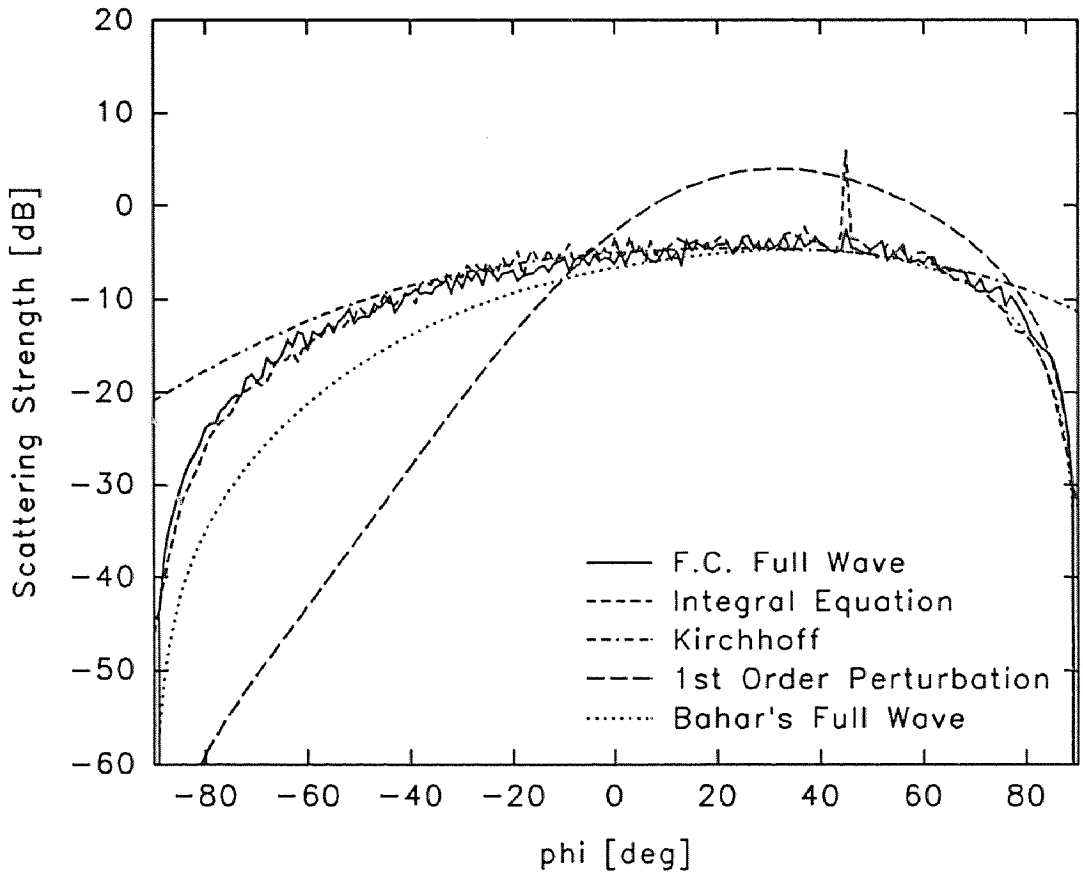

Figure 6.7 Comparison of rough surface scattering methods for $k_0\sigma = 1.319$, $k_0 l = 4.0$, $\gamma = 25^o$, $\phi_0 = 45^o$, TE polariazation.

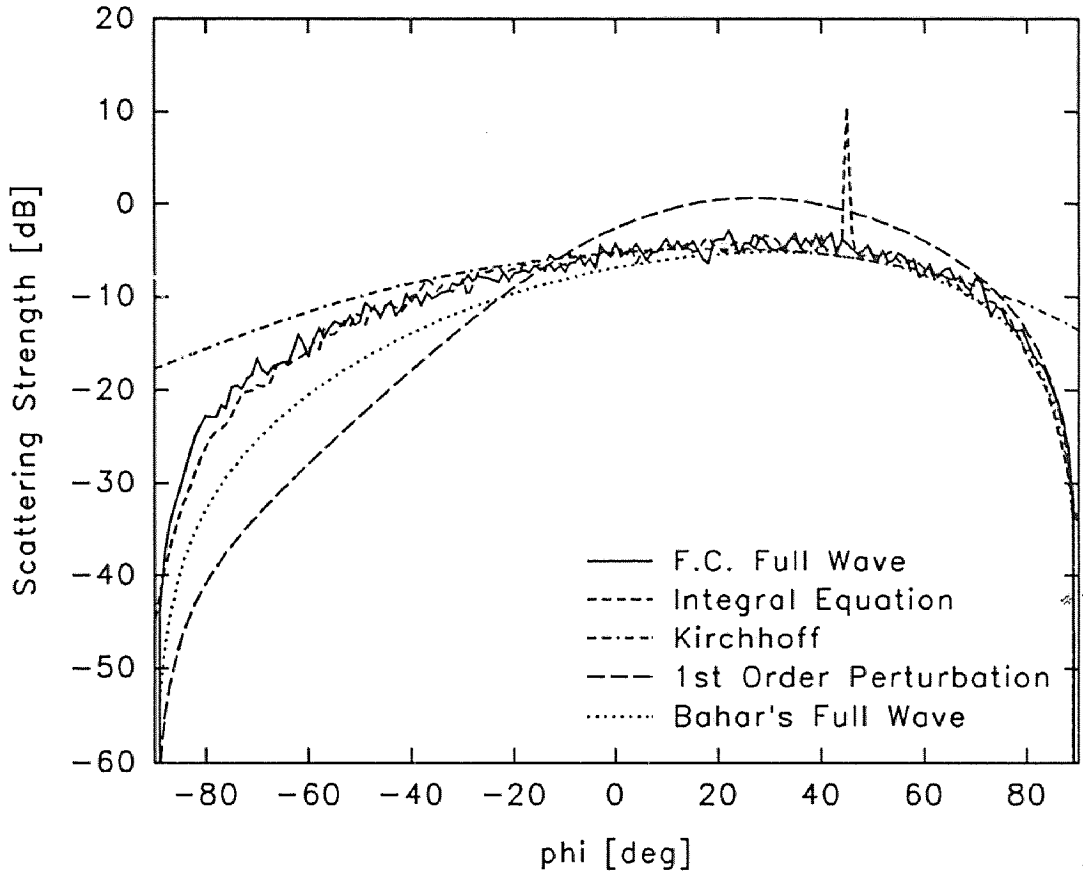

Figure 6.8 Comparison of rough surface scattering methods for $k_0\sigma = 1.0$, $k_0 l = 3.0$, $\gamma = 25.24°$, $\phi_0 = 45°$, TE polarization.

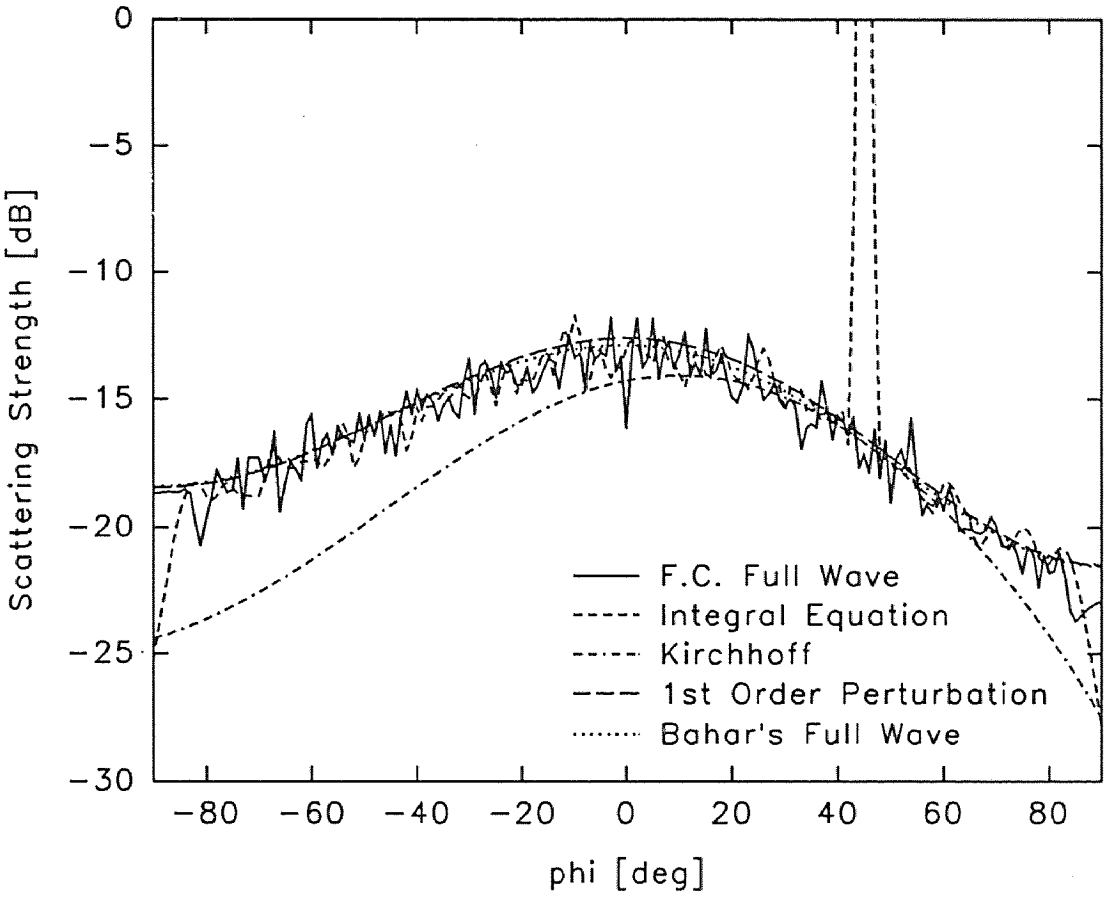

Figure 6.9 Comparison of rough surface scattering methods for $k_0\sigma = 0.2$, $k_0 l = 2.0$, $\gamma = 8^o$, $\phi_0 = 45^o$, TM polarization.

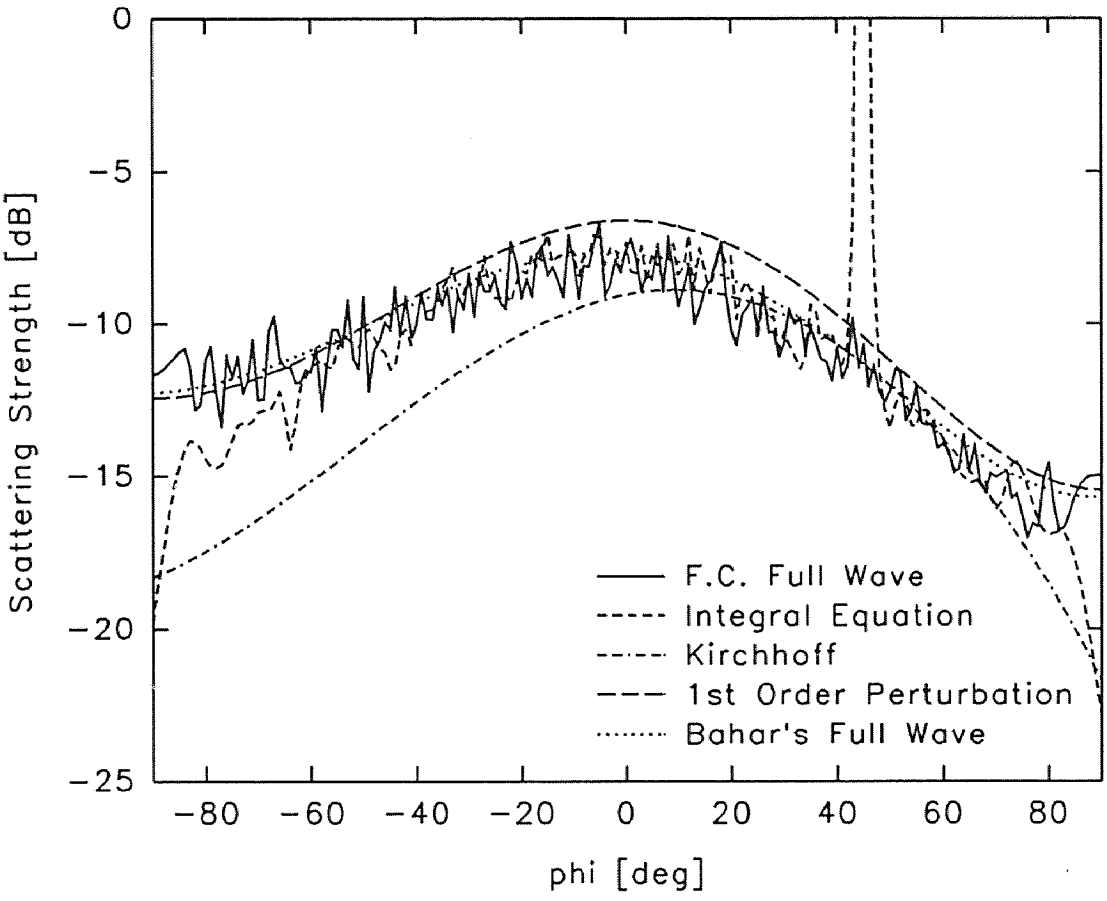

Figure 6.10 Comparison of rough surface scattering methods for $k_0\sigma = 0.4$, $k_0 l = 2.0$, $\gamma = 15.8^o$, $\phi_0 = 45^o$, TM polarization.

CHAPTER 7
CONCLUSION AND SUGGESTIONS

A new full wave theory has been formulated for scattering by rough perfectly conducting surfaces where the surface exists over a finite segment of the infinite conductor. Above the conductor, the field is initially approximated by a zero-order (primary) field that satisfies the boundary conditions and Maxwell's equations with a fictitious volume current source. This fictitious volume current source is cancelled by a higher order fictitious sheet current source which generates a higher order correction term to the field called the first-order field. The first-order field satisfies the boundary conditions and Maxwell's equations, but with a new first-order fictitious volume current source. At this point, the total field above the conductor is approximated by the superposition of the zero (primary) and first-order fields with the first-order fictitious volume current source present. The first-order volume source is cancelled by the next higher order sheet current source which produces a second-order field correction term. The process can be repeated until the desired field precision is obtained. Through use of currents induced on the metal surface, a quantitative measure of the accuracy of this method can be obtained.

This new full wave method generates a far field which is equivalent to Bahar's original full wave method plus an extra term proportional to the squared slope of the surface. For surfaces with small slope, both methods produce identical results. In the limit as the surface height and slope become small, the new full wave method reduces to the first-order perturbation result. Adding the first-order far field expressions for the TE and TM cases determined by the new full wave method and dividing by two gives the Kirchhoff result. This indicates that the Kirchhoff result, which is polarization independent, is essentially an average of the TE and TM cases. In the region where neither the Kirchhoff nor the first-order perturbation method are valid, the new full wave results agree with the "exact" integral equation solution more

closely than do Bahar's original full wave results; Bahar's modified full wave results are approximately equivalent to the Kirchhoff results [6] which as stated do not agree with the integral equation data.

Future work should be concerned with formulating a numerical procedure that uses the above mentioned induced surface current to measure the accuracy of the Fictitious Current Full Wave method for arbitrarily specified surface parameters. An efficient numerical method to evaluate the formal average for this method can also be obtained. The method can also be extended to include scattering by surfaces which are rough in two dimensions, and scattering by dielectric layers with rough interfaces, all of which are currently being investigated.

APPENDIX A

STOCHASTIC PROCESSES

A.1 General Processes

The purpose of this section is to provide a general overview of the analysis of stochastic, or random, processes. It is assumed that the reader is familiar with the basic theory of a single and multiple random variables (for a detailed discussion, see [12]).

Some basic definitions pertaining to stochastic processes are necessary for further discussion. A random variable (RV) X is a rule for assigning a real *number* $X(\zeta)$ to an outcome ζ in the sample space of an experiment. A stochastic, or random, process (RP) $X(z)$ is a rule for assigning a *function* $X(z,\zeta)$ to every outcome ζ. Therefore, a stochastic process is a family of spatial functions of the real variable z which depend on the parameter ζ. In all the cases considered here, z will be a continuous variable. The notation $X(z)$ will be used to represent the stochastic process, suppressing the ζ dependence. $X(z)$ has the following different interpretations[12]:

1. It is an *ensemble* of functions $X(z,\zeta)$ where both z and ζ are variables.

2. It is a single spatial function of z, or a *sample* of the random process, if z is a variable and ζ is a fixed parameter, i.e., if $\zeta = \zeta_1$ then $X(z,\zeta_1)$ varies over the range of z

3. $X(z)$ is a *random variable* equal to the state of the process at point $z = z_1$ if z_1 is fixed and ζ is variable, i.e., is the set of numbers $\{X(z_1,\zeta_1), X(z_1,\zeta_2), \dots\}$.

4. $X(z)$ is a *number* if both z and ζ are fixed, i.e., if $z = z_1$ and $\zeta = \zeta_1$ then $X = X(z_1,\zeta_1)$.

For the interpretation given in (3), a stochastic process is a collection of random variables $X(z_i, \zeta_j)$, $j = 1, \ldots, \infty$, for each $z = z_i$. If a specific point z is considered, $X(z)$ is an RV with the first-order probability distribution defined by

$$F(x, z) = P\{X(z) \leq x\}, \tag{A.1}$$

and first-order probability density function defined as

$$f(x, z) = \frac{\partial F(x, z)}{\partial x}, \tag{A.2}$$

where $P\{A\}$ means the probability that event A occurs. The second-order distribution is a joint distribution function of the RVs $X(z_1)$ and $X(z_2)$ such that

$$F(x_1, x_2; z_1, z_2) = P\{X(z_1) \leq x_1, X(z_2) \leq x_2\} \tag{A.3}$$

and the second-order probability density function is defined by

$$f(x_1, x_2; z_1, z_2) = \frac{\partial^2 F(x_1, x_2; z_1, z_2)}{\partial x_1 \partial x_2}. \tag{A.4}$$

This can be generalized to the nth-order distribution and density functions. Note, in order for the definition of the first-order distribution and density functions to be consistent with the second-order ones, it must be true that

$$F(x_1, z_1) = F(x_1, \infty; z_1, z_2) \quad , \quad f(x_1, z_1) = \int_{-\infty}^{\infty} f(x_1, x_2; z_1, z_2) dx_2. \tag{A.5}$$

For the stochastic process to be completely determined, its distribution function $F(x_1, \ldots, x_n; z_1, \ldots, z_n)$ must be known for every x_i, z_i, where $i = 1, \ldots, n$, and for all n. However, in most practical applications only a few properties of the stochastic process need to be specified. These include the mean, or ensemble average, which is defined as

$$m(z) = \langle X(z) \rangle = \int_{-\infty}^{\infty} x f(x, z) dx, \tag{A.6}$$

where $f(x,z)$ is the first-order probability density function (A.2). From (A.6), it follows that

$$\langle AX_1 \rangle = A\langle X_1 \rangle \quad , \quad \langle A + X_1 \rangle = A + \langle X_1 \rangle \quad , \quad \langle X_1 + X_2 + \cdots \rangle = \langle X_1 \rangle + \langle X_2 \rangle + \cdots \tag{A.7}$$

where $X_i = X(z_i)$. Also from (A.6), the mean of a function of X_1 is

$$\langle g(X_1) \rangle = \int_{-\infty}^{\infty} g(x) f(x, z_1) dx. \tag{A.8}$$

A second property of the RP $X(z)$ is its autocorrelation function which is defined as

$$R(z_1, z_2) = \langle X_1 X_2^* \rangle = \int_{-\infty}^{\infty} \int_{-\infty}^{\infty} x_1 x_2 f(x_1, x_2; z_1, z_2) dx_1 dx_2, \tag{A.9}$$

where the random variables X_1 and X_2 are, in general, complex. Related properties are the autocovariance which is defined as

$$C(z_1, z_2) = R(z_1, z_2) - \langle X_1 \rangle \langle X_2 \rangle^*, \tag{A.10}$$

the variance which is

$$C(z, z) = R(z, z) - |\langle X \rangle|^2, \tag{A.11}$$

and the correlation coefficient which is the ratio

$$r(z_1, z_2) = \frac{C(z_1, z_2)}{\sqrt{C(z_1, z_1) C(z_2, z_2)}}. \tag{A.12}$$

The standard deviation of an RP, also called the root mean squared (RMS), is defined as

$$\sigma = \sqrt{R(z_1, z_1)} = \sqrt{\langle X_1^2 \rangle} = \sqrt{\int_{-\infty}^{\infty} x^2 f(x, z_1) dx}. \tag{A.13}$$

Further properties include the characteristic function $\chi(\omega)$ of a first-order distribution $f(x,z)$,

$$\chi(\omega, z) = \int_{-\infty}^{\infty} f(x, z) e^{j\omega x} dx \tag{A.14}$$

and the characteristic function $\chi_2(\omega_1, \omega_2)$ of a second-order distribution function $f(x_1, x_2; z_1, z_2)$ which is

$$\chi_2(\omega_1, \omega_2; z_1, z_2) = \int_{-\infty}^{\infty} \int_{-\infty}^{\infty} f(x_1, x_2; z_1, z_2) e^{j\omega_1 x_1 + j\omega_2 x_2} dx_1 dx_2. \tag{A.15}$$

A stochastic process is called strict-sense stationary (SSS) if its statistical properties do not change with a shift in the origin, i.e., $X(z)$ and $X(z+c)$ have the same statistical properties for any real constant c. Two processes $X(z)$ and $Y(z)$ are called jointly stationary if their joint statistics are the same as the joint statistics of $X(z+c)$ and $Y(z+c)$. If a process is complex, i.e., $Z(z) = X(z) + jY(z)$, then it is SSS if $X(z)$ and $Y(z)$ are jointly stationary. If a random process has a constant mean and has an autocorrelation which depends only on the distance τ between two points z and $z+\tau$ then it is called wide sense stationary (WSS), i.e., if

$$\langle X(z) \rangle = m = const. \tag{A.16}$$

and

$$\langle X(z+\tau) X^*(z) \rangle = R(\tau) \tag{A.17}$$

then X is WSS. The autocovariance for a WSS process can now be written as

$$C(\tau) = R(\tau) - |m|^2 \tag{A.18}$$

and the correlation coefficient becomes

$$r(\tau) = \frac{C(\tau)}{C(0)}. \tag{A.19}$$

If two processes are to be considered jointly WSS then each must be WSS and the cross-correlation must only depend on τ, i.e.,

$$\langle X(z+\tau) Y^*(z) \rangle = R_{XY}(\tau). \tag{A.20}$$

It follows that the cross-covariance is given by

$$C_{XY}(\tau) = R_{XY}(\tau) - m_X m_Y^*. \tag{A.21}$$

Two WSS processes are considered uncorrelated if $C_{XY}(\tau) = 0$ for all τ, and are considered mutually orthogonal if $R_{XY}(\tau) = 0$ for all τ. If the two processes are uncorrelated, it follows from (A.21) that

$$R_{XY}(\tau) = \langle X(z+\tau)Y^*(z)\rangle = \langle X(z+\tau)\rangle \langle Y^*(z)\rangle = m_X m_Y^*. \tag{A.22}$$

It can be shown that if a process is SSS then it is automatically WSS. It is not true, in general, that if the process is WSS it is SSS.

If a stochastic process is the input to a system with a transfer function, or operator, T, the output is also a stochastic process, i.e.,

$$Y(z) = T[X(z)]. \tag{A.23}$$

A system is called memoryless if its output at a given point $z = z_1$, say $Y(z_1)$ depends only on $X(z_1)$, i.e.,

$$Y(z) = g[X(z)], \tag{A.24}$$

where g is only a function of X. The statistics of Y for a memoryless system can be expressed in terms of the density function of X, namely, f_X, as follows:

$$\langle Y(z)\rangle = \int_{-\infty}^{\infty} g(x) f_X(x; z) dx, \tag{A.25}$$

$$\langle Y(z_1)Y(z_2)\rangle = \int_{-\infty}^{\infty}\int_{-\infty}^{\infty} g(x_1)g(x_2) f_X(x_1, x_2; z_1, z_2) dx_1 dx_2. \tag{A.26}$$

If the system is linear then the operator T will be called L and

$$Y(z) = L[X(z)], \tag{A.27}$$

where the definition of a linear system is given by

$$L\left[a_1X_1(z) + a_2X_2(z)\right] = a_1L\left[X_1(z)\right] + a_2L\left[X_2(z)\right] \tag{A.28}$$

for any $a_1, a_2, X_1(z), X_2(z)$. Note, the output of a linear system is a convolution

$$Y(z) = X(z) * H(z) = \int_{-\infty}^{\infty} X(z-t)H(t)dt, \tag{A.29}$$

where H is the impulse response, i.e.,

$$H(z) = L\left[\delta(z)\right]. \tag{A.30}$$

For any linear system the mean of the output is

$$\langle L\left[X(z)\right]\rangle = L\left[\langle X(z)\rangle\right], \tag{A.31}$$

the cross-correlation between input X and output Y is

$$R_{XY}(z_1, z_2) = L_2\left[R_{XX}(z_1, z_2)\right], \tag{A.32}$$

where the subscript "2" means the system operates on z_2 holding z_1 as a fixed parameter, and the autocorrelation for the output is

$$R_{YY}(z_1, z_2) = L_1\left[R_{XY}(z_1, z_2)\right]. \tag{A.33}$$

For example, if the linear system is a differentiator then the above results can be used to find the statistics of the output. Hence, if

$$L\left[X(z)\right] = X'(z), \tag{A.34}$$

where

$$L\left[\cdot\right] = \frac{d}{dz}\cdot, \tag{A.35}$$

it follows that

$$m_{X'}(z) = L\left[m_X(z)\right] = m'_X(z), \tag{A.36}$$

and the cross-correlation and autocorrelation is expressed as

$$R_{XX'}(z_1, z_2) = L_2 \left[R_{XX}(z_1, z_2) \right] = \frac{\partial R_{XX}(z_1, z_2)}{\partial z_2} \tag{A.37}$$

and

$$R_{X'X'}(z_1, z_2) = L_1 \left[R_{XX'}(z_1, z_2) \right] = \frac{\partial^2 R_{XX}(z_1, z_2)}{\partial z_1 \partial z_2}. \tag{A.38}$$

In the above, and to follow, primes mean differentiation with respect to the argument. If the input process is WSS then the above relations become

$$m_{X'}(z) = L \left[m_X \right] = 0, \tag{A.39}$$

since the mean of the input process is constant. Since the autocorrelation of the input process is a function of only τ, i.e., $R_{XX}(z_1, z_2) = R_{XX}(\tau)$ with $\tau = z_2 - z_1$, then

$$\langle X(z+\tau) X'^*(z) \rangle = R_{XX'}(\tau) = -R'_{XX}(\tau) \tag{A.40}$$

$$\langle X'(z+\tau) X'^*(z) \rangle = R_{X'X'}(\tau) = -R''_{XX}(\tau) \tag{A.41}$$

The previous results can be specialized to give higher order correlations through the relationship

$$\left\langle \frac{\partial^m X(z_1)}{\partial z_1^m} \frac{\partial^n X^*(z_2)}{\partial z_2^n} \right\rangle = (-1)^n \frac{\partial^{m+n} R_{XX}(\tau)}{\partial \tau^{m+n}}. \tag{A.42}$$

If $z_1 = z_2 = z$ then higher order surface derivatives and RMS values can be found using

$$\left\langle \frac{\partial^m X(z)}{\partial z^m} \frac{\partial^n X^*(z)}{\partial z^n} \right\rangle = \left. \frac{\partial^{m+n} R_{XX}(\tau)}{\partial \tau^{m+n}} \right|_{\tau=0} \tag{A.43}$$

and

$$\left\langle \left| \frac{\partial^n X(z)}{\partial z^n} \right|^2 \right\rangle = \left. \frac{\partial^{2n} R_{XX}(\tau)}{\partial z^{2n}} \right|_{\tau=0}, \tag{A.44}$$

respectively.

A.2 Gaussian Stochastic Processes

Gaussian, or Normal, stochastic processes occur frequently in nature, mostly as a result of the central limit theorem which can be stated as follows. Given n independent RVs X_i, their sum is

$$X = X_1 + \cdots + X_n. \tag{A.45}$$

This new RV X has a mean $m = m_1 + \cdots + m_n$ and variance $\sigma^2 = \sigma_1^2 + \cdots + \sigma_n^2$. If X is a continuous RV, the central limit theorem states that as n approaches infinity, the density function of X approaches a Gaussian density function with the above mentioned mean and variance, i.e.,

$$f_X(x) = \frac{1}{\sigma\sqrt{2\pi}} e^{-(x-m)^2/2\sigma^2}. \tag{A.46}$$

Therefore, if the RP under consideration is everywhere a result of a large number of local events, the effects of which are cumulative, then the resulting RP is Gaussian distributed. This is the case with most natural processes which form rough surfaces [10].

A property of Gaussian RPs is that wide sense stationarity implies strict sense stationarity. Thus, if a Gaussian process under consideration has a constant mean and an autocorrelation function which is a function of only the distance between two points then it is automatically SSS. This considerably simplifies the analysis. Another property of a WSS Gaussian RP denoted by X is that X' is also Gaussian, and X and X' at the same point are uncorrelated [9].

For the remainder of this section, the Gaussian stochastic process under consideration will be denoted $D(z)$ and will be taken to be a WSS process having a zero mean and Gaussian autocorrelation. The associated first-order probability density function (PDF) is then

$$f_D(\zeta, z) = \frac{1}{\sigma\sqrt{2\pi}} e^{-\zeta(z)^2/2\sigma^2}, \tag{A.47}$$

where $\zeta(z)$ is one realization of the Gaussian RP $D(z)$ and σ is the RMS value of the RP. The second-order PDF is given by

$$f_D(\zeta_1, \zeta_2; z_1, z_2) = \frac{1}{2\pi\sigma^2\sqrt{1-r^2}} \exp\left\{-\frac{\zeta_1^2 - 2r\zeta_1\zeta_2 + \zeta_2^2}{2\sigma^2(1-r^2)}\right\}, \tag{A.48}$$

where r is the correlation coefficient

$$r = r(\tau) = \frac{R_{DD}(\tau)}{\sigma^2}, \tag{A.49}$$

and $R_{DD}(\tau)$ is the autocorrelation function, which is assumed to be Gaussian

$$R_D(\tau) \equiv R_{DD}(\tau) = \sigma^2 e^{-\tau^2/l^2}. \tag{A.50}$$

The parameter l called the correlation length, and the RMS value of the surface σ, are sufficient to characterize the surface.

Two other important quantities are the characteristic functions defined in (A.14) and (A.15), which reduce to [9]

$$\chi(\omega) = \left\langle e^{j\omega\zeta} \right\rangle = \int_{-\infty}^{\infty} f_D(\zeta, z) e^{j\omega\zeta} d\zeta = e^{-\sigma^2\omega^2/2} \tag{A.51}$$

and

$$\chi_2(\omega_1, \omega_2) = \left\langle e^{j\omega_1\zeta_1} e^{j\omega_2\zeta_2} \right\rangle = \int_{-\infty}^{\infty}\int_{-\infty}^{\infty} f(\zeta_1, \zeta_2; z_1, z_2) e^{j\omega_1\zeta_1 + j\omega_2\zeta_2} d\zeta_1 d\zeta_2$$
$$= e^{-\frac{1}{2}\sigma^2\left[\omega_1^2 + 2r\omega_1\omega_2 + \omega_2^2\right]}. \tag{A.52}$$

For the special case of $\omega_1 = -\omega_2 = \omega$, (A.52) becomes

$$\chi_2(\omega, -\omega) = \left\langle e^{j\omega(\zeta_1 - \zeta_2)} \right\rangle = e^{-\omega^2\sigma^2(1-r)}. \tag{A.53}$$

If ζ_1 and ζ_2 are independent (uncorrelated) then

$$\chi_2(\omega, -\omega) = \left\langle e^{j\omega\zeta_1} \right\rangle \left\langle e^{-j\omega\zeta_2} \right\rangle = \chi(\omega)\chi(\omega)^*, \tag{A.54}$$

which follows from (A.22).

If the Gaussian process is the input to a linear differentiator whose output equals

$$X(z) = D'(z), \tag{A.55}$$

then using (A.39) and (A.40) give

$$\langle D'(z) \rangle = 0 \quad ; \quad R_{D'}(\tau) \equiv R_{D'D'}(\tau) = -R''_D(\tau) \ , \tag{A.56}$$

or, explicitly,

$$R_{D'}(\tau) = \frac{2\sigma^2}{l^2} e^{-\tau^2/l^2} \left[1 - \frac{2\tau^2}{l^2} \right]. \tag{A.57}$$

Assume the output of the above system is the input to a memoryless square-law detector whose output is

$$Y(z) = X^2(z). \tag{A.58}$$

The statistics of Y can be found by noting that for the input process X, $X(z)$ and $X(z+\tau)$ are jointly normal RVs with zero mean and autocorrelation $R_X(\tau) = R_{D'}(\tau)$. Hence,

$$\left\langle X^2(z) X^2(z+\tau) \right\rangle = \left\langle X^2(z) \right\rangle \left\langle X^2(z+\tau) \right\rangle + 2 \left\langle X(z) X(z+\tau) \right\rangle^2 , \tag{A.59}$$

and through use of the Moment Theorem [12], the autocorrelation for the output Y is

$$R_{D'^2}(\tau) \equiv R_Y(\tau) = R_X^2(0) + 2R_X^2(\tau). \tag{A.60}$$

The mean of Y is seen to be

$$m_Y = \left\langle X^2(z) \right\rangle = R_X(0) = \frac{2\sigma^2}{l^2}. \tag{A.61}$$

Also note that the variance of Y is given by

$$\sigma_Y^2 = R_Y(0) = 3R_X^2(0). \tag{A.62}$$

The autocorrelation and variance of D'^2 can now be written explicitly as

$$R_Y(\tau) \equiv R_{D'^2}(\tau) = \frac{4\sigma^4}{l^4}\left\{1 + 2e^{-2\tau^2/l^2}\left[1 - \frac{2\tau^2}{l^2}\right]^2\right\} \tag{A.63}$$

and

$$\sigma_Y^2 = 12\frac{\sigma^4}{l^4}, \tag{A.64}$$

respectively.

APPENDIX B

BAHAR'S FULL WAVE METHOD

The full wave theory for rough surface scattering was first introduced by Bahar [1, 16, 17] to describe scattering by multilayered dielectric structures of arbitrary thickness. The method was applied to a one-dimensionally rough surface with the same geometry as was used in previous sections of this dissertation. It consists of expanding the x and z components of the field in terms of a set of local flat surface basis functions. Maxwell's equations are then written in the form of the telegraphist's equations for the right and left going amplitudes of the scattered fields. Since the fields are expanded in terms of basis functions, the telegraphist's equations become a set of coupled differential equations for the modes. This set of equations is solved by taking the surface slope as a small parameter and using the method of successive approximations, which is the same as assuming there is no mode coupling. Bahar removes the explicit dependence on the surface slope through use of integration by parts and discards the integrated term by assuming it is a negligible edge term. However, since the set of coupled equations is solved by assuming the surface slope is small, the method should only be valid if this condition is met. This method will be called Bahar's original full wave method.

Bahar later attempted to extend his method for the one dimensional surface to solve the problem of scattering from a surface which is rough in two dimensions [18]. He did this by leaving the inverse Fourier transform with respect to y uncompleted, and replaced the one dimensional surface profile $D(z)$ by the two dimensional one $D(y, z)$. This procedure was not justified mathematically by Bahar. However, Collin [3], with slight modifications to Bahar's theory, rigorously obtains Bahar's result for scattering form one- and two-dimensional rough surfaces.

In order to remove the small slope restriction, Bahar introduced a new coordinate system which conforms to the rough surface [18, 19]. In this formulation, angles of incidence and scatter used in the original method are referred to the local normal along the surface. This method will be referred to as Bahar's modified full wave theory. It has been shown that this modified theory does not reduce to the first-order perturbation theory in the limit of small height and slope variation [8] and provides results almost equivalent to those obtained with the Kirchhoff theory for all parameters studied. In order to correct this solution method, Bahar reintroduced the edge term before transforming to the local coordinate system. It was then shown by Collin [20] that this added term for vertical (TM) polarization yields radar cross sections that are more than an order of magnitude larger than when the term was not included. Bahar proceeded next to revise his method to overcome these problems [20] and again removed the edge term, which resulted in his obtaining more acceptable radar cross section calculations. However, this latest full wave method still does not reduce to the first-order perturbation result over its entire range of validity and does not bridge the gap between the regions of validity of the Kirchhoff and first-order perturbation theories [20]. It does, however, agree with the Kirchhoff result for high frequency and small slopes, but for large heights and slopes it produces a large enhancement of the diffuse radar cross section around the specular direction, which is considered to be nonphysical [20].

Experimentally, it was observed that rough surfaces can strongly backscatter [21]. This enhanced backscatter was not predicted by any of the standard first-order theories. In a 1989 paper, Bahar and Fitzwater [22] interpreted data generated by the modified full wave theory for a rough surface with $\epsilon_r = -56.6 - j21.3$ as evidence of backscatter enhancement. In this study, the radar cross section that they obtained was 20 times larger than Kirchhoff results in the backscatter direction. Collin [20] has

subsequently shown that this anomalous enhancement was a result of the assumption that the heights and slopes were uncorrelated and the slopes were perfectly correlated.

Since there is still some confusion as to which of Bahar's full wave theories is correct, this appendix will derive[1] the results for the original full wave theory and explain how it is modified to obtain Bahar's modified full wave theory. For a rigorous treatment of the full wave theory for two dimensional rough surfaces, the reader is referred to the excellent paper by Collin [3].

For the TE case, $E_x = E_z = H_y = 0$, with the same geometry as shown in Figure 2.3, Maxwell's equations reduce to

$$\eta_0 H_x = -\frac{j}{k_0}\frac{\partial E_y}{\partial z} \tag{B.1a}$$

$$\eta_0 H_z = \frac{j}{k_0}\frac{\partial E_y}{\partial x} \tag{B.1b}$$

$$jk_0 E_y = \eta_0 \left\{ \frac{\partial H_x}{\partial z} - \frac{\partial H_z}{\partial x} \right\}. \tag{B.1c}$$

Introducing the notation $g = k_0\eta_0 H_x$, $f = E_y$ and combining (B.1b) with (B.1c) result in a set of coupled differential equations:

$$\frac{\partial f}{\partial z} = jg \tag{B.2a}$$

$$\frac{\partial g}{\partial z} = j\left(k_0^2 f + \frac{\partial^2 f}{\partial x^2}\right). \tag{B.2b}$$

The field quantities are now expressed as a superposition of mode functions, with parameter u, of the form:

$$\psi_u(x,z) = \sin u\,(x - D(z))\,. \tag{B.3}$$

These mode functions are interpreted, for a fixed z value, as local modes of a waveguide with one boundary at infinity. The modal superpositions with a convenient

[1]The derivation in this section will closely follow that of Voronovich [23]

normalization are given by

$$f(x,z) = \frac{2}{\pi}\int_0^\infty F(z,u)\left(k_0^2-u^2\right)^{-1/4} e^{-juD}\sin u\,(x-D)\,du \qquad \text{(B.4a)}$$

$$g(x,z) = \frac{2}{\pi}\int_0^\infty G(z,u)\left(k_0^2-u^2\right)^{1/4} e^{-juD}\sin u\,(x-D)\,du, \qquad \text{(B.4b)}$$

which are considered as field transforms. Using the orthogonality properties of the sine function, the inverse transforms are written as

$$F(z,u) = \left(k_0^2-u^2\right)^{1/4} e^{juD}\int_D^\infty f(x,z)\sin u(x-D)dx \qquad \text{(B.5)}$$

$$G(z,u) = \left(k_0^2-u^2\right)^{-1/4} e^{juD}\int_D^\infty g(x,z)\sin u(x-D)dx. \qquad \text{(B.6)}$$

To transform the set of coupled differential equations, they are multiplied by the mode function $\psi_u(x,z)$ and integrated over x from D to ∞. Using Liebnitz rule, namely,

$$\frac{\partial}{\partial z}\int_D^\infty f(x,z)\sin u\,(x-D)\,dx = \int_D^\infty \frac{\partial f(x,z)}{\partial z}\sin u\,(x-D)\,dx - uD'\int_D^\infty f(x,z)\cos u\,(x-D)\,dx, \qquad \text{(B.7)}$$

the left hand side of (B.2a) becomes

$$\int_D^\infty \frac{\partial f}{\partial z}\sin u\,(x-D)\,dx = \frac{\partial}{\partial z}\int_D^\infty f(x,z)\sin u\,(x-D)\,dx + uD'\int_D^\infty f(x,z)\cos u\,(x-D)\,dx. \qquad \text{(B.8)}$$

By substituting the transform of f and (B.4a) into (B.8) and using the orthogonality relations for the improper integrals involving sines and cosines from Appendix E, i.e., (E.6), (E.7) and (E.8), the transformed version of the left hand side of (B.2a) is deduced as

$$\left\{\frac{\partial F(z,u)}{\partial z} - juD'F(z,u)\right\}\left(k_0^2-u^2\right)^{-1/4} e^{-juD} + \frac{D'}{\pi}\int_0^\infty F(z,u')\left(k_0^2-u'^2\right)^{-1/4} e^{-ju'D}\mathcal{P}\left\{\frac{2uu'}{u'^2-u^2}\right\}du', \qquad \text{(B.9)}$$

where the $\mathcal{P}$ means the principal value of the integral. The right hand side of (B.2a) is transformed in the same way and the complete transformed version of (B.2a) is expressed as

$$\frac{\partial F}{\partial z} + j\left(k_0^2 - u^2\right)^{1/2} G = juD'F + \frac{D'}{\pi}\int_0^\infty F(z,u')\left(\frac{k_0^2-u^2}{k_0^2-u'^2}\right)^{1/4} e^{j(u-u')D}\mathcal{P}\left\{\frac{2uu'}{u'^2-u^2}\right\}du'. \quad \text{(B.10)}$$

The second differential equation (B.2b) is transformed by the same method as used on the first equation (B.2a), except that the term with the second derivative is integrated by parts twice. The result is the transformed version of (B.2b):

$$\frac{\partial G}{\partial z} + j\left(k_0^2 - u^2\right)^{1/2} F = juD'G + \frac{D'}{\pi}\int_0^\infty G(z,u')\left(\frac{k_0^2-u^2}{k_0^2-u'^2}\right)^{1/4} e^{j(u-u')D}\frac{2uu'\mathcal{P}}{u'^2-u^2}du'. \quad \text{(B.11)}$$

Introducing the new variables

$$a(z,u) = F(z,u) + G(z,u) \quad , \quad b(z,u) = F(z,u) - G(z,u), \quad \text{(B.12)}$$

into the coupled integro-differential equations (B.10) and (B.11) yields the generalized telegraphist's equations:

$$\frac{da}{dz} + j\left(k_0^2 - u^2\right)^{1/2} a = juD'a + \frac{D'}{\pi}\int_0^\infty e^{j(u-u')D}\frac{uu'\mathcal{P}}{u'^2-u^2}\left[T_1(u,u')a + T_2(u,u')b\right]du' \quad \text{(B.13)}$$

and

$$\frac{db}{dz} + j\left(k_0^2 - u^2\right)^{1/2} b = juD'b + \frac{D'}{\pi}\int_0^\infty e^{j(u-u')D}\frac{uu'\mathcal{P}}{u'^2-u^2}\left[T_2(u,u')a + T_1(u,u')b\right]du', \quad \text{(B.14)}$$

where

$$T_1(u,u') = \frac{\beta(u)+\beta(u')}{\sqrt{\beta(u)\beta(u')}}, \tag{B.15}$$

$$T_1(u,u') = \frac{\beta(u)-\beta(u')}{\sqrt{\beta(u)\beta(u')}}, \tag{B.16}$$

and, as in previous sections,

$$\beta(u) = \sqrt{k_0^2 - u^2}. \tag{B.17}$$

If equations (B.13) and (B.14) are solved for a flat surface, $D = 0$, the solutions a and b are waves propagating in the positive and negative z directions, respectively. For a rough surface, the equations can be solved by the method of successive approximations, taking the surface slope $D'(z)$ to be small for all z. An initial approximation for the total field is constructed by adding together an incident plane wave and a plane wave reflected by an infinite conducting flat surface that is adjusted to the local surface height $x = D(z)$. This field is the same as the primary field used in Chapter 2 and is

$$E_y^p \equiv f_0 = E_0^i e^{-j\beta_0 z + ju_0 D} \sin u\,(x - D)\,. \tag{B.18}$$

The transformed primary wave is expressed as

$$F_0 = \frac{\pi}{2} E_0^i e^{-j\beta_0 z + j2u_0 D} \left(k_0^2 - u_0^2\right) \delta(u - u_0) \tag{B.19}$$

and the amplitude terms are $a_0 = 2F_0$ and $b_0 = 0$. By the method of successive approximations, the first-order solution is found by substituting $a = a_0$ into the right side of (B.13) and $a = a_1$ in the left side, i.e.,

$$\frac{da_1}{dz} + j\beta(u)a_1 = Q(z,u) \tag{B.20}$$

where

$$Q(z,u) = \pi E_0^i \sqrt{\beta_0} e^{-j\beta_0 z + j2u_0 D} D' \left[ju\delta(u-u_0) + \frac{1}{\pi} e^{j(u-u_0)D} \frac{uu_0 \mathcal{P}}{u^2 - u_0^2} T_1(u,u_0)\right]. \tag{B.21}$$

Since the amplitude a represents a wave traveling to the right, $a = 0$ for the region $z < L$. Using this condition, the solution to (B.20) for $z > L$ is

$$a_1 = e^{-j\beta z} \int_{-L}^{L} Q(z', u) e^{j\beta z'} dz'. \tag{B.22}$$

The delta function term in (B.21) represents the specularly reflected wave and can be ignored as long as the solution is not examined in the specular direction. The first-order field is now inverse transformed to yield

$$E_y^{(1)} \equiv f_1(x, z) = \frac{1}{\pi} \int_0^{\infty} a_1(z, u) \sqrt{\beta} e^{-juD} \sin u\,(x - D)\,. \tag{B.23}$$

Since the field is being considered for $z > L$, the surface height in this region is zero and the field in (B.23) is given explicitly as

$$f_1(x, z) = \frac{E_0^i}{\pi} \int_0^{\infty} \int_{-L}^{L} \widetilde{D}' e^{-j(\beta_0 - \beta)z'} e^{j(u+u_0)\widetilde{D}} dz' \frac{uu_0}{\beta_0 - \beta} e^{-j\beta z} \sin uxdu. \tag{B.24}$$

where $\widetilde{D} = D(z')$. An integration by parts is performed to remove the explicit dependence on $\widetilde{D}'$ by noting that

$$\widetilde{D}' e^{j(u+u_0)D} = \frac{1}{j\,(u + u_0)} \frac{d}{dz} \left[e^{j(u+u_0)\widetilde{D}} \right]. \tag{B.25}$$

Thus,

$$\int_{-L}^{L} \widetilde{D}' e^{-j(\beta_0 - \beta)z'} e^{j(u+u_0)\widetilde{D}} dz' = \frac{e^{j(u+u_0)\widetilde{D}} e^{-j(\beta_0 - \beta)z'}}{j\,(u + u_0)} \Bigg|_{-L}^{L} + \frac{\beta_0 - \beta}{u + u_0} \int_{-L}^{L} e^{j(u+u_0)\widetilde{D}} e^{-j(\beta_0 - \beta)z'} dz'. \tag{B.26}$$

The integrated term is rewritten as an integral, i.e.,

$$\frac{e^{j(u+u_0)\widetilde{D}} e^{-j(\beta_0 - \beta)z'}}{j\,(u + u_0)} \Bigg|_{-L}^{L} = -\frac{\beta_0 - \beta}{u + u_0} \int_{-L}^{L} e^{-j(\beta_0 - \beta)z'} dz'. \tag{B.27}$$

As mentioned previously, in Bahar's original formulation of the full wave theory he discarded this "edge" term as negligible, but later found it to be important. Therefore, it is included in this example The scattered field is now written as

$$f_1(x,z) = -\frac{E_0^i}{\pi}\frac{uu_0}{u_0+u}\int_0^{\infty}\int_{-L}^{L}\left\{1-e^{j(u+u_0)\tilde{D}}\right\}e^{-j(\beta_0-\beta)z'}dz'e^{-j\beta z}\sin uxdu. \tag{B.28}$$

To obtain the far field, the u integration is approximated by using stationary phase as was done in Chapter 2, and the resulting expression becomes

$$E_y^{(1)ff}(x,z) = \frac{k_0}{\sqrt{2\pi}}G_0A_0^iR^{TE}(\phi,\phi_0), \quad 0\le\phi<\pi/2, \tag{B.29}$$

where

$$G_0 = \frac{e^{-j[k_0\rho-\pi/4]}}{\sqrt{k_0\rho}}, \tag{B.30}$$

$$A_0^i = \frac{E_0^i}{2j}, \tag{B.31}$$

and

$$R_B^{TE}(\phi,\phi_0) = \frac{2\cos\phi\cos\phi_0}{\cos\phi+\cos\phi_0}\int_{-L}^{L}\left\{1-e^{jk_0D_0(\cos\phi+\cos\phi_0)}\right\}e^{jk_0z_0(\sin\phi-\sin\phi_0)}dz_0. \tag{B.32}$$

The angles ϕ and ϕ_0 are defined in Figure 2.5. If the analysis is performed for $z<-L$, the same expression is obtained, which implies (B.29) is valid for $-\pi/2\le\phi\le\pi/2$.

The method outlined above can be performed for the TM case and results in a scatter pattern of the form

$$R_B^{TM} = \frac{2\left(1-\sin\phi\sin\phi_0\right)}{\cos\phi+\cos\phi_0}\int_{-L}^{L}\left\{1-e^{jk_0D_0(\cos\phi+\cos\phi_0)}\right\}e^{jk_0z_0(\sin\phi-\sin\phi_0)}dz_0. \tag{B.33}$$

As was mentioned above, Bahar later modified this formula by referring the angles ϕ and ϕ_0 to the local normal (see Figure B.1), i.e.,

$$\phi^{\gamma} = \phi+\gamma, \tag{B.34}$$

and

$$\phi_0^\gamma = \phi - \gamma, \tag{B.35}$$

where the angle γ is defined by

$$\tan\gamma = D'(z). \tag{B.36}$$

The integration must now be performed along the rough surface, which means dz_0

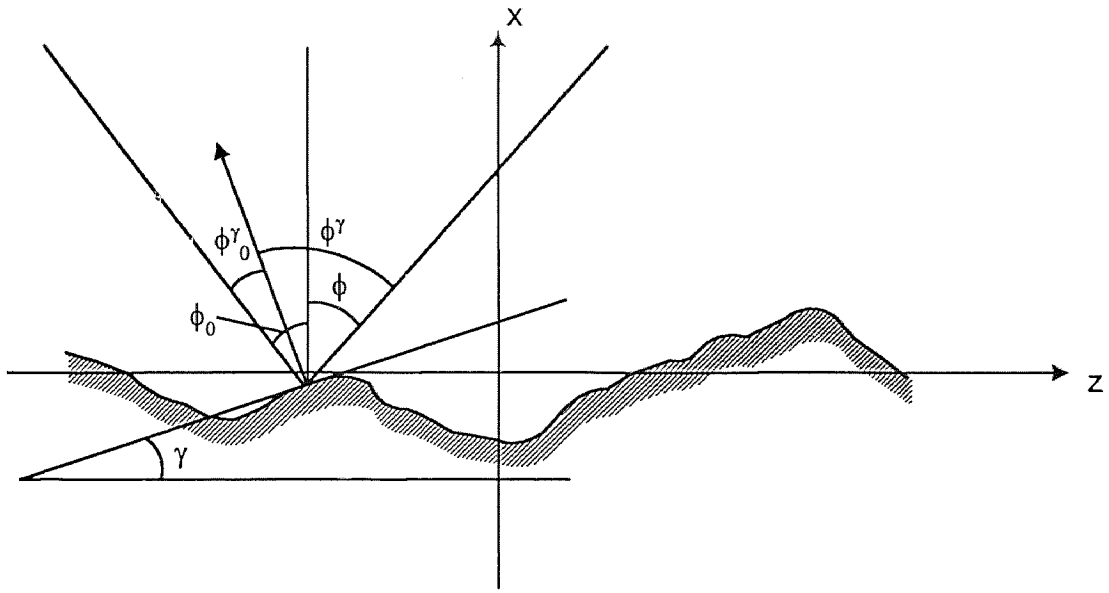

Figure B.1 Referring incident and scatter angles to local normal.

must be replaced by an element of length along the surface:

$$dz_0 \rightarrow \frac{dz_0}{\cos\gamma} = dz_0\sqrt{1 + D_0'^2}. \tag{B.37}$$

The scatter pattern now becomes

$$R_B = \int_{-L}^{L} S\left(\phi^\gamma, \phi_0^\gamma\right)\left\{1 - e^{jk_0 D_0(\cos\phi + \cos\phi_0)}\right\} e^{jk_0 z_0(\sin\phi - \sin\phi_0)}\frac{dz_0}{\cos\gamma}, \tag{B.38}$$

where

$$S\left(\phi^\gamma, \phi_0^\gamma\right) = \begin{cases} 2\cos\phi^\gamma\cos\phi_0^\gamma / \left(\cos\phi^\gamma + \cos\phi_0^\gamma\right) = S^{TE} \\ 2\left(1 - \sin\phi^\gamma\sin\phi_0^\gamma\right) / \left(\cos\phi^\gamma + \cos\phi_0^\gamma\right) = S^{TM} \end{cases}. \tag{B.39}$$

The statistical analysis of the radar cross section for this modified full wave method is particularly difficult and requires use of conditional probability density functions. Since Thorsos and Winebrenner [8] have shown that this method does not reduce to the first-order perturbation results, and because of other shortcomings of this method [20], it will not be considered here.

APPENDIX C
KIRCHHOFF (PHYSICAL OPTICS) METHOD

The most commonly used theory for predicting rough surface scattering is the physical optics, or Kirchhoff, method[1]. The reason the method is so popular is its simplicity of use and its validity over a fairly wide range of surface parameters. The method consists of using the Kirchhoff approximation of the boundary conditions which are then used in the Helmholtz integral.

The notation for this section is basically the same as that used for the previous sections, i.e., the propagation vector always lies in the xz plane, $\boldsymbol{\rho}$ is the radius vector

$$\boldsymbol{\rho} = x\hat{\mathbf{x}} + z\hat{\mathbf{z}}. \tag{C.1}$$

The vector from the origin to the point (D_0, z_0) on the surface S_0 is

$$\boldsymbol{\rho}_0 = D(z_0)\hat{\mathbf{x}} + z_0\hat{\mathbf{z}}, \tag{C.2}$$

and the vector from the point (D_0, z_0) on the surface S_0 to the observation point (x, z) is

$$\mathbf{R} = (x - D_0)\hat{\mathbf{x}} + (z - z_0)\hat{\mathbf{z}}, \tag{C.3}$$

where $D_0 = D(z_0)$. The angle of incidence is measured from the x axis to the incident propagation vector $\mathbf{k}^i$ in a counter-clockwise direction and is denoted by ϕ_0; the scattering angle ϕ is measured from the x axis to the scattered propagation vector $\mathbf{k}$ in a clockwise direction as shown in Figure C.1 for a finite scatterer, where

$$\mathbf{k}^i = -\hat{\mathbf{x}}k_0 cos\phi_0 + \hat{\mathbf{z}}k_0 sin\phi_0 \tag{C.4a}$$

$$\mathbf{k} = +\hat{\mathbf{x}}k_0 cos\phi + \hat{\mathbf{z}}k_0 sin\phi \tag{C.4b}$$

$$|\mathbf{k}| = |\mathbf{k}^i| = k_0 = \omega\sqrt{\mu_0\epsilon_0} \tag{C.4c}$$

[1]The material in this section essentially follows the procedure outlined in Beckmann and Spiziccino [9].

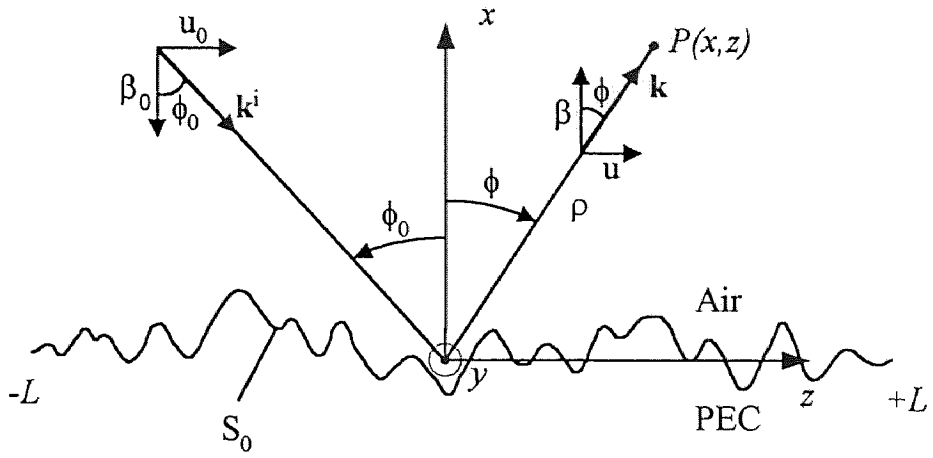

Figure C.1 Finite one-dimensional rough surface S_0 with incident and scattered angles illustrated.

An incident electric field is assumed to be expressed as

$$\mathbf{E}^i = \hat{\mathbf{e}} E_0^i e^{-j\mathbf{k}^i \cdot \rho}, \tag{C.5}$$

where for TE (or horizontal) polarization $\hat{\mathbf{e}} = +\hat{\mathbf{y}}$, and for TM (or vertical) polarization $\hat{\mathbf{e}} = \hat{\mathbf{x}} \cos\phi + \hat{\mathbf{z}} \sin\phi$ with the incident $\mathbf{H}$ field in the $+\hat{\mathbf{y}}$ direction. Henceforth, only the scalar portion of $\mathbf{E}^i$ in (C.5) will be used; a superscript "+" will refer to the TM case and a superscript "-" to the TE case. A time dependence of $e^{j\omega t}$ is assumed and suppressed. If P is the observation point and $R = |\mathbf{R}|$ is the distance from a point (D_0, z_0) on S_0 to the observation point P then the scattered field from a finite surface is obtained using the Helmholtz integral [24],

$$E^s(P) = -\int_{-L}^{L} \left[\psi \frac{\partial E}{\partial n} - E \frac{\partial \psi}{\partial n} \right] dS_0, \tag{C.6}$$

where E is the total field above the surface and

$$\psi = -\frac{j}{4} H_0^{(2)}(k_0 R), \tag{C.7}$$

which is the two-dimensional free-space Green's function. If the observation point is removed to the far-field (Fraunhofer zone), i.e., $R \to \infty$, then the asymptotic form

of the Hankel function

$$H_0^{(2)}(k_0R) \sim \sqrt{\frac{2}{\pi}}\frac{e^{-jk_0R+j\pi/4}}{\sqrt{k_0R}} \quad , \qquad k_0\rho \to \infty, \tag{C.8}$$

is used along with the parallel ray approximation (illustrated in Figure C.2)

$$k_0R \simeq k_0\rho - \mathbf{k}\cdot\boldsymbol{\rho}_0, \tag{C.9}$$

to give the far-field form of the Green's function which is

$$\psi \sim -\frac{j}{2\sqrt{2\pi}}G_0e^{j\mathbf{k}\cdot\boldsymbol{\rho}_0}, \tag{C.10}$$

where

$$G_0 = \frac{e^{-j[k_0\rho-\pi/4]}}{\sqrt{k_0\rho}}. \tag{C.11}$$

To obtain the scattered field $E^s(P)$, the integral in (C.6) is evaluated, where E and

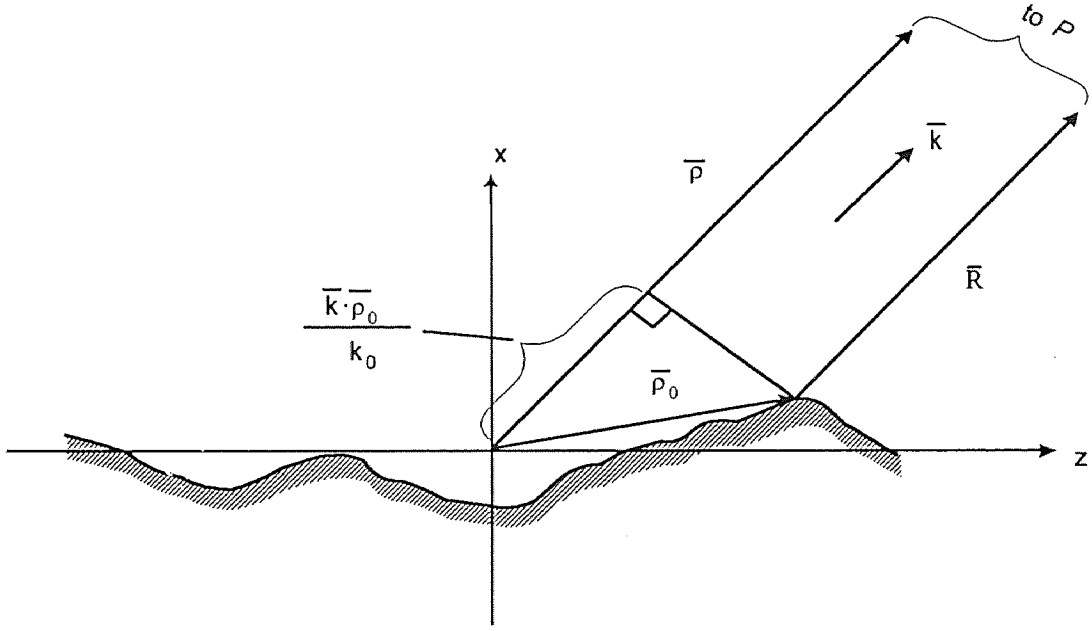

Figure C.2 The parallel ray approximation.

$\partial E/\partial n$ are the field and its normal derivative on the surface S_0. In general, these two quantities are unknown.

The Kirchhoff or Physical Optics approximation consists of approximating the values of E and $\partial E/\partial n$ on S_0 by the field that would be present on the infinite tangent plane at that point (Figure C.3) and then evaluating (C.6). This approximation

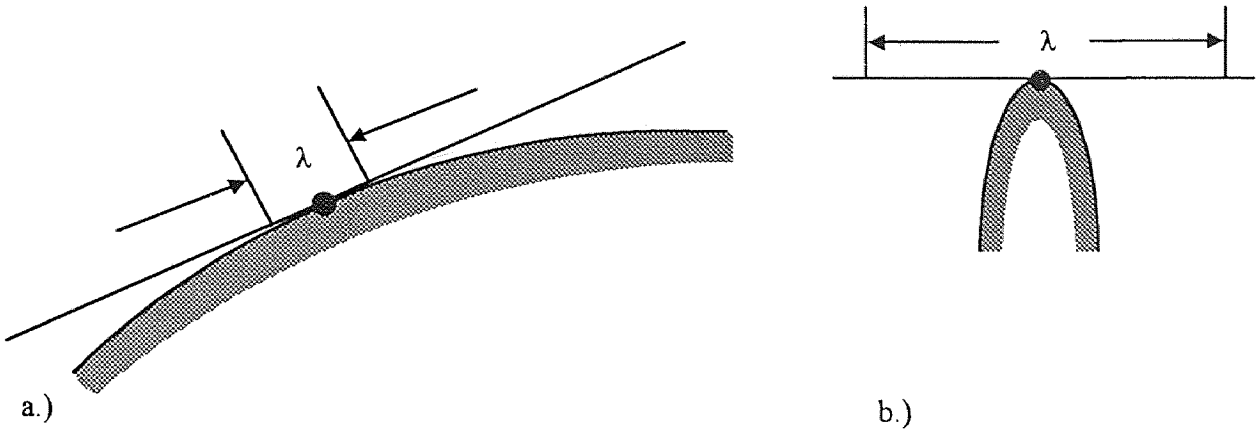

Figure C.3 Tangent plane at a specific point on a rough surface. (a) Radius of curvature is large compared to wavelength. (b) Radius of curvature is small compared to wavelength.

will obviously be very good when the radius of curvature of the irregularities is large compared with the wavelength, but will be inaccurate if the roughness includes sharp edges or points. Using this approximation, the field on S_0 is

$$E|_S = (1+\Gamma)E^i \tag{C.12a}$$

$$\left.\frac{\partial E}{\partial n}\right|_S = -j\mathbf{k}^i \cdot \mathbf{n}(1-\Gamma)E^i \tag{C.12b}$$

where $\mathbf{n}$ is the normal to the surface at the point under consideration and Γ is the reflection coefficient of a smooth infinite plane, i.e., for the case of a perfectly conducting surface, $\Gamma^+ = 1$ for the TM case and $\Gamma^- = -1$ for the TE case. Equation (C.12b) is obtained by differentiating the incident and reflected fields.

Substituting (C.10) and (C.12a,b) into (C.6) gives the scattered field at P :

$$E_s = \frac{E_0^i}{2\sqrt{2\pi}} G_0 \int_{-L}^{L} (\Gamma\mathbf{v} - \mathbf{p}) \cdot \mathbf{n} e^{-j\mathbf{v}\cdot\boldsymbol{\rho}_0} dS_0, \tag{C.13}$$

where

$$\mathbf{v} = -k_0(cos\phi_0 + cos\phi)\hat{\mathbf{x}} + k_0(sin\phi_0 - sin\phi)\hat{\mathbf{z}} \tag{C.14a}$$

$$\mathbf{p} = k_0(cos\phi - cos\phi_0)\hat{\mathbf{x}} + k_0(sin\phi_0 + sin\phi)\hat{\mathbf{z}} \tag{C.14b}$$

$$\mathbf{n} = \frac{[\hat{\mathbf{x}} - D'(z_0)\hat{\mathbf{z}}]}{\sqrt{1 + D'^2(z_0)}} \tag{C.14c}$$

$$dS_0 = \sqrt{1 + D'^2(z_0)}dz_0 \tag{C.14d}$$

Equation (C.13) may be written for a finite surface extending from $[-L, L]$ as

$$E_s = -\frac{k_0}{\sqrt{2\pi}} G_0 \frac{E_0^i}{2} \int_{-L}^{L} (aD_0' - b)\, e^{-jv_z z_0 - jv_x D_0} dz_0, \tag{C.15}$$

where $D_0 \equiv D(z_0)$, v_x and v_z are the x and z components respectively of $\mathbf{v}$, and

$$a = (1 - \Gamma)sin\phi_0 + (1 + \Gamma)sin\phi, \tag{C.16}$$

$$b = (1 + \Gamma)cos\phi - (1 - \Gamma)cos\phi_0. \tag{C.17}$$

Integration by parts is performed on (C.15) by noting that

$$aD_0' e^{-jv_x D_0} = j\frac{a}{v_x}\frac{d}{dz_0}\left[e^{-jv_x D_0}\right]. \tag{C.18}$$

Thus,

$$E_s = -\frac{k_0}{\sqrt{2\pi}} G_0 E_0^i \left\{ \frac{1}{2} \int_{-L}^{L} \left(\frac{av_z}{v_x} + b \right) e^{-jv_z z_0 - jv_x D_0} dz_0 + j\frac{a}{v_x} e^{-jv_z z_0 - jv_x D_0} \Big|_{-L}^{L} \right\}. \tag{C.19}$$

Employing the same normalization as used in (2.28), the scatter pattern is seen to be the negative of the term in the large brackets, i.e.,

$$R^{\pm}(\phi, \phi_0) = \pm\frac{1 + cos(\phi + \phi_0)}{cos\phi + cos\phi_0} \int_{-L}^{L} e^{-jk_0 z_0(sin\phi_0 - sin\phi) + jk_0 D_0(cos\phi_0 + cos\phi)} dz_0 + e^{\pm}(L) \tag{C.20}$$

where,

$$e^{\pm}(L) = -j\,\frac{2sin\phi^{\pm}}{k_0(cos\phi_0 + cos\phi)} e^{-jk_0 z_0(sin\phi_0 - sin\phi) + jk_0 D_0(cos\phi_0 + cos\phi)} \Big|_{-L}^{L} \tag{C.21}$$

with $\phi^+ = \varphi$ and $\phi^- = \phi_0$ represents "edge" effects. It has been rigorously shown that these "edge" effects go to zero if $\lambda \ll L$ [8]. The scatter pattern for a finite rough surface of length $2L$ can, therefore, be written as

$$R^{\pm}(\phi,\phi_0) = \pm\frac{1+cos(\phi+\phi_0)}{cos\phi+cos\phi_0}\int_{-L}^{L} e^{-jk_0z_0(sin\phi_0-sin\phi)+jk_0D_0(cos\phi_0+cos\phi)}dz_0 \tag{C.22}$$

where, again, the "+" superscript means the TM case and the "-" means the TE case. It should be noted that in the full wave case, the surface under consideration is a finite rough surface of length $2L$ with a flat surface ($D(z) = 0$) in the region $|z| > L$.

The scatter pattern for the full wave case is obtained by subtracting from the approximate field (first-order field), the incident field and specularly reflected field from an infinite flat surface. Therefore, the Kirchhoff scatter pattern in (C.22) must be modified in order for a comparison to be made to the full wave solution. If the original geometry (see Figure 2.1) is considered with an incident plane wave as the excitation, the total field above the conducting surface is

$$\mathbf{E}^t = \mathbf{E}^i + \mathbf{E}^s. \tag{C.23}$$

The field scattered by a flat metal plate of length $2L$ centered about the origin, $\mathbf{E}^f$, is added to and subtracted from (C.23) to produce

$$\mathbf{E}^t = \mathbf{E}^i + \mathbf{E}^f + \mathbf{E}^s - \mathbf{E}^f. \tag{C.24}$$

The scattered field $\mathbf{E}^s$ can now be written as the sum of two fields, one scattered by the finite rough surface in the region $|z| \leq L$ denoted $\mathbf{E}^L$, and one scattered by the flat surface in the region $|z| > L$ denoted $\mathbf{E}^\infty$. Thus,

$$\mathbf{E}^t = \mathbf{E}^i + \mathbf{E}^f + \mathbf{E}^\infty + \mathbf{E}^L - \mathbf{E}^f \tag{C.25}$$

Note that $\mathbf{E}^f + \mathbf{E}^\infty$ is the field specularly reflected from an infinite flat conducting surface which is designated $\mathbf{E}^r$. The field needed to calculate the scatter pattern $\mathbf{E}^{sp}$

is equal to the total field minus the incident and specularly reflected fields, i.e.,

$$\mathbf{E}^{sp} = \mathbf{E}^{t} - \mathbf{E}^{i} - \mathbf{E}^{r} = \mathbf{E}^{L} - \mathbf{E}^{f}. \tag{C.26}$$

The scatter pattern for $\mathbf{E}^{L}$ is given in (C.22) and the scatter pattern for $\mathbf{E}^{f}$ is obtained by setting $D_0 = 0$ in (C.22). Therefore, the scatter pattern obtained using the Kirchhoff approximation for the geometry in Figure 2.1 is

$$R_K^{\pm}(\phi, \phi_0) = \mp \frac{1 + cos(\phi + \phi_0)}{cos\phi + cos\phi_0} \int_{-L}^{L} \left\{1 - e^{+jk_0 D_0 (cos\phi_0 + cos\phi)}\right\} e^{-jk_0 z_0 (sin\phi_0 - sin\phi)} dz_0. \tag{C.27}$$

APPENDIX D

FIRST ORDER PERTURBATION METHOD

The small perturbation method was first introduced in 1951 by Stephen O. Rice [25] for the solution of the problem of scattering of electromagnetic waves by slightly rough surfaces. The solution is obtained by expanding the scattered field in a perturbation series and satisfying the boundary conditions to the first-order. In the aforementioned paper by Rice, the solution is formulated for the three-dimensional case, with the roughness on a finite patch. The solution for the two-dimensional case can be constructed from the three-dimensional solution by restricting the source and observation points to the xz-plane (see Figure D.1) and using the $2-D$

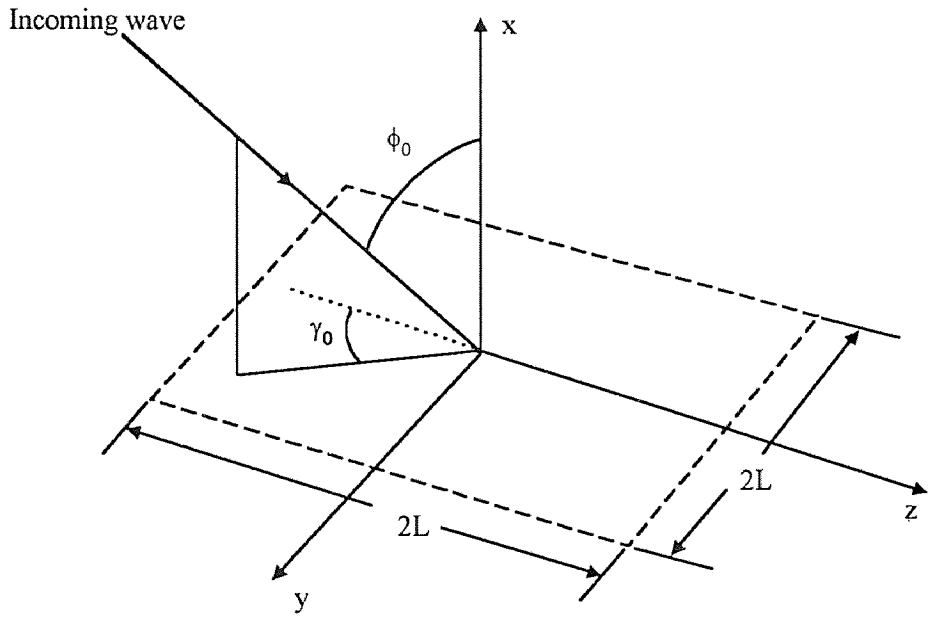

Figure D.1 Scattering geometry for a two-dimensionally rough surface.

Green's function to obtain the far field. However, it is instructive to obtain the two-dimensional solution by assuming no y dependence from the outset. In this appendix, the $2-D$ analysis will be performed for the TE case.

If the surface is taken to be a one-dimensionally rough surface (see Figure 2.5) with height $D(z)$, the conditions under which the perturbation method is applicable can be written as

$$|k_0 D(z)\cos\phi_0| \ll 1 \quad ; \quad |D'(z)| \ll 1. \tag{D.1}$$

Since the TE case is being considered ($E_x = E_z = H_y = 0$), Maxwell's equations become

$$\frac{\partial E_y}{\partial z} = jk_0\eta_0 H_x \tag{D.2}$$

$$\frac{\partial E_y}{\partial x} = -jk_0\eta_0 H_z \tag{D.3}$$

$$jk_0 E_y = \eta_0\left[\frac{\partial H_x}{\partial z} - \frac{\partial H_z}{\partial x}\right] \tag{D.4}$$

where $\eta_0 = \sqrt{\mu_0/\epsilon_0}$ and $k_0 = \omega\sqrt{\mu_0\epsilon_0}$. Take the same incident field as used in all the previous methods, i.e.,

$$E_y^i(x,z) = E_0^i e^{-j\beta_0 z + ju_0 x}, \tag{D.5}$$

where $\beta_0 = k_0\sin\phi_0$ and $u_0 = k_0\cos\phi_0$. The field reflected by a smooth surface of infinite extent is

$$E_y^r(x,z) = -E_0^i e^{-j\beta_0 z - ju_0 x}. \tag{D.6}$$

The total field in the region above the rough surface $x \geq D(z)$ is assumed to be

$$E_y(x,z) = E_y^i + E_y^r + E_y^s = 2jE_0^i e^{-j\beta_0 z}\sin u_0 x + E_y^s. \tag{D.7}$$

Since the rough surface is of finite length $2L$, the scattered field can be represented by a Fourier series in the z direction:

$$E_y^s(x,z) = \sum_{n=-\infty}^{\infty} A_n E(x,z;\nu) \tag{D.8a}$$

$$E(x,z;\nu) = \exp\left[-j(\pi/L)(\nu+n)z - jb(n;\nu)x\right], \tag{D.8b}$$

provided the dimension L is taken to be large. Since E_y^s satisfies the Helmholtz equation, $b(n;\nu)$ satisfies

$$\left[\frac{\pi}{L}(\nu+n)\right]^2 + b^2(n;\nu) = k_0^2. \tag{D.9}$$

For purposes of coefficient matching, the incident wavenumber β_0 is defined by the integrer ν as

$$\beta_0 = (\pi/L)\nu; \tag{D.10}$$

this means that β_0 is restricted to discrete values, but as L becomes large can take on any value.

It should be noted that (D.8a) contains only waves propagating in the $+x$ direction (outgoing) and not incoming propagating waves. As a result of this omission (D.8a) is not complete and cannot be considered valid in the regions between the peaks and valleys of the rough surface unless the incoming propagating waves are added. However, numerical investigation[26] shows that as long as the slope of the surface is small (<0.4) and the field is examined at a point sufficiently far from the surface, (D.8a) gives a good approximation. The approximation that the scattered field is represented by only outgoing propagating waves is the Rayleigh hypothesis.

The boundary condition that the tangent electric field be zero on the surface is

$$\hat{\mathbf{n}} \times \mathbf{E}|_{x=D(z)} = \mathbf{0} \quad ; \quad \hat{\mathbf{n}} = \left[\hat{\mathbf{x}} - D'(z)\hat{\mathbf{z}}\right] / \sqrt{1 + D'^2(z)} \tag{D.11}$$

and for the TE case becomes

$$E_y(x = D(z), z) = 0. \tag{D.12}$$

Since a perturbation solution for slightly rough surfaces is sought, the small parameter can be either the height or slope of the surface :

$$\varepsilon \sim |k_0 D| \sim |D'(z)|\,. \tag{D.13}$$

In general, the surface normal, and hence the boundary condition in (D.11), is expanded in powers of the small parameter ε; however, for the TE case this is not necessary. The Fourier coefficient in (D.8a) can also be expanded in a power series in terms of ε :

$$A_n = A_n^{(1)} + A_n^{(2)} + \cdots . \tag{D.14}$$

Note that for the case of a smooth flat surface ($D(z) \to 0$), the scattered field should be zero; hence, it is at least of order ε. Therefore, $A_n^{(1)}$ is order ε, $A_n^{(2)}$ is order ε^2, and so on.

The exponential involving x in (D.8a) is now expanded in a Taylor series about $x = 0$, as is the incident plus reflected field (D.7):

$$E(x,z;\nu) = E(0,z;\nu)\left(1 - jb(n;\nu)x + \cdots\right) \tag{D.15}$$

$$E_y^i(x,z) + E_y^r(x,z) = 2jE_0^i e^{-j\beta_{0z}}\left(u_0 x - \frac{(u_0 x)^3}{3!} + \cdots\right). \tag{D.16}$$

The boundary condition (D.12) can now be written as

$$2jE_0^i e^{-j\beta_{0z}}\left(u_0 D + \cdots\right) + \sum_{n=-\infty}^{\infty}\left[A_n^{(1)} + A_n^{(2)} + \cdots\right] E(0,z;\nu)\left(1 - jb(n;\nu)D + \cdots\right) = 0. \tag{D.17}$$

Keeping only terms up to $O(\varepsilon)$:

$$2jE_0^i e^{-j\beta_{0z}} u_0 D + \sum_{n=-\infty}^{\infty} A_n^{(1)} e^{-j(\pi/L)(\nu+n)z} = 0. \tag{D.18}$$

The surface height is now expanded in a Fourier series:

$$D(z) = \sum_{n=-\infty}^{\infty} P(n) e^{-j(\pi/L)nz}, \tag{D.19}$$

and coefficients for each n are equated, giving

$$A_n^{(1)} = -2ju_0 E_0^i P(n), \tag{D.20}$$

remembering that

$$e^{-j(\pi/L)\nu z} = e^{-j\beta_{0z}}. \tag{D.21}$$

The total field to order ε becomes

$$E_y \sim 2jE_0^i e^{-j\beta_0 z}\sin u_0 x - 2ju_0 E_0^i \sum_{n=-\infty}^{\infty} P(n)e^{-j(\pi/L)(\nu+n)z}e^{-jb(n;\nu)x}. \tag{D.22}$$

The expression for the scattered far-field is obtained using the Helmholtz integral (C.6), which for the case of a one dimensional surface with the electric field equal to zero on the surface is

$$E_y^{sff}(x,z) = \int_{-L}^{L} \psi_{2-D}(x,z;x_0,z_0)\frac{\partial E_y(D_0,z_0)}{\partial n}\sqrt{1+D'^2(z_0)}dz_0, \tag{D.23}$$

where

$$\psi_{2-D} = -\frac{j}{4}H_0^{(2)}\left(k_0\left|\boldsymbol{\rho}-\boldsymbol{\rho}_0\right|\right); \tag{D.24}$$

$\boldsymbol{\rho}$ and $\boldsymbol{\rho}_0$ are defined in (C.1) and (C.2), respectively. By using the asymptotic expansion of the Hankel function and the parallel ray approximation (see Figure C.2),

$$\psi_{2-D} \sim -\frac{j}{2\sqrt{2\pi}}G_0 e^{j\mathbf{k}\cdot\boldsymbol{\rho}_0}, \tag{D.25}$$

where the term G_0 is the $2-D$ asymptotic Green's function

$$G_0 = \frac{e^{-j[k_0\rho-\pi/4]}}{\sqrt{k_0\rho}}, \tag{D.26}$$

$\mathbf{k}\cdot\boldsymbol{\rho}_0 = k_0 D_0\cos\phi + k_0 z_0\sin\phi$ (see (C.2) and (C.4b)) and $D_0 = D(z_0)$. The normal derivative of E_y can be calculated using the relation

$$\frac{\partial E_y}{\partial n} = \hat{\mathbf{n}}\cdot\nabla E_y = \frac{1}{\sqrt{1+D'^2}}\left[\frac{\partial E_y}{\partial x} - D'\frac{\partial E_y}{\partial z}\right]. \tag{D.27}$$

Evaluating the factors in (D.27) on the surface $x = D_0$, $z = z_0$ gives

$$\frac{\partial E_y}{\partial x} \sim \cdot\ 2ju_0 E_0^i e^{-j\beta_0 z_0} - 2u_0 E_0^i \sum_{n=-\infty}^{\infty} b(n;\nu)P(n)e^{-j(\pi/L)(\nu+n)z_0} \tag{D.28a}$$

$$\frac{\partial E_y}{\partial z} \sim 2j\beta_0 D_0 E_0^i e^{-j\beta_0 z_0} - 2\frac{\pi}{L}u_0 E_0^i \sum_{n=-\infty}^{\infty}(\nu+n)P(n)e^{-j(\pi/L)(\nu+n)z_0} \tag{D.28b}$$

Since all the terms in the above expressions except the first one in (D.28a) are at least order ε, only the first is kept, which from (D.23) produces

$$E_y^{sff} \sim -\frac{k_0}{\sqrt{2\pi}} G_0 E_0^i \frac{2u_0}{k_0} \int_{-\infty}^{\infty} e^{jk_0 D_0 \cos\phi} e^{-jk_0 z_0(\sin\phi_0 - \sin\phi)} dz_0. \tag{D.29}$$

The exponential involving D_0 is now expanded in a Taylor series, ignoring terms of order greater than ε, yields

$$E_y^{sff} \sim -\frac{k_0}{\sqrt{2\pi}} G_0 E_0^i \frac{2u_0}{k_0} \int_{-\infty}^{\infty} (1 + jk_0 D_0 \cos\phi)\, e^{-jk_0 z_0(\sin\phi_0 - \sin\phi)} dz_0. \tag{D.30}$$

The above expression is the field scattered by a finite metal strip of rough surface as depicted in Figure C.1. In order to compare this result to the full wave result, which is the field scattered by a finite rough strip surrounded by a flat plate, the field scattered by a finite metal flat plate over $|z| \leq L$ needs to be subtracted from (D.30) (see Appendix C for a more detailed explanation). This is done by subtracting from (D.30) the same expression with $D_0 = 0$. Thus,

$$E_y^{sff} \sim -\frac{k_0}{\sqrt{2\pi}} G_0 E_0^i 2jk_0 \cos\phi_0 \cos\phi \int_{-\infty}^{\infty} D_0 e^{-jk_0 z_0(\sin\phi_0 - \sin\phi)} dz_0. \tag{D.31}$$

Normalizing the field expression gives the scatter pattern:

$$R_P^{TE}(\phi, \phi_0) = -2jk_0 \cos\phi_0 \cos\phi \int_{-\infty}^{\infty} D_0 e^{-jk_0 z_0(\sin\phi_0 - \sin\phi)} dz_0. \tag{D.32}$$

The same procedure is performed to obtain the scatter pattern for the TM case, which is

$$R_P^{TM}(\phi, \phi_0) = 2jk_0 (1 - \sin\phi \sin\phi_0) \int_{-\infty}^{\infty} D_0 e^{-jk_0 z_0(\sin\phi_0 - \sin\phi)} dz_0. \tag{D.33}$$

APPENDIX E
MATHEMATICAL APPENDIX

An integral of the following form arises from the procedure used to obtain (2.16)

$$\int_0^\infty e^{j\kappa x} d\kappa. \tag{E.1}$$

Using relations found in Heitler [27], this integral is evaluated as follows:

$$-j \lim_{K\to\infty} \int_0^K e^{j\kappa x} d\kappa = \lim_{K\to\infty} \frac{1 - e^{jKx}}{x} = \lim_{K\to\infty} \left(\frac{1 - \cos Kx}{x} - j\frac{\sin Kx}{x} \right) \equiv \frac{\mathcal{P}}{x} - j\pi\delta(x). \tag{E.2}$$

The $\mathcal{P}/x$ is called the principal value of $1/x$. When $x \neq 0$ it behaves like $1/x$, but for $x = 0$, it vanishes. When multiplied by a function and integrated, it has the effect of removing a small interval $(-\epsilon, +\epsilon)$ symmetrically about $x = 0$, i.e.

$$\int_{-\infty}^{\infty} f(x)\frac{\mathcal{P}}{x} dx = \int_{-\infty}^{-\epsilon} \frac{f(x)}{x} dx + \int_{+\epsilon}^{\infty} \frac{f(x)}{x} dx. \tag{E.3}$$

The function $\delta(x)$ is the Dirac delta function which is undefined unless in the integrand of an integral. It has the following properties

$$\int_{-\infty}^{\infty} \delta(x) dx = 1 \tag{E.4}$$

$$\int_{-\infty}^{\infty} f(x)\delta(x - x_0) dx = f(x_0). \tag{E.5}$$

If the expression in (E.2) is combined in the proper way, improper integrals of the sine and cosine functions are obtained, i.e.,

$$\int_0^\infty \sin ax \sin bx dx = \frac{\pi}{2} [\delta(a - b) - \delta(a + b)] \tag{E.6}$$

$$\int_0^\infty \cos ax \cos bx dx = \frac{\pi}{2} [\delta(a - b) + \delta(a + b)] \tag{E.7}$$

$$\int_0^\infty \cos ax \sin bx dx = \mathcal{P}\left\{ \frac{b}{b^2 - a^2} \right\} \tag{E.8}$$

If $a > 0$ and $b > 0$ then $\delta(a+b) = 0$.

In order to find the far fields in Sections 2.1 and 2.2, the stationary phase method is used, which is given by Felsen and Marcuvitz [4] to be

$$\int_{x_a}^{x_b} f(x)e^{j\Omega q(x)}dx \sim I_s(\Omega)U\left[(x_s - x_a)(x_b - x_s)\right] + I_e(\Omega) + O\left(\frac{1}{\Omega^{3/2}}\right), \quad \Omega \to \infty \tag{E.9}$$

where $\Omega > 0$, $U(\alpha)$ is the Heaviside step function which is zero for $\alpha < 0$ and unity for $\alpha > 0$; I_s is the contribution from the stationary-phase point, which is

$$I_s(\Omega) = \sqrt{\frac{2\pi}{\Omega\left|q''(x_s)\right|}} f(x_s)e^{j\Omega q(x_s) \pm j\pi/4}, \quad q''(x_s) \gtrless 0, \tag{E.10}$$

and I_e is the contribution from the endpoints, namely

$$I_e(\Omega) = \frac{1}{j\Omega}\left[\frac{f(x_b)}{q'(x_b)}e^{j\Omega q(x_b)} - \frac{f(x_a)}{q'(x_a)}e^{j\Omega q(x_a)}\right]. \tag{E.11}$$

The stationary point is the point at which $q'(x_s) = 0$ and is assumed to lie within the interval $x_a < x_s < x_b$.

REFERENCES

1. E. Bahar, "Electromagnetic wave propagation in inhomogeneous multilayered structures of arbitrary thickness—full wave solutions," *J. Math. Phys.*, vol. 14, no. 8, pp. 1030–1036, 1973.

2. W. J. Plant, "Comment on the full-wave controversy," *J. Geophys. Res.*, vol. 96, no. C9, pp. 17,105–17,106, 1991.

3. R. E. Collin, "Electromagnetic scattering from perfectly conducting rough surfaces," *IEEE Trans. Antennas Propag.*, vol. AP-40, no. 12, pp. 1466–1477, 1992.

4. L. B. Felsen and N. Marcuvitz, *Radiation and Scattering of Waves.* New York: IEEE Press, 1994.

5. C. A. Balanis, *Advanced Engineering Electromagnetics.* New York: Wiley, 1989.

6. E. I. Thorsos, "The validity of the Kirchhoff approximation for rough surface scattering using a gaussian roughness spectrum," *J. Acoust. Soc. Am.*, vol. 83, no. 1, pp. 78–92, 1988.

7. E. I. Thorsos and D. R. Jackson, "The validity of the perturbation approximation for rough surface scattering using a Gaussian roughness spectrum," *J. Acoust. Soc. Am.*, vol. 86, no. 1, pp. 261–277, 1989.

8. E. I. Thorsos and D. P. Winebrenner, "An examination of the 'full-wave' method for rough surface scattering in the case of small roughness," *J. Geophys. Res.*, vol. 92, no. C9, pp. 17,107–17,121, 1991.

9. P. Beckmann and A. Spizzichino, *The Scattering of Electromagnetic Waves from Rough Surfaces.* New York: Macmillan, 1963.

10. J. Ogilvy, *Theory of Wave Scattering from Random Rough Surfaces.* Philadelphia: Institute of Physics, 1991.

11. I. Gradshteyn and I. Ryzhik, *Table of Integrals, Series, and Products.* San Diego: Academic Press, corrected and enlarged ed., 1980.

12. A. Papoulis, *Probability, Random Variables, and Stochastic Processes.* New York: McGraw-Hill, third ed., 1991.

13. M. Priestly, *Spectral Analysis and Time Series, vol. I: Univariate Series.* London: Academic Press, 1981.

14. P. J. Davis and P. Rabinowitz, *Methods of Numerical Integration.* Orlando: Academic Press, second ed., 1984.

15. E. I. Thorsos and A. Ishimaru, "An examination of the 'full-wave' method for rough surface scattering," in *National Radio Science Meeting*, (Boulder, Colorado), 1988.

16. E. Bahar, "Radio wave propagation over a rough variable impedence boundary, ii, application of full wave analysis," *IEEE Trans. Antennas Propag.*, vol. AP-20, pp. 362–368, 1972.

17. E. Bahar and G. Rajan, "Depolarization and scattering of electromagnetic waves by irregular boundaries for arbitrary incident and scatter angles—full wave solutions," *IEEE Trans. Antennas Propag.*, vol. AP-27, pp. 214–225, 1979.

18. E. Bahar, "Full-wave solutions for the depolarization of the scattered radiation fields by rough surfaces of arbitrary slope," *IEEE Trans. Antennas Propag.*, vol. AP-29, pp. 443–454, 1981.

19. E. Bahar, "Full-wave solutions for the scattered radiation fields from rough surfaces with arbitrary slope and frequency," *IEEE Trans. Antennas Propag.*, vol. AP-28, no. 1, pp. 11–21, 1980.

20. R. E. Collin, "Full wave theories for rough surface scattering: An updated assessment," *Radio Science*, vol. 29, no. 5, pp. 1237–1254, 1994.

21. E. Mendez and K. O'Donnell, "Observations of depolarization and backscattering from Gaussian random surfaces," *Opt. Commun.*, vol. 61, pp. 91–95, 1987.

22. E. Bahar and M. Fitzwater, "Depolarization and backscatter enhancement in light scattering from random rough surfaces: Comparison of full-wave theory with experiment," *J. Opt. Soc. Am.*, vol. A Opt. Image Sci., pp. 33–43, 1989.

23. A. G. Voronovich, *Wave Scattering from Rough Surfaces.* Berlin: Springer-Verlag, 1994.

24. J. Kong, *Electromagnetic Wave Theory.* New York: Wiley, second ed., 1990.

25. S. O. Rice, "Reflection of electromagnetic waves from slightly rough surfaces," *Commun. Pure Appl. Math.*, vol. 4, pp. 351–378, 1951.

26. L. Fortuin, "Survey of literature on reflection and scattering of sound waves at the sea surface," *J. Acoust. Soc. Am.*, vol. 50, pp. 1209–1228, 1970.

27. W. Heitler, *The Quantum Theory of Radiation.* New York: Dover, 1984.